INVESTIGATION OF EFFECTS OF NEUROLOGICAL DISEASES ON HUMAN BRAIN METABOLISM: COMPUTATIONAL SYSTEMS BIOLOGY APPROACH

by

Mustafa SERTBAŞ

B.S., Chemical Engineering, Hacettepe University, 2009

Submitted to the Institute for Graduate Studies in
Science and Engineering in partial fulfillment of
the requirements for the degree of
Master of Science

Graduate Program in Chemical Engineering

Boğaziçi Univerisity

2013

ACKNOWLEDGEMENTS

I would like to express my sincere gratitude to my supervisors, Prof. Kutlu Ülgen and Assist. Prof. Tunahan Çakır for their never-ending support and encouragement throughout my study. I would like to thank the other members of my thesis committee, Prof. Zeynep Petek Çakar, Assist. Prof. Arzucan Özgür, and Assist. Prof. A. Kerem Uğuz, for the time they devoted to reading my thesis and their comments.

I gratefully acknowledge Gebze Institute of Technology for financial support (Project Code: BAP 2011-A-27). Erasmus Office at Gebze Institute of Technology is acknowledged due to financial contribution to attend ECCE9 in The Hague within the framework of staff mobility. I also acknowledge Office of International Relations at Boğaziçi University for invaluable experience as graduate exchange student at North Carolina State University.

I would like to thank my friend, Res. Asst. Özgün Yücel, for his continuous support in programming. I am also thankful to all members of Biosystems Engineering Research Group at Boğaziçi University and Computational Systems Biology Group at Gebze Institute of Technology for providing me a friendly working atmosphere.

I am deeply indebted to my family, Muammer, Aynur, and Büşra Sertbaş, for their everlasting support and patience.

ABSTRACT

INVESTIGATION OF EFFECTS OF NEUROLOGICAL DISEASES ON HUMAN BRAIN METABOLISM: COMPUTATIONAL SYSTEMS BIOLOGY APPROACH

The objective of this study is the investigation of the effects of Parkinson's disease on human brain metabolism by using computational systems biology approach. A new brain metabolic model originated from Çakır *et al*., (2007) is substantially improved by expanding the lumped reactions in the model into elementary reactions and adding several new reactions existed in the literature. In addition, available gene information of each reaction based on HumanCyc is included in the developed brain model to be used in transcriptome data analysis. The new brain model comprises 630 reactions (571 internal, 59 exchange) and 524 metabolites (465 internal, 59 external) with the 670 genes. The applicability of the new brain model is tested by predicting resting (healthy) condition fluxes by using flux balance analysis. Since estimated flux results are consistent with the resting state, the new brain model is used in prediction of fluxes by using constraint-based modeling in hypoxia and Parkinson's disease. Flux changes in these two cases are computed by using minimization of metabolic adjustment (MOMA) and regulatory on / off minimization (ROOM) approaches. Hypoxia results are in agreement with the results in Çakır *et al*., (2007). Many of the metabolic fluxes in Parkinson's disease are found to be almost the same as in resting state. Apart from constraint based modeling, integrative modeling of the transcriptome data and brain metabolism is performed by using different approaches. Reporter metabolite analysis (RMA) is applied in Parkinson's disease and other neurological diseases. Significant changes are estimated in glycolysis, oxidative phosphorylation and ATPase pathway, isoleucine, and methionine metabolism in Parkinson's disease by using reporter pathway analysis. Lastly, transcription factor binding site analysis is performed for the reporter metabolites in Parkinson's disease by grouping up-regulated and down-regulated genes. SOX17, FOXF2, PBX1, Mycn, and Myb are identified as over-represented transcription factors with a high frequency among many others, pointing to these transcription factors as putative regulators of Parkinson's disease.

ÖZET

NÖROLOJİK HASTALIKLARIN İNSAN BEYİN METABOLİZMASI ÜZERİNE OLAN ETKİLERİNİN İNCELENMESİ: HESAPLAMALI SİSTEM BİYOLOJİSİ YAKLAŞIMI

Bu çalışmanın amacı Parkinson hastalığının insan beyin metabolizmasına etkisinin hesaplamalı sistem biyoloji yaklaşımı kullanarak incelenmesidir. Çakır ve ark. (2007) tarafından yapılan çalışması kaynak alınarak toplu reaksiyonların basit (elementer) reaksiyonlara genişletilmesiyle ve literatürde var olan birçok yeni reaksiyon eklenmesiyle yeni bir beyin metabolik modeli geliştirilmiştir. Ek olarak, modelde yer alan her bir reaksiyonun mevcut gen bilgisi Humancyc.org'dan alınarak model transkriptom verisi analizinde kullanılmaya uygun hale getirilmiştir. Yeni beyin modeli 670 gen, 630 reaksiyon (571 içsel, 59 değişim) ve 524 metabolit (465 içsel, 59 dışsal) içermektedir. Modelinin uygulanabilirliği akı denge analizi kullanarak sağlıklı koşul akıları tahmin edilmesiyle test edilmiştir. Tahmin edilen akı sonuçları sağlıklı durum ile uyumlu olduğundan, yeni beyin modeli kısıta-dayalı modelleme kullanarak oksijen yetmezliği ve Parkinson hastalığında akıların tahmininde kullanılmıştır. Bu iki koşulda akı değişimleri metabolik düzenlemenin minimizasyonu ve düzenleyici aç / kapa minimizasyonu yaklaşımları kullanarak hesaplanmıştır. Oksijen yetmezliği sonuçları Çakır ve ark. (2007) sonuçları ile uygun bulunmuştur. Parkinson hastalığında metabolik akıların çoğunun hemen hemen dinlenme koşulundaki ile aynı olduğu hesaplanmıştır. Kısıta-dayalı modelleme dışında, transkriptom verisinin ve beyin metabolizmasının birleştirici modellemesi farklı yaklaşımlar kullanılarak gerçekleştirilmiştir. Bilgi verici metabolit analizi Parkinson hastalığı ve diğer nörolojik hastalıklar için uygulanmış olup Parkinson hastalığında glikoliz, oksidatif fosforilasyon ve ATPase yolizi, izolösin ve metiyonin metabolizmalarında önemli değişiklikler tahmin edilmiştir. Son olarak, bilgi verici metabolitler için artan ve azalan genleri gruplayarak Parkinson hastalığı için transkripsiyon faktörü bağlama yeri analizi gerçekleştirilmişir. Diğer birçoğu arasında, SOX17, FOXF2, PBX1, Mycn ve Myb transkripsiyon faktörleri Parkinson hastalığında düzenleyiciler olarak bulunmuştur.

TABLE OF CONTENTS

LIST OF FIGURES

LIST OF TABLES

LIST OF SYMBOLS

D	Euclidean distance
m	Number of metabolites
n	Number of reactions
S	Stoichiometric coefficient matrix
v	Flux distribution
w	Wild type flux distribution
Z	Objective function
μ	Mean
σ	Standard deviation
Θ.	Normal cumulative distribution
Θ^{-1}	Inverse normal cumulative distribution
ε	Absolute ranges of tolerance
δ	Relative ranges of tolerance

LIST OF ACRONYMS / ABBREVIATIONS

AD	Alzheimer's disease
ALS	Amyotrophic lateral sclerosis
CMR	Cerebral metabolic rate
CNS	Central nervous systems
CoA	Coenzyme-A
DOPA	Dihydroxyphenylalanine
FBA	Flux balance analysis
GABA	γ-aminobutyric acid
GEO	Gene expression omnibus
Hc	Hydrogen in oxidative phosphorylation
HD	Huntington's disease
KIC	α-ketoisocapriate
KIV	α-ketoisovalerate
KMV	α-keto-β-methylvalerate
lb	Lower bound
MILP	Mixed-integer linear programming
MOMA	Minimization of metabolic adjustment
MS	Multiple Sclerosis
PD	Parkinson's disease
PPP	Pentose phosphate pathway
RMA	Reporter metabolite analysis
ROOM	Regulatory on / off minimization
ROS	Reactive oxygen species
RPA	Reporter pathway analysis
SCH	Schizophrenia
TCA	Tricarboxylic acid,
TF	Transcription Factor
ub	Upper bound

1. INTRODUCTION

Systems biology is a new branch of science, investigating cell as a whole with the help of biological data and computational methods rather than focusing solely on individual cellular components [1,2]. Transcriptomics, high-throughput measurement of the messenger RNA molecules, constitutes the basis of the systems biology and enables scientists to understand the complexities occurring in the cells simultaneously [3,4]. One of the important research area in systems biology is metabolism, which is the sets of all chemical reactions existing in the cell to sustain life. Investigation of the brain metabolism depending on the interactions between astrocytes and neurons draws many researchers' attention due to advancement in transcriptomics technology. Any change in a certain metabolite of brain metabolism may result in a fatal perturbation in the central nervous system due to the complexity. Parkinson's disease is an age-related neurological disease resulting in decreased level of the dopamine metabolite due to the loss of dopaminergic neurons in the substantia nigra region of the brain. Aside from Parkinson's disease, Alzheimer's disease, amyotrophic lateral sclerosis, Huntington's disease, multiple sclerosis, and schizophrenia are common neurological diseases affecting thousands of people all over the world.

Developments in the computing science lead to computational examination of complex metabolism in a collaborative manner with state-of-the-art experimental technology. Flux balance analysis (FBA) is the most prevalent constraint-based computational method enabling researchers to predict experimental results of metabolic fluxes *in silico* with respect to a defined objective function. Other two widely used constraint-based methods are minimization of metabolic adjustment (MOMA) approach which aims to calculate a flux distribution as close as possible to the resting condition by calculating minimal Euclidean distance between the wild-type and perturbed condition, and regulatory on / off minimization (ROOM) approach, minimizing the number of significant fluxes changing due to the perturbed condition. Apart from constrain-based modeling, computational techniques are used in integrative modeling of transcriptome data and metabolism. One method in these techniques is reporter metabolite analysis which

determines the metabolites affected most by transcriptional changes due to any perturbation [5]. Another remarkable method is prediction of transcription factor binding sites to elucidate regulatory networks in the cells.

The objective of this study is the investigation of the effects of neurological diseases on human brain metabolism by using computational systems biology approach. The general information about the topics covered in this study is presented in the second chapter under the name of "Background Aspects". The following three chapters include research performed in this study.

The third chapter details development of the brain model. The brain reaction model, 217 metabolic reactions and 216 metabolites, constructed by Çakır et al. (2007) is augmented by (i) expanding the lumped reactions in the model into elementary reactions and (ii) adding new reactions existed in the literature [6]. Since it is aimed to integrate transcriptome data with the brain reaction model, gene information for each elementary reaction is included based on HumanCyc, which is a database supplying the information about the human metabolism reactions. After transformation of lumped reactions in Çakır et al. (2007) into elementary reactions and addition of scientifically supported metabolisms, the new brain model comprises 630 reactions and 524 metabolites with 670 genes in total.

The fourth chapter focuses on the prediction of fluxes by using constraint-based modeling in resting (healthy) condition, hypoxia, and Parkinson's disease. Resting state predictions are performed by flux balance analysis and compared with the literature studies for the applicability of the developed brain model. Flux changes in two different hypoxia states, namely cerebral and astrocytic, are computed by using MOMA and ROOM approaches. Low-expressed genes are determined from the transcriptome data and inactivated in the calculation of fluxes via MOMA and ROOM in Parkinson's disease.

The fifth chapter covers the integrative modeling of the transcriptome data and brain metabolism for neurological diseases. The first analysis in this chapter is reporter metabolite analysis (RMA) for the different regions of the brain in Parkinson's disease and in other neurological diseases. Second one is reporter pathway analysis in which each

pathway is scored with a p-value based on the p-value of their metabolites calculated from RMA. Lastly, transcription factor binding site analysis is performed for the reporter metabolites in Parkinson's disease by grouping up-regulated and down-regulated genes.

The summary of the main results and recommendations for future work are given in the "Conclusion and Recommendations" chapter.

2. BACKGROUND ASPECTS

2.1. Systems Biology

The existence and function of individual cellular biomolecules have been studied enormously. It has been deduced that existence of a biomolecule does not necessarily mean proper functioning in the cell. The reason underlying this result is interactions between biomolecules. It is necessary to measure many biomolecules in the cell simultaneously in order to understand the interactions between them. In the last decade, cutting-edge technologies have enabled the researchers to measure hundreds of biomolecules (gene, protein, metabolite) in the same experiment [7–9]. Therefore, a new approach called systems biology has emerged. It is a new branch of science, investigating cell as a whole with the help of biological data and computational methods rather than focusing solely on individual cellular components [1,2]. Behaviors of the cell are predicted *in silico* by systems biology approaches using biological data.

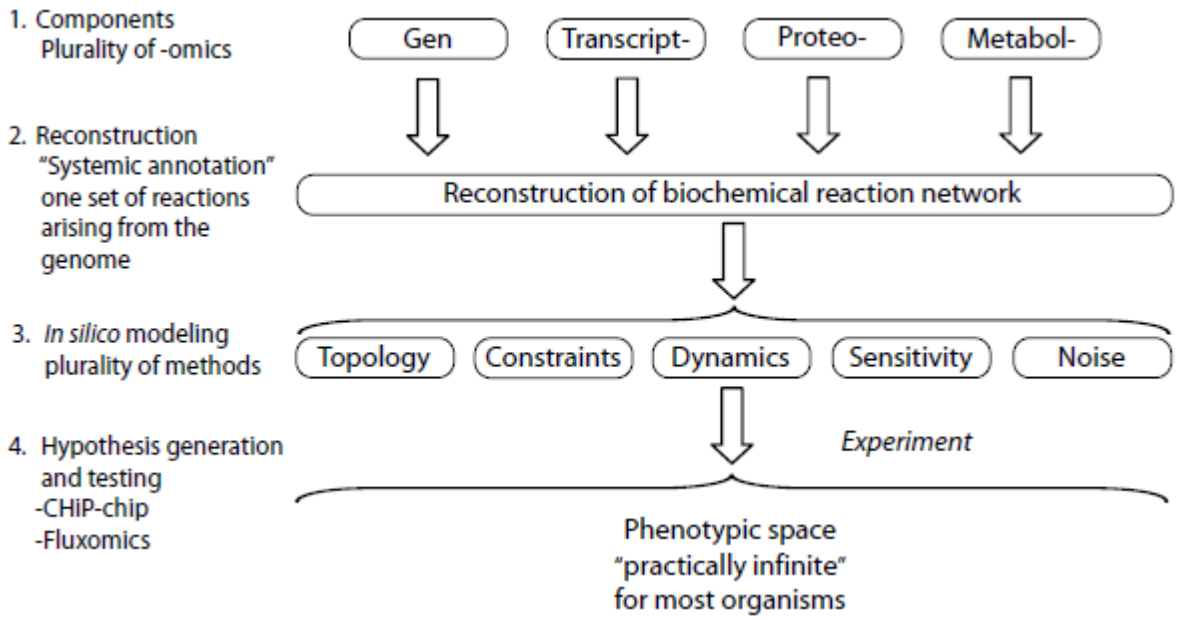

Figure 2.1. The four principal steps in the implementation of systems biology [10].

Analysis of systems biology is made up of four steps as shown in Figure 2.1 [10]. First, the list of biological components that participate in the process of interest is

enumerated. Second, the interactions between these components are studied, and the biological networks of genomic data are constructed. Third, reconstructed networks are described mathematically and their properties are analyzed. Computer models are then generated to analyze, interpret, and predict the biological functions that can arise from the reconstructed networks. Fourth, the models are used to analyze, interpret, and predict experimental outcomes. Prediction essentially corresponds to generating specific hypotheses that can then be experimentally tested. These *in silico* models of reconstructed networks are then improved in an iterative manner.

2.1.1. Omics Technologies

Omics data developed by high-throughput technology constitutes the basis of the systems biology and enables scientists to understand the complexities occurring in the cells simultaneously [3,4]. By comparing omics data obtained at different conditions, changes in the cell are unraveled comprehensively. Genomics, transcriptomics, proteomics, metabolomics, and fluxomics are the main omics technologies used in systems biology approach and their scope are listed in Table 2.1 briefly [10].

Table 2.1. High-throughput omics technologies and their definitions [10].

Omics Technology	**Function**
Genomics	Whole genome sequencing and annotation
Transcriptomics	Simultaneous measurement of the messenger RNA molecules
Proteomics	Simultaneous measurement of the protein abundance
Metabolomics	Simultaneous measurements of the concentration of metabolites
Fluxomics	Simultaneous measurements of metabolic fluxes

Transcriptomics is the high-throughput measurement of the messenger RNA molecules in the cell. Relative amounts of transcriptions of thousands of genes at various conditions are determined simultaneously by transcriptome analysis [11]. Mainly this technique is used to specify which genes are expressed at different conditions by comparing relative expression levels.

2.2. Metabolism

One of the important research area in systems biology is metabolism, which is the sets of all chemical reactions existing in the cell to sustain life. As shown in Figure 2.2, metabolism is divided into two classes: catabolism and anabolism. Catabolism covers the degradation of complex molecules to low-carbon metabolites by producing ATP and NADPH. Sugar-phosphates, pyruvate, acetyl-coA, and succinyl-coA are the common cellular metabolites produced in catabolic reactions. On the other hand, anabolism includes the synthesis of complex molecules such as amino acids, nucleotides, and fatty acids from low-carbon metabolites by using ATP and NADPH. Along with the energy from catabolism, complex molecules produced by anabolic reactions take place in cellular growth.

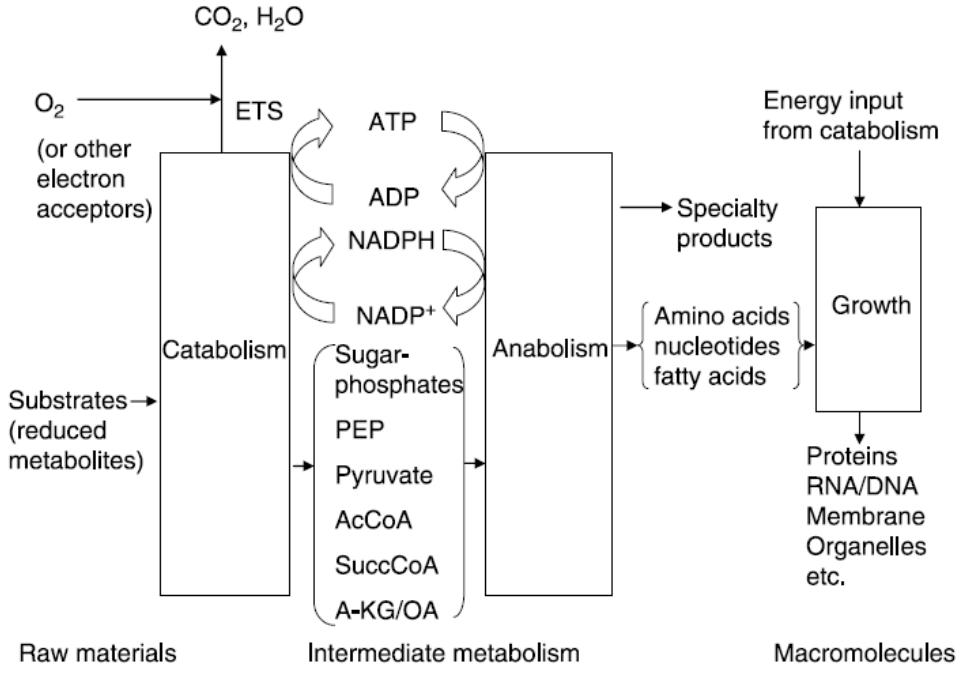

Figure 2.2. Major components of the cellular metabolism [12].

2.2.1. Brain Metabolism

Brain is one of the most active and complex organs of human body. Even though the human brain is 2% of the body weight, it uses 20% of the total oxygen consumed by the body at rest [13]. It regulates human behavior and quantities of metabolites circulating in

the body thanks to specialized cells as a response to received impulses. The major cells constituting brain are neurons and astrocytes. Neurons are responsible for receiving and transmitting impulses. Impulses are transmitted from neuron to another across a small gap called synapse. Astrocytes help to provide necessary chemicals for neurons. Metabolic reactions take place in and between these cells as illustrated in Figure 2.3 [6].

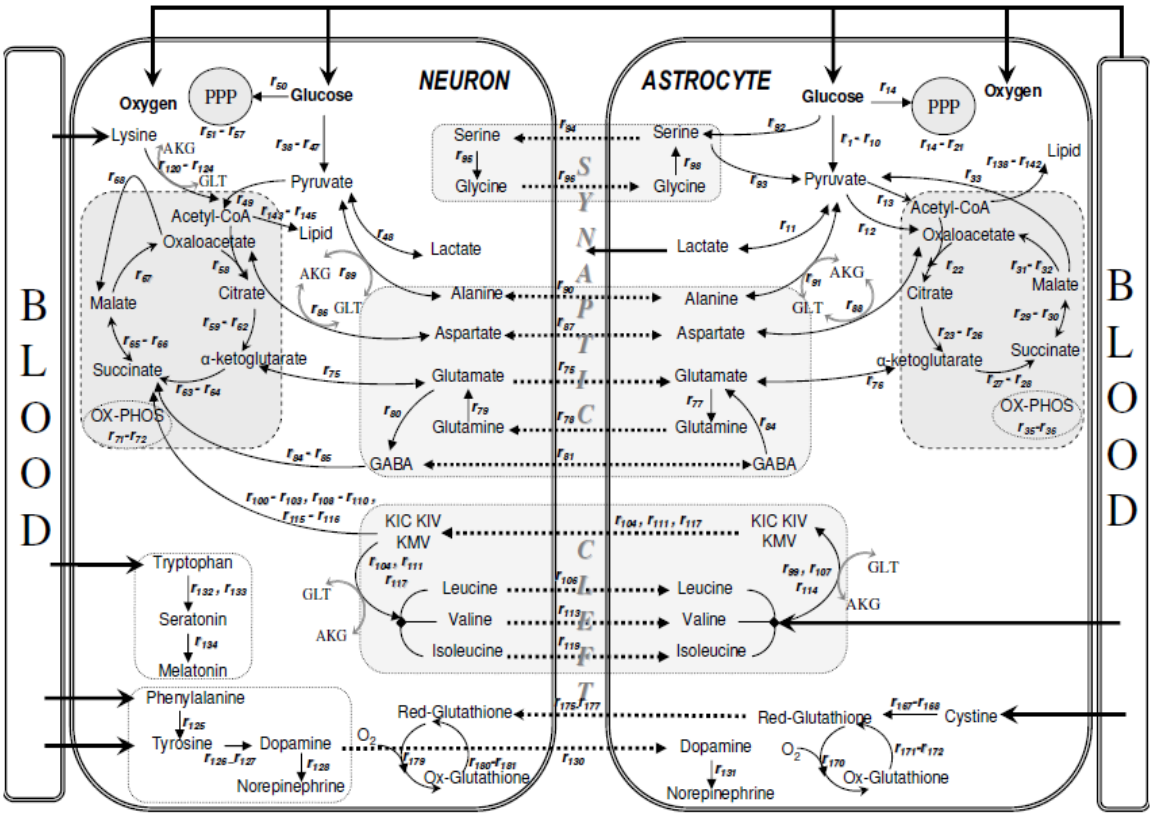

Figure 2.3. Illustration of brain metabolism and some of the metabolic reactions occurring in neuron and astrocyte [6].

Brain is protected from harmful chemicals existing in the blood by blood-brain-barrier, which is a layer of endothelial cells. Blood-brain-barrier has specific transport mechanisms. Therefore entry of protein and long chain fatty acids are restricted by blood brain barrier, and blood glucose is used as the main energy supplying substrate in the brain cells through the blood-brain-barrier [13].

2.3. Neurological Diseases

Neurological diseases stem from any disorder in the central nervous systems (CNS). Any change in a certain metabolite may result in a fatal perturbation in the central nervous system due to its complexity. There are many identified neurological diseases affecting thousands of people all over the world. However, further investigations are required for the full understanding of the mechanisms of these diseases and improvement of successive treatment techniques by using state of the art technology. Figure 2.4 demonstrates search results of the "neurological disease" term on PubMed for the last 50 years. As seen, there is an increasing trend in neurological disease research performed.

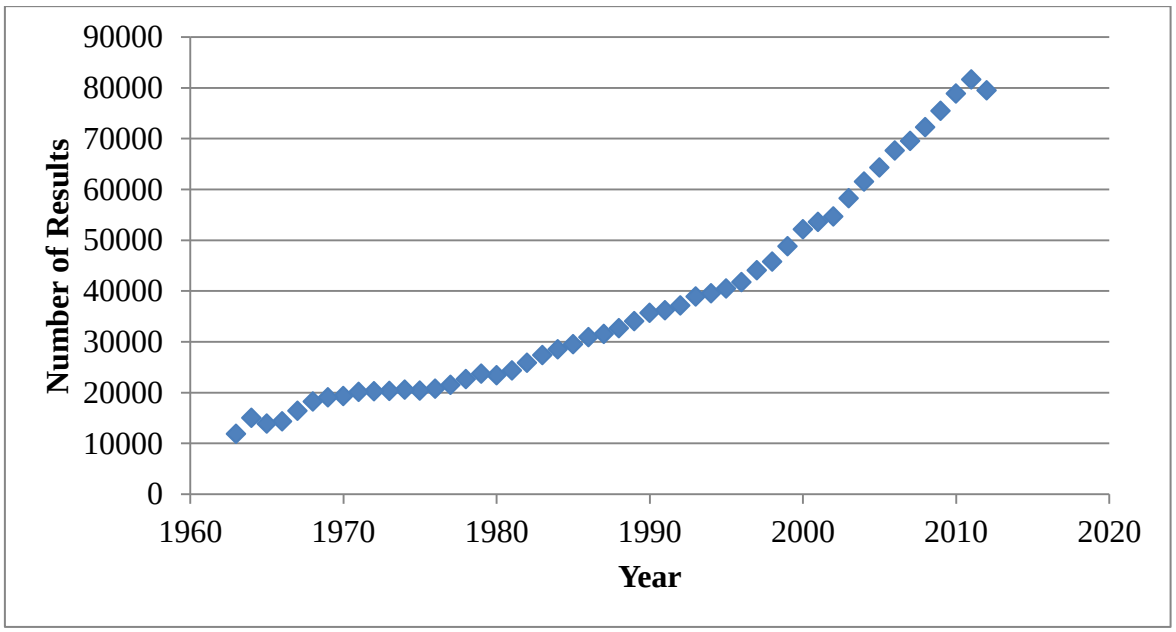

Figure 2.4. Search results of the "neurological disease" term on PubMed for the last 50 year.

The main neurological diseases affecting human being are Alzheimer's disease, Parkinson's disease, Huntington's disease, amyotrophic lateral sclerosis, multiple sclerosis, and schizophrenia. The results of searching these neurological diseases as a keyword on PubMed are listed in Table 2.2.

Table 2.2. Number of results found on PubMed search for main neurological diseases.

Keyword	Number of Results
Schizophrenia	103512
Alzheimer’s disease	91357
Parkinson’s disease	68202
Multiple Sclerosis	56520
Amyotrophic Lateral Sclerosis	15757
Huntington’s disease	13216

2.3.1. Parkinson's Disease

Parkinson’s disease is an age-related neurological disease and it was identified by James Parkinson in 1817. It is one of the most important neurological diseases from which thousands of people are suffering around the world. The main symptoms of PD are tremor, rigidity, akinesia and postural problems [14]. In addition to genetic factors Parkinson’s disease is mainly caused by environmental factors, such as rular living, herbicides, pesticides and heavy metals [15,16].

Search results of the "Parkinson’s disease" term on PubMed for the last 50 years are plotted in Figure 2.5. It is obviously seen that there is a steep increase in scientific research of this disease especially in the last 2 decades, due to the discovery of genes causing Parkinson’s disease by using high-throughput technologies .

Genetic studies have elucidated the mutated genes causing Parkinson’s disease [17–20]. SNCA, PARK2, LRRK2, PINK1, and PARK7 are the main identified genes and they are responsible for the synthesis of proteins of α-synuclein, Parkin, DJ1, PTEN-induced putative kinase 1, and Leucine-rich repeat kinase, respectively. Mutations in these genes result in dysfunction in their proteins and familial Parkinson’s disease.

In the Parkinson’s disease, the level of the dopamine metabolite is decreased due to the loss of dopaminergic neurons in the substantia nigra region of the brain. Insoluble protein, called Lewy bodies, is accumulated within the brain. These changes in the brain

metabolism give rise to symptoms of this disease including rigidity, shaking, and lack of movement since dopamine is responsible for control of the movement ability [20–22].

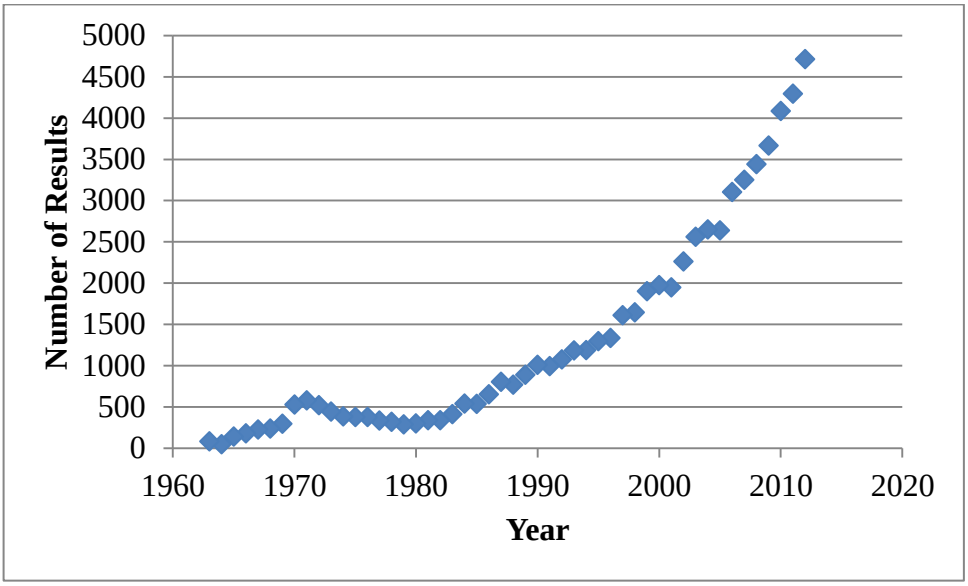

Figure 2.5. Search results of the "Parkinson's disease" term on PubMed for the last 50 year.

Dopamine is an important neurotransmitter in brain metabolism. It is produced from tyrosine via L-DOPA intermediate metabolite in neurons [23]. The strategy underlying the current treatment of this disease is to provide supplemental dopamine to the brain in order to compensate the decrease in dopamine level due to loss of neurons. This is done by using L-DOPA which is the precursor of dopamine synthesis in the treatment on account of the fact that dopamine does not cross the blood-brain barrier [13,24].

2.3.2. Other Neurological Diseases

Alzheimer's disease (AD) is the most common neurological disease affecting elderly people. Main symptom of AD is the lack of cognitive ability due to loss of neurons in the cerebral cortex [20]. In AD, amyloid plaques and neurofibrillary tangles accumulation occurs in the brain [20]. Different types of inhibitors and strategies are used in the treatment of AD [25].

Huntington's disease (HD) stems from impairment of neurons in the basal ganglia part of the brain and results in unintentional movements called chorea [20]. Most of the HD cases are genetic, resulting from repeated CAG codon in the huntingtin gene [26]. Despite absence of effective treatments, there are different therapeutic strategies in research [26].

Amyotrophic lateral sclerosis (ALS) is a rare age-dependent neurological disease. The most common symptoms of this disease is muscle weakness and atrophy. ALS is caused by a degeneration of motor neurons in the brain and spinal cord [20]. In order to slow the progress of ALS, riluzole, a modulator of glutamate transmission, is used in the treatment [27].

Multiple Sclerosis (MS), mainly seen among young adults, is characterized by loss of myelin in the brain and leads decreased vision, dysarthria, and paresthesias [20]. In addition to clinical findings, magnetic resonance imaging of the brain and analysis of cerebrospinal fluid are used in the diagnosis of MS [28]. Drug therapy is performed to reduce the progression of the disease [28].

Schizophrenia is an important mental disorder, affecting 1% of the population [29]. Magnetic resonance imaging of identical twins demonstrated that it is related to enlargement of the brain ventricles [13,29]. The medical symptoms include delusions, hallucinations, memory impairment and loss of rational behavior. In the treatment of this disease drug therapy is used integrated with psychosocial support [29].

2.4. Constraint-based Modeling of Metabolism

2.4.1. Flux Balance Analysis

Several methods have been developed for computational analysis of metabolism. Flux balance analysis (FBA) is the most widely used one among these computational methods with the aim of estimating conversion rates of metabolites in biochemical networks [30,31]. Since metabolism is the sets of all chemical reactions occurring in living organisms, FBA enables researchers to predict experimental results of metabolic fluxes *in*

silico. Prediction of growth rate of an organism and production rates of biologically important metabolites are the main applications of flux balance analysis.

Flux Balance Analysis comprises three main steps: (i) definition of the system, (ii) definition of constraints, and (iii) optimization.

2.4.1.1. Definition of the System: The first step of flux balance analysis is the description of the biological system. All known reactions (internal and exchange) as well as metabolites should be included in the definition of the system. Figure 2.6 indicates a sample system investigated by flux balance analysis. The model system comprises three internal metabolites (A, B and C) with four internal reactions (v_1, v_2, v_3, v_4) and three exchange fluxes (b_1, b_2, b_3).

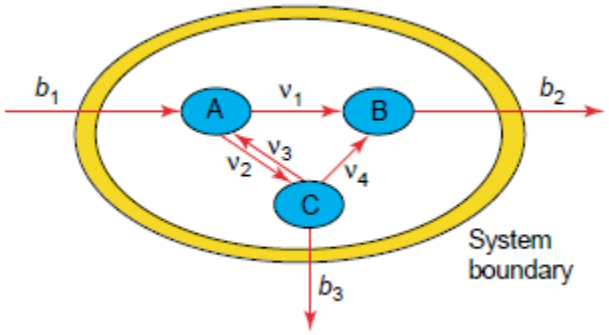

Figure 2.6. Sample system comprising reversible and irreversible conversion reactions between metabolites A, B, and C with exchange fluxes [30].

2.4.1.2. Definition of Constraints: There are three types of constraints in flux balance analysis, which are equality, reversibility, and measurement constraints. They are briefly explained below.

Equality Constraints: After the system is defined, mass balances of metabolites, known as equality constraints, are required. Mass balance equations accounting for all reactions as well as transport mechanisms within the system boundary are written around each internal metabolite as shown in Eqs. (2.1), (2.2), and (2.3).

$$\frac{dA}{dt} = -v_1 - v_2 + v_3 + b_1 \tag{2.1}$$

$$\frac{dB}{dt} = v_1 + v_4 - b_2 \tag{2.2}$$

$$\frac{dC}{dt} = v_2 - v_3 - v_4 - b_3 \tag{2.3}$$

The set of differential equations are then rewritten in matrix form.

$$\underbrace{\begin{bmatrix} -1 & -1 & 1 & 0 & 1 & 0 & 0 \\ 1 & 0 & 0 & 1 & 0 & -1 & 0 \\ 0 & 1 & -1 & -1 & 0 & 0 & -1 \end{bmatrix}}_{\mathbf{S}} \underbrace{\begin{bmatrix} v_1 \\ v_2 \\ v_3 \\ v_4 \\ b_1 \\ b_2 \\ b_3 \end{bmatrix}}_{\mathbf{v}} = \begin{bmatrix} \frac{dA}{dt} \\ \frac{dB}{dt} \\ \frac{dC}{dt} \end{bmatrix} \tag{2.4}$$

By taking into consideration steady state condition, where there is no flux change with respect to time, matrix notation is reduced to;

$$\underbrace{\begin{bmatrix} -1 & -1 & 1 & 0 & 1 & 0 & 0 \\ 1 & 0 & 0 & 1 & 0 & -1 & 0 \\ 0 & 1 & -1 & -1 & 0 & 0 & -1 \end{bmatrix}}_{\mathbf{S}} \underbrace{\begin{bmatrix} v_1 \\ v_2 \\ v_3 \\ v_4 \\ b_1 \\ b_2 \\ b_3 \end{bmatrix}}_{\mathbf{v}} = \begin{bmatrix} 0 \\ 0 \\ 0 \end{bmatrix} \tag{2.5}$$

In a general expression:

$$\mathbf{S}_{mxn} . \mathbf{v}_{nx1} = 0_{mx1} \tag{2.6}$$

where **S**, **v**, m, and n represent stoichiometric coefficient matrix, flux vector, number of metabolites, and number of reactions, respectively.

Reversibility Constraints: Direction of the biological reactions also plays an important role in flux values. For reversible reactions, flux value is either positive or

negative; however, for irreversible reactions, flux value of a reaction is only positive. Negative value of flux means opposite direction of the reaction. This reversibility information is used as a constraint in FBA. Irreversible reactions and reversible reactions are constrained to take values between [0,∞) and (-∞, ∞), respectively. Mathematically expressing, upper and lower bounds of fluxes are specified as follows:

$$v_i^{lb} \leq v_i \leq v_i^{ub} \qquad for\ i = 1,2,\dots,n \qquad (2.7)$$

Measurement Constraints: The objective of the flux balance analysis is to predict metabolic fluxes at steady state. Since there are more reactions than metabolites, the system of the equations is underdetermined, which means many solutions for the system. Degrees of freedom can be reduced by measuring some fluxes. That is, flux measurements can be used as a third type of constraint in FBA. This is mathematically expressed by setting the lower and upper bounds defined in Eq. 2.7 to the measured value.

2.4.1.3. Optimization: Metabolic reaction systems are underdetermined systems, which have degrees of freedom higher than zero and include more reactions than metabolites. Therefore, optimization based on objective functions is a technique that is used in flux balance analysis as a last step. Thanks to optimization, a single solution satisfying a selected objective function is computed among many solutions, satisfying the constraints. Figure 2.7 demonstrates optimization of the system with the objective function, Z, giving a single optimal point.

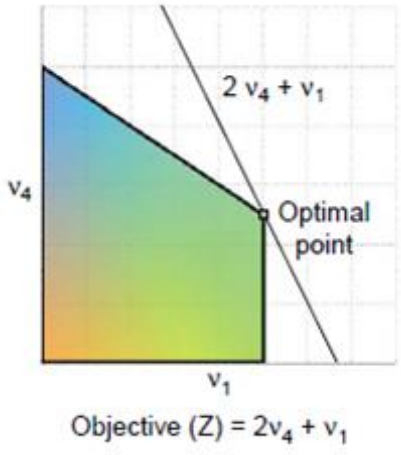

Figure 2.7. Illustration of optimization with only one optimal point for defined objective function [30].

In general, maximization of growth rate is used as the objective function in microorganisms since microorganisms are known to have tendency to grow faster [32]. However, in mammals, there is no common objective function. The objective function of the cells in different tissues of mammals can be different due to the fact that each tissue is specialized in different functions.

2.4.2. Minimization of Metabolic Adjustment

Minimization of Metabolic Adjustment (MOMA) predicts the optimum solution of the reaction set in the case of perturbed condition by taking resting (in microorganisms, wild type) condition into consideration [33]. Cells in perturbed condition tend to stay closer to the resting condition. In other words, MOMA hypothesizes that the closer is the flux distribution to the resting condition, the more accurate is the flux distribution. Therefore, in MOMA approach, the objective function is chosen as the minimization of the Euclidean distance between resting condition flux distribution and perturbed state flux distribution rather than using the resting-state objective function as done by FBA. In Figure 2.8, point *a* and *b* respectively represent optimum solution of flux distribution in resting and perturbed condition by using FBA. The resting state solution is not taken into account in the computation of FBA in perturbed condition. In contrast, MOMA approach finds the optimum solution of flux distribution in perturbed state by taking into consideration the resting condition. As seen in Figure 2.8, point *c* stands for flux distribution in the perturbed state by using MOMA. This approach states that point *c* is more probable than point *b*. It was shown that MOMA predicts perturbed-case metabolic fluxes more accurately [33].

Mathematical formulation of MOMA is given below:

$$\mathrm{D}(\mathbf{w}, \mathbf{v}) = \sqrt{\sum_{i=1}^{N} (w_i - v_i)^2} \tag{2.8}$$

where D represents the Euclidean distance between the wild-type flux distribution vector **w** and perturbed condition flux distribution vector **v**. The equation is expanded in the form of

$$\mathrm{D}(\mathbf{w},\mathbf{v}) = \sqrt{\sum_{i=1}^{N}({w_i}^2 - 2w_i v_i + {v_i}^2)} \tag{2.9}$$

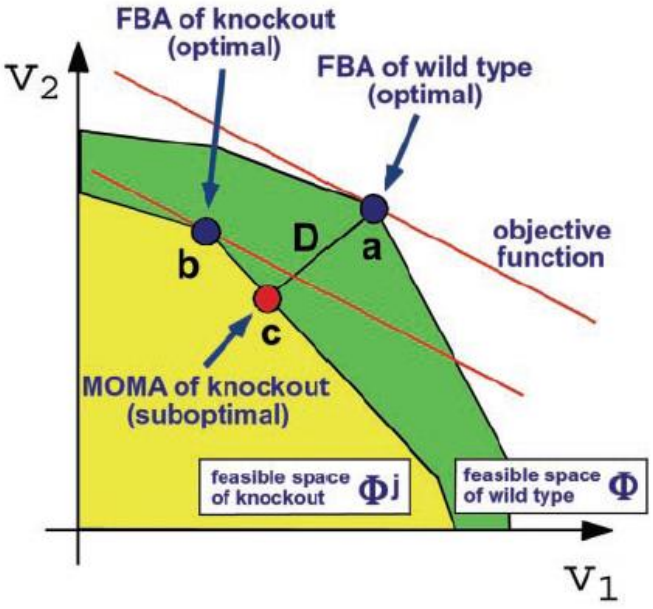

Figure 2.8. Illustration of optimal points determined by FBA and MOMA [33].

Since vector **w** represents wild type flux distribution and assumed to be known, the value of ${w_i}^2$ term is constant. Therefore, minimization of Euclidean distance D is equal to minimization of sum of remaining terms in the equation (sum of $-2w_i v_i$ and ${v_i}^2$ terms). Our aim is to find values of perturbed condition flux distribution vector v_i that satisfy

$$min(-2w_i v_i + {v_i}^2) \tag{2.10}$$

Since it has quadratic terms, quadratic programming is used to solve this problem. Quadratic programming solvers of major optimization softwares are based on the following general expression:

$$f(x) = L.x + \frac{1}{2}x^T Qx \tag{2.11}$$

where L and Q represent a vector and matrix, respectively. x^T is the transpose of x. Quadratic programming finds the values of x by minimizing $f(x)$ function. By letting $x = x_i$, $L = -2w_i$, and $Q = 2I$, where $I = unit\ matrix$, objective function of quadratic programming is converted into the minimization of $(-2w_i x_i + {x_i}^2)$ term, which is equivalent to Eq. 2.10.

2.4.3. Regulatory On / Off Minimization

Regulatory On / Off Minimization (ROOM) minimizes the number of significant fluxes changing in perturbed condition by using the same constraints as FBA and taking the resting condition into account [34]. In terms of physical meaning, the goal behind ROOM and MOMA is the same: both aim to calculate a perturbed flux distribution as close to resting condition as possible. However, they differ in mathematical formulation. ROOM minimizes the significant flux change rather than minimizing squared difference of the fluxes. The behavior underlying minimization of significant flux changes is that cells tend to eliminate any perturbation by using already active reactions occurring in them because activation of a new reaction which does not exist in the resting condition requires extra effort for cells (eg. production of new enzymes). Therefore, ROOM approach suggests a minimum number of significant change in fluxes with respect to the resting case. Mixed-integer linear programming (MILP) is used in ROOM calculation, which is formalized as:

$$min \sum_{i=1}^{n} y_i \tag{2.12}$$

where $y_i = 1$ for significant flux change and $y_i = 0$ otherwise. In addition to Eq. 2.6 and Eq. 2.7, a new set of reversibility constraint is specified as follows:

$$v_i - y_i\left(v_i^{ub} - w_i^{ub}\right) \leq w_i^{ub} \tag{2.14}$$

$$v_i - y_i\left(v_i^{lb} - w_i^{lb}\right) \geq w_i^{lb} \tag{2.15}$$

where y_i is either 0 or 1. For $y_i = 1$, which states no change in fluxes with respect to resting condition, Eq. 2.14 and Eq. 2.15 reduce to Eq. 2.7. In case of change in fluxes in comparison with resting state (i.e. $y_i = 0$), Eq. 2.14 and Eq. 2.15 become:

$$w_i^{lb} \leq v_i \leq w_i^{ub} \tag{2.16}$$

To solve reconstructed system in a short time computationally, the following two parameters are specified: relative ranges of tolerance, δ, and absolute ranges of tolerance, ε [34]. δ and ε are added to the system as additive and multiplicative term, respectively. In case of existence of a very small term like 10^{-15} from resting state solution, it is time consuming to evaluate such a small number. Therefore, running time is reduced by introducing ε, (10^{-5}), and δ, (0.03) as stated below and this does not change the optimization result:

$$w_i^{ub} = w_i + \delta|w_i| + \varepsilon \tag{2.17}$$

$$w_i^{lb} = w_i - \delta|w_i| - \varepsilon \tag{2.18}$$

The mathematical formulation of ROOM is quite different from MOMA and FBA formulations. In the ROOM method, there are $2n$ unknowns that are v_i and y_i. The mathematical system is therefore to be reformulated to be solved by optimization softwares. To this aim, augmented matrices are formed as follows:

$$v_{2nx1}^{all} = \begin{bmatrix} v_{nx1} \\ y_{nx1} \end{bmatrix}_{2nx1} \tag{2.19}$$

$$A_{mx2n} = \left[[S]_{mxn} \quad \vdots \quad \begin{bmatrix} 0 & 0 & 0 \\ 0 & 0 & 0 \\ 0 & 0 & 0 \end{bmatrix}_{mxn} \right]_{mx2n} \tag{2.20}$$

Equality constraint defined in Eq. 2.6 becomes

$$A_{mx2n} . v_{2nx1}^{all} = 0_{mx1} \tag{2.21}$$

Reversibility constraints in Eq. 2.14 and 2.15 are expressed in matrix form by defining matrices B and C as follows:

$$B_{nx2n} = \left[\left| \begin{matrix} 1 & 0 & \dots & 0 \\ 0 & 1 & \dots & 0 \\ \dots & \dots & \dots & \dots \\ 0 & 0 & \dots & 1 \end{matrix} \right|_{nxn} \left| \begin{matrix} -\left(v_1^{ub} - w_1^{ub}\right) & 0 & \dots & 0 \\ 0 & -\left(v_2^{ub} - w_2^{ub}\right) & \dots & 0 \\ \dots & \dots & \dots & \dots \\ 0 & 0 & 0 & -\left(v_n^{ub} - w_n^{ub}\right) \end{matrix} \right|_{nxn} \right]_{nx2n} \quad (2.22)$$

$$B_{nx2n} . v_{2nx1}^{all} \leq w_{nx1}^{ub} \quad (2.23)$$

$$C_{nx2n} = \left[\left| \begin{matrix} 1 & 0 & \dots & 0 \\ 0 & 1 & \dots & 0 \\ \dots & \dots & \dots & \dots \\ 0 & 0 & \dots & 1 \end{matrix} \right|_{nxn} \left| \begin{matrix} -\left(v_1^{lb} - w_1^{lb}\right) & 0 & \dots & 0 \\ 0 & -\left(v_2^{lb} - w_2^{lb}\right) & \dots & 0 \\ \dots & \dots & \dots & \dots \\ 0 & 0 & 0 & -\left(v_n^{lb} - w_n^{lb}\right) \end{matrix} \right|_{nxn} \right]_{nx2n} \quad (2.24)$$

$$C_{nx2n} . v_{2nx1}^{all} \geq w_{nx1}^{lb} \quad (2.25)$$

Combining two reversibility constraints into one:

$$\begin{bmatrix} B_{nx2n} \\ -C_{nx2n} \end{bmatrix}_{2nx2n} [v^{all}]_{2nx1} \leq \begin{bmatrix} w_{nx1}^{ub} \\ -w_{nx1}^{lb} \end{bmatrix}_{2nx1} \quad (2.26)$$

Equality and reversibility constraints are defined as stated above. Since minimization of the sum of y_i's is aimed, objective function for the system is expressed as follows:

$$f = [|0\ 0\ 0\ 0\ \dots\ 0|_{1xn} |1\ 1\ 1\ 1\ \dots\ 1|_{1xn}]_{1x2n}\ [v^{all}]_{2nx1} \quad (2.27)$$

2.5. Integrative Modeling of Transcriptome Data and Metabolism

2.5.1. Reporter Metabolite Analysis

Reporter metabolites are defined as metabolites having the most significant transcriptional changes around due to any perturbation, such as genetic and environmental [5]. Genetic perturbations include gene deletion and insertion to develop genetically modified cells for industrial applications or research activities. Environmental perturbations cover changes in growth medium such as temperature, oxygen concentration,

and carbon source. In addition, the diseases in human metabolism are considered to be a type of perturbation due to the fact that all of these perturbations enable the cells to use a different combination of metabolic pathways than they use in unperturbed (healthy) condition. Changes in metabolic network are elucidated by looking at transcriptional changes. Since any metabolite in the cellular metabolic network can be involved in many metabolic reactions, reporter metabolite analysis (RMA) determines the metabolites around which the most significant transcriptional changes occur due to perturbation. RMA takes expression levels of all genes controlling the reactions of the related metabolite into account as demonstrated in Figure 2.9. In the literature, RMA is applied to the different types of studies including gene deletions in *Saccharomyces cerevisiae* [5], and diabetes in human [35].

In RMA, each metabolite is scored by depending on the p-values of its neighbor genes which are responsible for reactions of the metabolite in question. p-values of each gene (p_i), representing the significance of differential gene data, are transformed into Z score (Z_i) by using the inverse normal cumulative distribution (Θ^{-1}).

$$Z_i = \Theta^{-1}(1 - p_i) \tag{2.31}$$

New aggregated Z scores of the k neighbor genes are computed for each metabolite node in the metabolic graph.

$$Z_{metabolite} = \frac{1}{\sqrt{k}} \sum Z_i \tag{2.32}$$

Then, Z scores are corrected by using mean (μ_k) and standard deviation (σ_k) of the aggregated Z scores of many sets of randomly selected k genes from metabolic network.

$$Z_{metabolite}^{corrected} = \frac{(Z_{metabolite} - \mu_k)}{\sigma_k} \tag{2.33}$$

In the last step, corrected Z scores are converted to p-values by using Eq. 2.31, and metabolites having p-values less than the selected cut-off are named as reporter metabolites. RMA calculation was performed using the online BioMet Toolbox [36].

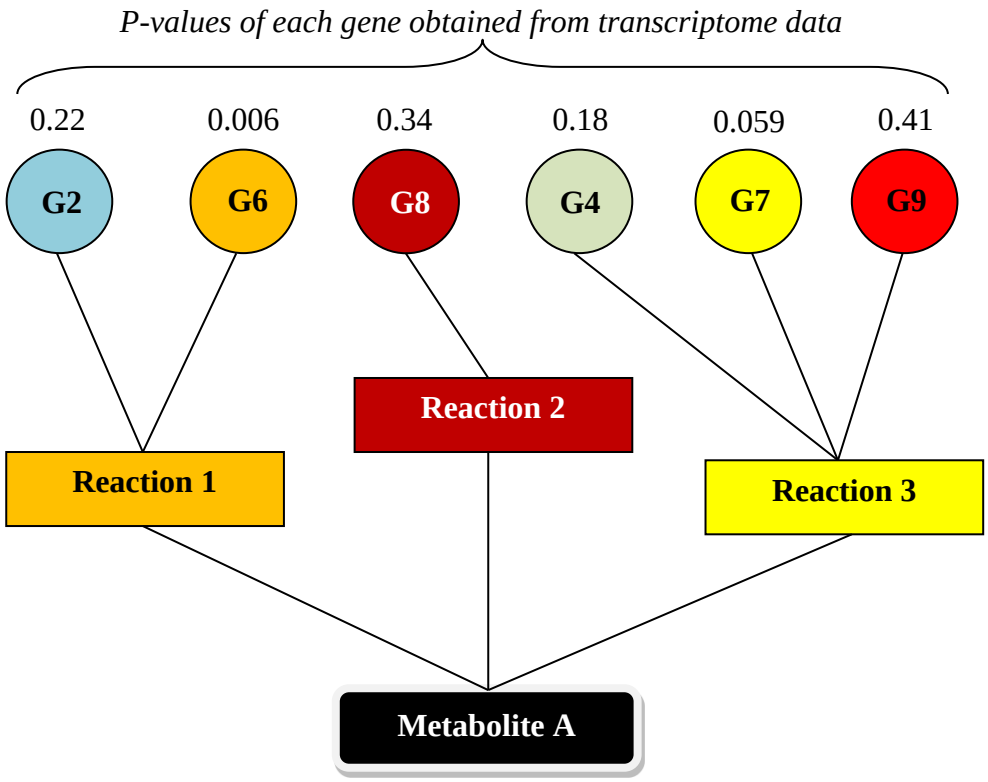

Figure 2.9. Outline of reporter metabolite analysis in which each metabolite is scored by depending on the p-values of its neighbor genes which are responsible for reactions of the metabolite in question. In case of multiple available genes for a particular reaction, gene having minimum p-value is used in the present study for related reaction in RMA. For example, G6, G8, and G7 are selected in RMA for Reactions 1, 2, and 3, respectively.

2.5.2. Computational Binding Site Analysis

Transcription factors are proteins binding to specific sequence in DNA so as to regulate transcription process. The regulation takes place by activating or repressing the transcription of genes. Activation leads to increased transcription level and repression brings about decreased level of transcription. Each gene is controlled by one or more transcription factor due to the presence of one or more transcription factor binding sites.

Prediction of transcription factor binding site is a key assessment in order to understand the gene regulations. Integration of high-throughput sequencing techniques with computational methods puts this prediction into practice. For the prediction of the transcription factor binding site, a database storing the sequence of different binding sites is initially generated [37,38]. There are mainly 4 steps in building database for different transcriptional factor binding sites as given in Figure 2.10 [39]. The first step is to collect the experimentally verified binding site sequence information available in the literature and align with the best matching. In the second step, position frequency matrix (PFM), representing the frequency of each nucleotide in corresponding position, is constructed from the aligned binding sites. Then, position frequency matrix is transformed into position weight matrix (PWM) in which normalized frequency values are converted to log-scale. In the last step, sequence logo (motif) is generated to demonstrate alignment in each column measured in terms of information content [40]. The reason in the use of sequence logo is to perform fast and visual evaluation of pattern properties. JASPAR [37] and TRANSFAC [38] are two main internet-based databases storing information of position matrices and consequently sequence logo for different transcription factors. After building the database, each motif is aligned with the gene of interest to see whether there is a corresponding transcriptional factor.

Transcriptional factors play also an important role in multiple gene expression due to possibility of regulation of many genes by a single transcriptional factor. Especially, improvements in transcriptomic technology enable collection of gene expression data for thousands of genes and a comprehensive investigation of these data elucidate over-represented transcriptional factor binding sites. Pscan is an internet-based software tool finding these sites by using co-regulated genes [41]. It compares co-regulated gene sequences with the motifs of known transcription factors from JASPAR or TRANSFAC database. It computes significantly over-represented and under-represented motifs, specifying transcriptional factors, with the location in the sequence. It results in common regulatory transcriptional factors for investigated genes.

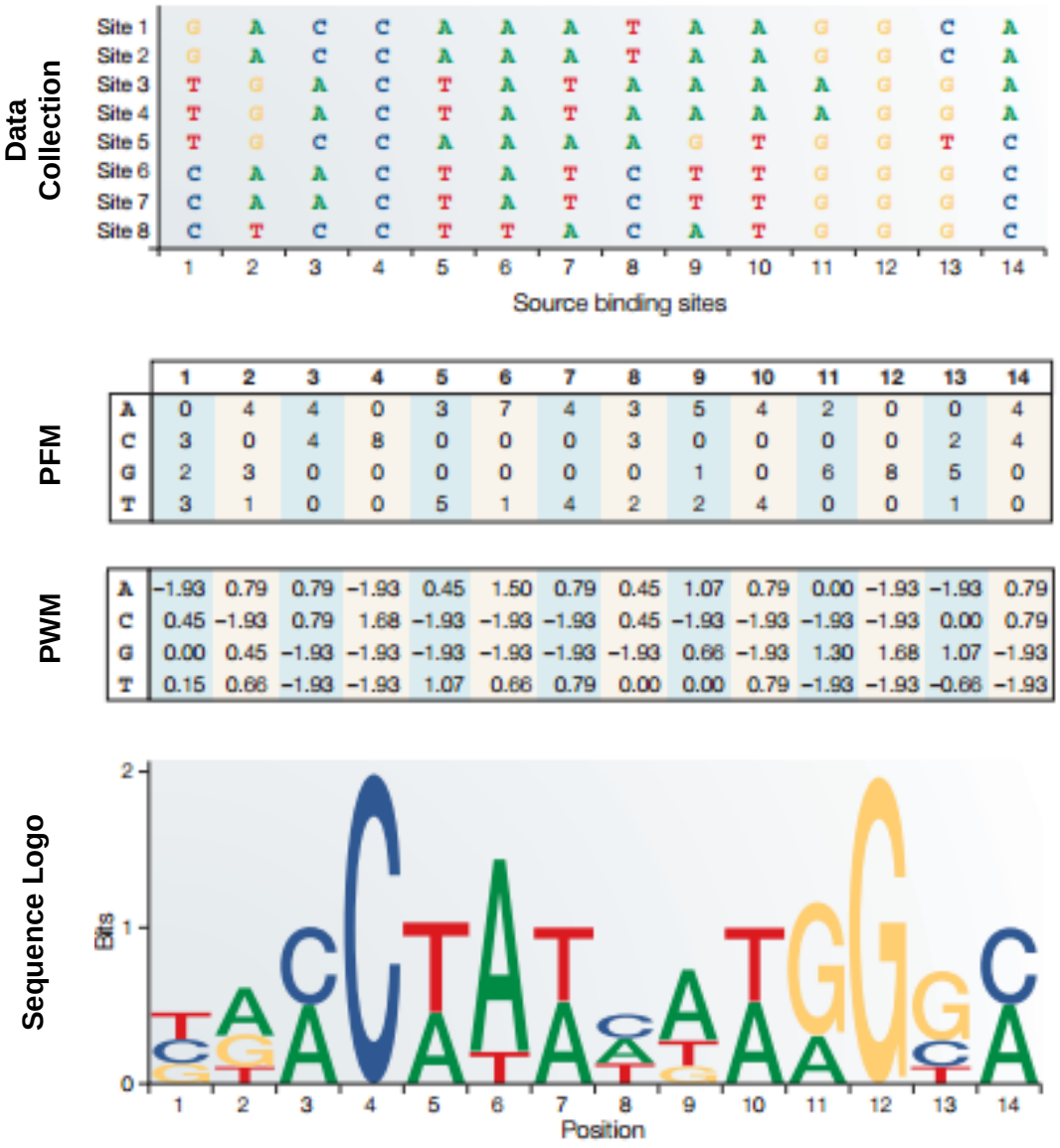

Figure 2.10. Steps in building database for transcriptional factor binding sites [39].

3. MODEL DEVELOPMENT

Flux balance modeling approach of the brain metabolism was firstly investigated by Chatziioannou et al. (2003) [42]. This study, focusing on interaction and Krebs cycle reactions between neuron and astrocyte metabolism, includes 16 reactions. Many pathways (glycolysis, pentose phosphate pathway, Krebs cycle, amino acid metabolism and ROS pathway, lipid metabolism) constituting metabolism was taken into consideration by Çakır et al. (2007) [6]. This study is more advantageous than the previous study since Çakır et al.'s model contained 217 reactions and 216 metabolites totally. Moreover, the results of this study, modeling with flux balance analysis, are in accordance with experimentally published data. In the same year, another study of 108 reactions was published on brain metabolism by Occhipinti et al. (2007) [43]. A new study with about 1000 reactions, derived from generalized human metabolism, was published by Lewis et al. (2010) [44]. Although the last study has more reactions than Çakır et al.'s model, it was derived from a model not specific to brain metabolism and therefore has some disadvantages.

In this study, the brain reaction model constructed by Çakır et al. (2007) is augmented by (i) expanding the lumped reactions in the model (ii) adding new reactions existed in the literature. Since we aimed to integrate transcriptome data with the brain reaction model, gene and enzyme information for each elementary reaction in the Çakır model are obtained from HumanCyc, which is a database supplying the information about the human metabolism reactions (www.humancyc.org) [45].

3.1. Expanding Lumped Reactions

The reactions including two or more steps and stated as only one lumped reaction are transformed into elementary reactions constituting them. To illustrate, in Çakır model, the formation of propionyl-coa and acetyl-coa from methylbutyryl-coa is expressed as;

Methylbutyryl-CoA + FAD + NAD -> FADH2 + NADH + Propionyl-CoA + Acetyl-CoA

To use this reaction in transcriptome data analysis, it is converted into 4 elementary reactions by using HumanCyc as shown in Table 3.1. The same procedure is applied to all lumped reactions in the model. The new reaction set is tabulated with the information of gene name in order to be used in the future part of the study.

Table 3.1. Reaction name and gene name of 4 elementary reactions constituting propionyl-CoA and acetyl-CoA formation from methylbutyryl-CoA.

Reaction Name	**Gene Name**
Methylbutyryl-CoA + FAD -> FADH2 + E-2-methylcrotonoyl-CoA	ACADSB
E-2-methylcrotonoyl-CoA -> 2-methyl-3-hydroxybutyryl-CoA	HADHA; EHHADH; HS15845; HS17054; ECHS1
2-methyl-3-hydroxybutyryl-CoA + NAD -> NADH + 2-methylacetoacetyl-CoA	HSD17B10
2-methylacetoacetyl-CoA <-> Propionyl-CoA + Acetyl-CoA	HADHB; ACAA1; ACAT1

It is observed that some lumped reactions that existed in Çakır model are made up of 2 or 3 steps but a few of them consist of more than 30 steps (eg. cholesterol synthesis reaction). By writing all reactions in the form of elementary reactions, the number of reactions in the model is considerably increased. More importantly, new reaction set became suitable for transcriptome analysis. Comparison of the number of reactions in some metabolic pathways existing in Çakır model and this study after expanding lumped reactions is demonstrated in Table 3.2.

Table 3.2. Comparison of the number of reactions in some metabolic pathways existing in Çakır model and this study after expanding lumped reactions.

Pathway Name	Çakır et al. (2007)	This Study
Alanine Metabolism	10	12
Leucine Metabolism	8	11
Valine Metabolism	7	13
Isoleucine Metabolism	6	9
Lysine Metabolism	5	11
Phenylalanine-Tyrosine Metabolism	7	9
Tryptophan Metabolism	3	4
Cholesterol Metabolism	2	52
Fatty Acid Synthesis	10	94
Lipid Synthesis	19	27
Reactive Oxygen Species (ROS) Pathway	16	17
Glycogen Degradation Metabolism	2	3
Oxidative Phosphorylation*	2	5

* The related reactions are expanded, and P/O ratios for FADH and NADH is updated to 1.5, and 2.5 respectively, in accordance with information given by Rosenthal and Glew (2009) [46].

3.2. Workflow of Finding Active Pathways

In addition to transforming lumped reactions into elementary reactions, new reactions and pathways, supported by literature survey, are added to the Çakır model as outlined in Figure 3.1.

The ultimate goal is to construct a metabolic model with correct representation of the healthy brain metabolism. To this aim, transcriptome data of different brain regions for healthy (control) condition is used to determine active genes in healthy brain. For that purpose, control part of transcriptome data for 7 different regions of the brain are obtained from Gene Expression Omnibus (GEO). Corresponding GSE number of the data for each region is given in Table 3.3. An example of how to use GEO dataset is detailed in Appendix A. Since the aim of the present study is to develop a general model for whole

brain, as many as different regions are included in the study. Therefore, the brain model constructed in this study is not region-specific.

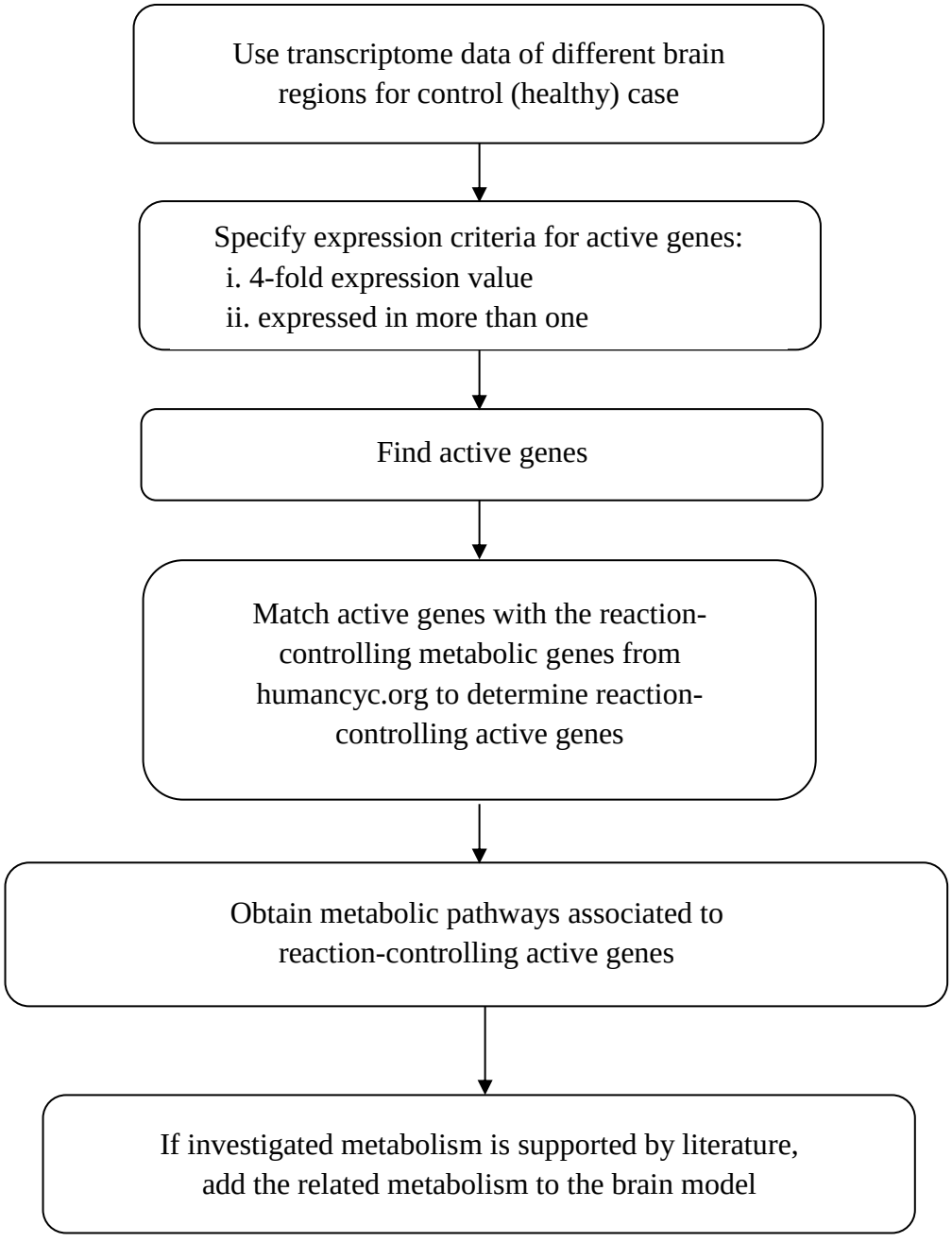

Figure 3.1. Outline of workflow in adding new pathways to the brain model.

In the determination of active genes in healthy brain, it is assumed that if any gene has very high expression value with respect to other genes, it must be active in the healthy brain. 4-fold is selected to be the criterion for this assumption from Figures 3.2 and 3.3. It

means if expression value of a gene that is higher than 4-fold of average of expression values of all genes in the same transciptome data, it is considered to be active in the healthy brain. Being expressed in more than one investigated region is used as a second criterion in order to minimize false positives.

Table 3.3. GSE code and brain regions used in expansion of model.

GSE Code	**GPL Code**	**Brain Region**
GSE20168	GPL96	Prefrontal Area 9
GSE20291	GPL96	Putamen
GSE20292	GPL96	Substantia Nigra
GSE28894	GPL6104	Medulla
GSE28894	GPL6104	Striatum
GSE28894	GPL6104	Frontal Cortex
GSE28894	GPL6104	Cerebellum

In addition to the reaction-controlling genes functioning in metabolism, there are active genes responsible for biological processes such as signaling in the brain. Therefore, after finding active genes by using the specified criteria based on transcriptome data, they are matched with the reaction-controlling metabolic genes obtained from humancyc.org in order to get only reaction-controlling active genes. Since humancyc.org also gives the associated metabolic pathway information for most of the reactions, metabolic pathways covering these active genes are used in literature survey as a guideline. If the investigated pathway is supported by literature, it is added to the brain model. If a pathway includes many reactions and only a few genes are found to be active in this pathway in transcriptome data analysis, the related pathway is disregarded. The underlying reason is that such genes are active probably because of different function than reaction control. Moreover, reaction-controlling genes that are active in all 7 regions and do not have pathway information are also checked. If a reaction does not have any connection with the current brain metabolic network via its metabolites, it is not added to the brain model. As a result, the improved brain model covers many more metabolites and reactions taking place in the brain compared to the Çakır model.

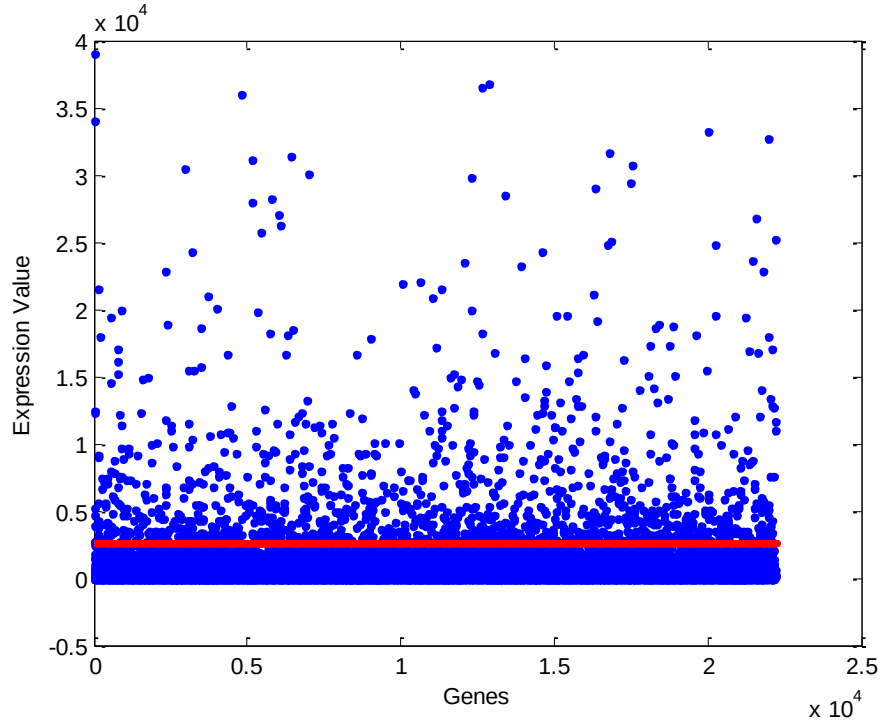

Figure 3.2. Representation of expression value of genes in determining active genes for cerebellum dataset in GSE28894. Red line shows 4-fold of average of expression values.

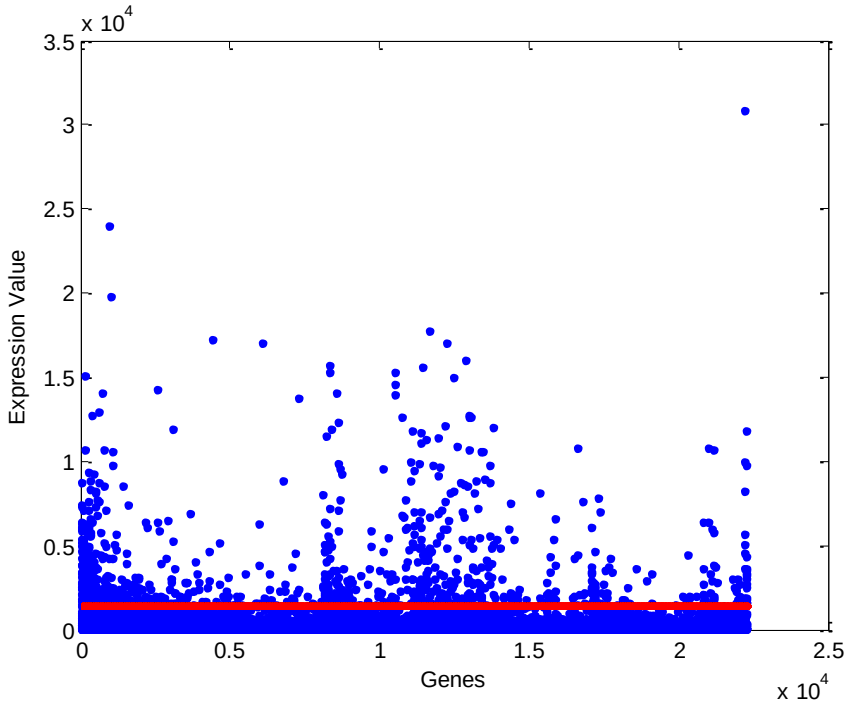

Figure 3.3. Representation of expression value of genes in determining active genes for substantia nigra dataset in GSE20292. Red line shows 4-fold of average of expression values.

Total number of genes and active genes satisfying the criteria in the related transcriptome data for investigated brain regions are given in Table 3.4. By applying the procedure mentioned above and outlined in Figure 3.1., numbers of genes found in each step are summarized in Figure 3.4. Total number of genes available in Transcriptome datasets is 20334. Total number of genes active in any one of the considered brain regions is 2785. Of these, 2118 genes are active in 2 and more brain regions. By matching 2118 active genes with the genes from humancyc.org, 544 genes are found to be metabolic reaction-controlling. 178 of these genes have an associated pathway information. Arginine, creatine, heme, histidine, inositol, methionine, pyrimidine nucleoside, polyamine, purine nucleoside, sphingomyelin, and threonine metabolisms in brain are found to have active genes by using this method and supported by literature. Therefore, related reactions and metabolisms are added to the brain model. In addition, proline, cardiolipin, ketone body, and asparagine metabolisms are found to be active in the brain and investigated in the literature. Therefore, they are also included in the current brain model.

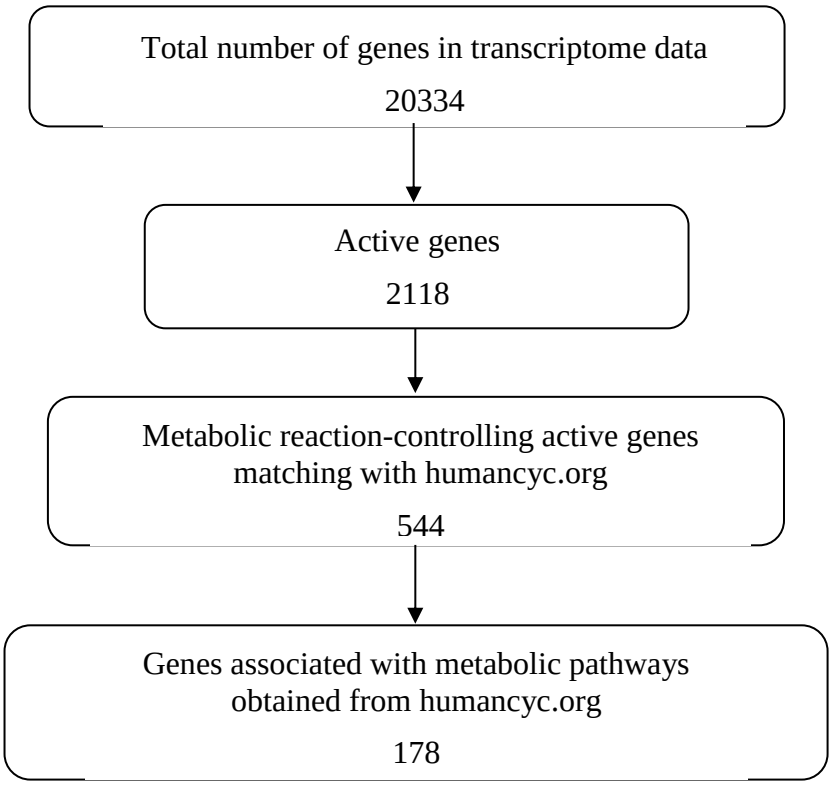

Figure 3.4. Summary of results in adding new pathways to the brain model.

Table 3.4. Number of total and active genes in related GSE dataset.

Brain Region (GSE Code)	**Number of Total Genes**	**Number of Active Genes***
Prefrontal Area 9 (20168)	13211	911
Putamen (20291)	13211	856
Substantia Nigra (20292)	13211	823
Medulla (28894)	18196	1200
Striatum (28894)	18196	1248
Frontal Cortex (28894)	18196	1258
Cerebellum (28894)	18196	1259

*Active gene criteria are defined as having 4-fold of average of expression values of all genes in the same transciptome data and being expressed in more than one region.

After transformation of lumped reactions in Çakır model into elementary reactions and addition of scientifically supported metabolisms as described above, the new brain model comprises 630 reactions (571 internal, 59 exchange) and 524 metabolites (465 internal, 59 external). Comparison of number of reactions and metabolites with Çakır model are tabulated in Table 3.5. 460 out of 571 internal reactions have gene information obtained from humancyc.org. Due to high coverage (81%) of gene-associated reactions in the model, in addition to FBA, it is possible to use this brain model for the integrated computational analysis of brain metabolism and transcriptome data. The total number of genes in the model is 670. After addition of the new reactions to the brain model, the number of the metabolic pathways included in the brain model is considerably increased. Comparison of the metabolic pathways in Çakır model (2007) and improved brain model in this study are given in Table 3.6.

Table 3.5. Comparison of Çakır model and improved model in this study in terms of included number of reactions and metabolites.

Comparison Criteria	**Çakır Model**	**This Model**
Internal Reaction	184	571
Exchange Reaction	33	59
Total Reaction	217	630
Internal Metabolite	183	465
External Metabolite	33	59
Total Metabolite	216	524
Total Number of Genes	-	670

Table 3.6. Comparison of metabolisms existing in Çakır model and improved brain model in this study.

Metabolism	**Çakır Model**	**This Model**
Glycolysis (Astrocytes)	+	+
Pentose Phosphate Pathway (Astrocytes)	+	+
TCA Cycle (Astrocytes)	+	+
Oxidative Phosphorylation and Atpase	+	+
Glutamate - Glutamine Cycle	+	+
GABA Cycle	+	+
Aspartate Metabolism	+	+
Asparagine Metabolism	-	+
Alanine Metabolism	+	+
Glycine-Serine Metabolism	+	+
Leucine Metabolism	+	+
Valine Metabolism	+	+
Isoleucine Metabolism	+	+
Lysine Metabolism	+	+
Phenylalanine-Tyrosine Metabolism	+	+
Tryptophan Metabolism	+	+
Acetylcholine Metabolism	+	+

Table 3.6. Comparison of metabolisms existing in Çakır model and improved brain model in this study (cont.).

Metabolism	**Çakır Model**	**This Model**
Proline metabolism	-	+
Histidine Metabolism	-	+
Methionine Metabolism	-	+
Threonine Metabolism	-	+
Cholesterol Synthesis	+	+
Fatty Acid Synthesis	+	+
Glycerol-3-phosphate Shuttle	+	+
CDP-Diacylglycerol biosynthesis	+	+
Phosphatidylethanolamine Metabolism	+	+
Phosphatidylcholine Metabolism	+	+
Cardiolipin Metabolism	-	+
Sphingomyelin Metabolism	-	+
Inositol Metabolism	-	+
Lipid Synthesis	+	+
Reactive Oxygen Species Pathway	+	+
Glycogen Degradation Metabolism	+	+
Ketone Body Metabolism	-	+
Arginine Metabolism	-	+
Polyamine Metabolism	-	+
Creatine Metabolism	-	+
Heme Metabolism	-	+
Purine Nucleoside Metabolism	-	+
Pyrimidine Nucleoside Metabolism	-	+

3.3. Reactions Added to the Çakır Model

In the present study, Çakır model (2007) is mainly improved by transforming lumped reactions into elementary reactions and identifying pathways present in the brain from

transcriptome data by using high gene expression values. Detailed literature survey about the existence of corresponding pathways in the brain is also performed for the further verification as mentioned below.

3.3.1. Glycolysis

Literature survey yielded a number of reactions related to the central carbon metabolism which is not accounted for in the Çakır model. They are included in the current model. In glycolysis, 3-phosphoglycerate is also produced from 1-3-biphosphoglycerate without yielding ATP in both astrocytes and neurons in addition to a direct production ($r_{7,}$ r_{52}). First, 1-3-biphosphoglycerate is converted to 2-3-Disphospho-D-glycerate (r_{16}, r_{60}) [47]. Then, 2-3-Disphospho-D-glycerate is transformed into 3-phosphoglycerate (r_{15}, r_{59}). In addition to the already accounted NADPH dependence, NADH is also used in the production of glutamate from alpha–ketoglutarate in astrocytes and neurons (r_{90}, r_{93}) [48]. Phosphoenolpyruvate carboxykinase, transforming oxaloacetate and GTP to Phosphoenol pyruvate, CO_2, and GDP, is expressed in both astrocytes and neurons (r_{14}, r_{58}) [49,50]. In addition to isocitrate biosynthesis, citrate reacts with ATP to give oxaloacetate, acetyl-coa, and ADP in neurons as well as astrocytes enzymatically (r_{28}, r_{72}) [51]. Also conversion of citrate to oxaloacetate and acetate is included in the astrocytes part of the present brain model because of the fact that citrate lyase subunit beta-like protein, responsible for this reaction, is highly expressed and astrocyte-specific enzyme according to Cahoy et al. (2008) study (r_{29}) [9].

3.3.2. Ketone Body Metabolism

Acetoacetate and 3-hydroxybutyrate are the ketone bodies that play an important role in human brain energy metabolism. They are produced by liver and transported by blood to brain where they can be used in ATP production as an alternative to glucose [52]. The uptake rates of ketone bodies from blood-brain barrier into brain are very small in comparison to glucose in resting condition; however, they significantly change in case of starvation in which uptake rates of ketone bodies increase with a decline in glucose uptake rate [53]. Ketone body metabolism in the brain is illustrated in Figure 3.5. Acetoacetate and 3-hydroxybutyrate are converted into acetyl-coa (r_{438}-r_{444}, r_{127}-r_{128}, r_{164}) which

participates in TCA cycle reactions or other metabolic reactions both in astrocytes and neurons [54].

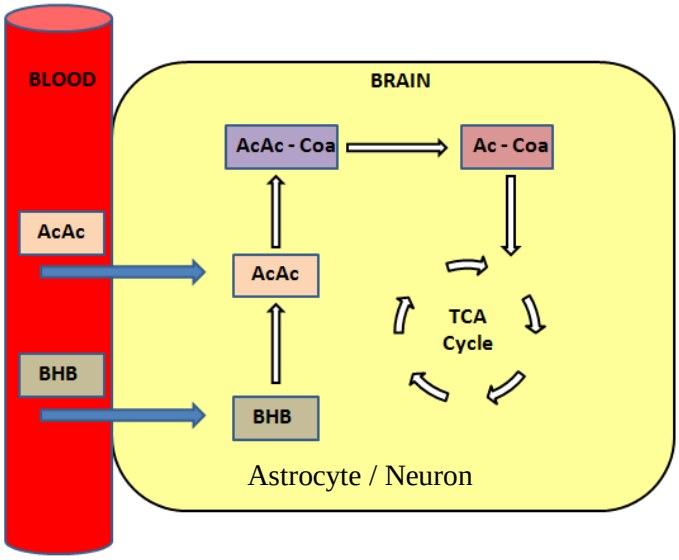

Figure 3.5. Representation of ketone body reactions in the astrocytes and neurons (BHB: 3-hydroxybutyrate, AcAc: Acetoacetate, AcAc-Coa: Acetoaacetyl-coa, Ac-Coa: Acetyl-coa).

3.3.3. Arginine, Polyamine and Creatine Metabolisms

Arginine is taken up by the astrocytes (r_{628}) [55]. As illustrated in Figure 3.6, it is used to produce agmatine (r_{446}) [55,56] and ornithine (r_{447}) [57] in astrocytes. Arginine is also transfered to neurons by astrocytes to synthesize agmatine (r_{453}) [58], citrulline (r_{455}) [59], and ornithine (r_{458}) [57]. Agmatine synthesized in neurons is converted into putrescine (r_{454}) [60,61] to be utilized both in polyamine metabolism including interconversion of precursor putrescine, spermidine, and spermine in neurons (r_{467}-r_{473}) [62] and in GABA synthesis from putrescine in astrocytes (r_{461}-r_{464}) [63,64]. In addition to its uptake, arginine is also produced in neurons from aspartate and citrulline (r_{456}-r_{457}) [57,65,66]. Ornithine is also taken up by both cell types, besides its production in astrocytes and neurons [67]; however, production of putrescine from ornithine is neuron-specific (R459) [68] and glutamate production from ornithine and alpha-ketoglutarate is astrocyte-specific reactions (r_{448}-r_{450}) [69]. In the cytosol of astrocytes, pyrroline-5-carboxylate, an intermediate metabolite in glutamate synthesis from ornithine, and NADPH are degraded into proline and $NADP^+$ (r_{179}). In astrocytic mitochondria, proline and FAD are converted to pyrroline-5-carboxylate and $FADH_2$ (r_{180}). These two proline

producing and consuming reactions are considered in only astrocytes in the brain model, due to the fact that Cahoy et al. (2008) work states Pyrroline-5-carboxylate reductase-like protein (PYCRL) and Proline dehydrogenase (PRODH) as astrocyte-specific [9].

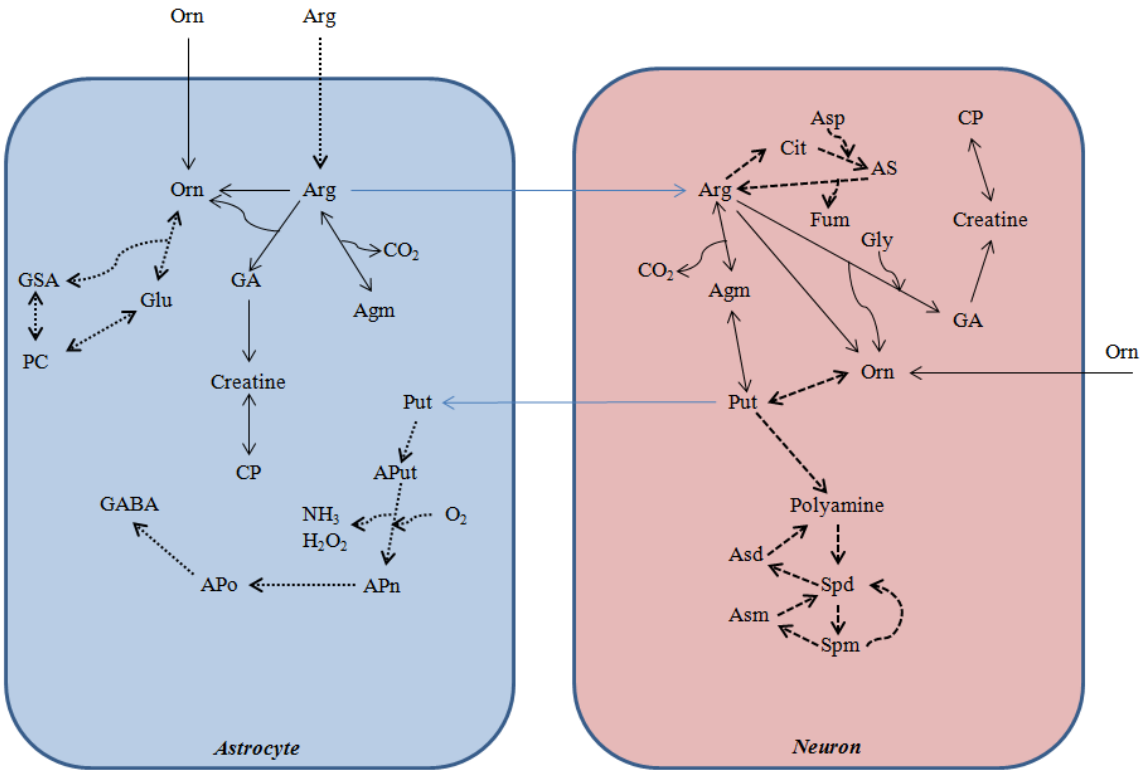

Figure 3.6. Representation of the reactions added to Çakır model including polyamine pathway, arginine metabolism, and creatine metabolism in astrocytes and neurons.

Another important metabolism consuming arginine and functioning in both neurons and astrocytes is creatine metabolism (r_{474}-r_{479}) consisting of ornithine and guanidinoacetate production from glycine and arginine [70]. Then guanidinoacetate is converted to creatine to be used in creatine phosphate synthesis (r_{475}-r_{476}, r_{478}-r_{479}) [69].

3.3.4. Asparagine and Histidine Metabolism

Asparagine is a non-essential amino acid and its biosynthesis is taken into account only in neurons, since asparagine synthetase, responsible for enzymatic biosynthesis of glutamate, asparagine, and AMP from glutamine, aspartate, and ATP, is found to be neuron-specific by Cahoy et al. (2008) study (r_{106}) [9].

Histidine, an essential amino acid, is taken up by the brain [71]. Then, it is enzymatically converted into neurotransmitter histamine in neurons by histidine decarboxylase (r_{107}) [72,73]. Neurons are also capable of synthesizing histamine N-methyltransferase producing S-adenosyl-L-homocysteine and methylhistamine from histamine and S-adenosyl-L-methionine (r_{108}) [74].

3.3.5. Methionine and Threonine Metabolism

Methionine, an essential amino acid, is taken up by brain [71]. It is converted into cysteine via transsulfuration pathway in astrocytes and neurons (r_{181}-r_{186}, r_{189}-r_{194}) [75,76]. In this pathway, homocysteine is formed by three reactions in series and reacts with serine to produce cystathionine which is transformed into cysteine, alpha-ketobutyrate (2-oxobutanoate), and ammonia. Homocysteine is also recycled to methionine due to the activity of 5-methyltetrahydrofolate-homocysteine methyltransferase enzyme in the brain (r_{187}, r_{195}) [77]. Conversion of alpha-ketobutyrate to propionyl-coa is thought to be active in astrocytes due to the control of this reaction by astrocyte-specific branched-chain α-keto acid dehydrogenase complex (r_{188}) [9].

Threonine is an essential amino acid and can cross the blood-brain barrier with a slow rate compared to other amino acids [71]. Its metabolism contains only 2 enzymatic reactions in the brain cells (r_{196}-r_{201}) [78]. First, threonine is converted to 2-amino-3-ketobutyrate by threonine 3-dehydrogenase. Then, 2-amino-3-ketobutyrate is catabolized to glycine and acetyl-CoA via 2-amino-3-ketobutyrate ligase.

3.3.6. Cardiolipin, Sphingomyelin, and Inositol Metabolisms

Cardiolipin is a phospholipid and found in mitochondria membrane [79]. It is synthesized from CDP-diacylglycerol and Glycerol-3-phosphate by three enzymatic reactions in series in the brain (r_{366}-r_{371}) [80].

Sphingomyelin, a type of sphingolipid, is localized in the brain [79,81]. Precursors of sphingomyelin synthesis are serine and palmitoyl-CoA. Astrocytes use its own serine; however, neurons utilize serine transported from astrocytes in sphingomyelin synthesis

since there is no serine synthesis in neurons (r_{372}-r_{376}, r_{378}-r_{382}) [82–84]. Sphingomyelin biosynthesis includes five metabolic reactions with 3-dehydrosphinganine, sphinganine, dihydroceramide, and ceramide intermediate metabolites. Sphingomyelin is also converted to ceramide and phosphoryl-choline due to availability of sphingomyelinase in the brain (r_{377}, r_{383}) [85].

Inositol is both taken up by brain [86], and synthesized from glucose in the brain in the cell from vasculature [87]. Since present study takes interactions between astrocytes and neuron into consideration, synthesis of inositol is not included in the brain model. Inositol is used to produce diacyglycerol, complex inositol phosphate, and phosphatidylinositol (r_{388}-r_{415}) [88,89].

Heme is an iron containing chemical compound and found in brain metabolism. Heme metabolism is included in present study in both neurons and astrocytes since it has active genes satisfying current criteria and supported by literature [90,91]. Heme is synthesized from glycine and succinyl-coa by eight reactions in series and degraded to bilirubin via biliverdin intermediate enzymatically (r_{480}-r_{499}) [92].

3.3.7. Purine and Pyrimidine Nucleoside Metabolism

Adenosine, guanosine, uridine, and cytidine are nucleosides taking place in brain metabolism and they are mainly synthesized in liver and transported into the brain through the blood-brain barrier [93]. In addition to a five-carbon sugar, adenosine, guanosine, uridine, and cytidine include adenine, guanine, uracil and cytosine in their structure as base, respectively. These nucleosides are converted into related nucleotides which are utilized in metabolic processes or recycled to their nucleosides in the brain (r_{500}-r_{571}) [93].

4. PREDICTIONS BY CONSTRAINT-BASED MODELING

4.1. Resting (Healthy) Condition

Çakır model includes 217 metabolic reactions (184 internal, 33 exchange) and 216 metabolites (183 internal, 33 external). The current model has 630 reactions (571 internal, 59 exchange) and 524 metabolites (465 internal, 59 external) in the brain metabolism. Çakır et al. (2007) has already analyzed resting state behavior of metabolic fluxes of astrocytes and neurons with their model. In this section, this analysis is repeated with the newly developed model to demonstrate the predictive power of the model.

Flux balance analysis (FBA) is applied to the current reaction set in two steps as stated below.

The first step, maximization of Glutamate/Glutamine/GABA Cycle, is selected as primary objective function of healthy (resting) astrocytes and neurons since it gives flux distribution consistent with experimental data [6]. Moreover, it is in agreement with the metabolic behaviors of neurons and astrocytes. These two cell types are known to have an active trafficking in between, and glutamate – glutamine cycle forms the most active part of this trafficking. Three reactions given in Figure 4.1 represent Glutamate/Glutamine/GABA cycle between astrocyte and neuron.

R91: Glutamate_N + ATP_A -> Glutamate_A + ADP_A
R95: Glutamine_A -> Glutamine_N
R98: GABA_N <-> GABA_A

Figure 4.1. Representation of Glutamate/Glutamine/GABA cycle between astrocyte and neuron.

Mathematical expression of maximization of the sum of Glutamate/Glutamine/GABA cycle-flux by using linear programming is given below:

$$\text{Max}(v_{91} + v_{95} + v_{98}) \tag{4.1}$$

$$subject\ to \quad S.v = 0 \tag{4.2}$$

$$f^T v = Z_{obj} \tag{4.3}$$

$$v_{min} \leq v \leq v_{max} \qquad for\ i = 1, 2, \dots, n \tag{4.4}$$

A second optimization, minimization of Euclidean norm (squared sum) of the internal fluxes, is applied to the system to eliminate the possibility of multiple optimum solutions. It is also aimed that the results obtained from second optimization must satisfy the first optimization outcomes. The underlying physical reason in the second optimization is to carry out cellular functions with minimum effort or minimal enzyme production.

Result of the maximization of the sum of Glutamate/Glutamine/GABA cycle flux is used to augment an equality constraint for second optimization as follows:

$$v_{91} + v_{95} + v_{98} = Z_{obj} \tag{4.5}$$

$$S_{m+1,i} = 0 \qquad for\ i = 1, 2, \dots, n \qquad and \qquad i \neq 75, 78, 81 \tag{4.6}$$

$$S_{m+1,i} = 1 \qquad for\ \ i = 91, 95, 98 \tag{4.7}$$

Since reaction numbers of 91, 95, and 98 represent Glutamate/Glutamine/GABA cycle reactions and maximum value of sum of these three reactions are calculated as Z_{obj} in the 1st optimization, 91st, 95th, and 98th terms in $(m+1)^{th}$ row of stoichiometric matrix are 1 and rest of the term in the same row are 0. Z_{obj} is added as $(m+1)^{th}$ term to zero vector at right hand side. Augmented equality constraint is:

$$\begin{bmatrix} \begin{bmatrix} & & & & & & & & & & & & & & & & & & & & \\ & & & & & & & & S_{mxn} & & & & & & & & & & & & \\ & & & & & & & & & & & & & & & & & & & & \end{bmatrix} \\ \begin{bmatrix} 0 & 0 & 0 & \dots & \underbrace{1}_{S_{m+1,91}} & 0 & 0 & \underbrace{1}_{S_{m+1,95}} & 0 & 0 & \underbrace{1}_{S_{m+1,98}} & \dots & 0 & 0 & 0 \end{bmatrix} \end{bmatrix} \begin{bmatrix} v_1 \\ v_2 \\ v_3 \\ . \\ . \\ . \\ . \\ v_{n-2} \\ v_{n-1} \\ v_n \end{bmatrix} = \begin{bmatrix} 0 \\ 0 \\ 0 \\ . \\ . \\ . \\ . \\ 0 \\ 0 \\ Z_{obj} \end{bmatrix} \tag{4.8}$$

By adding $(m+1)^{th}$ row to the stoichiometric matrix and Z_{obj} to the zero vector, a new equality constraint satisfying maximum value of the sum of Glutamate/Glutamine/GABA cycle flux is reconstructed so as to be used in the 2nd optimization as follows:

$$Min \sum_{i=1}^{n} v_i^2 \tag{4.9}$$

$$subject\ to \quad S_{m+1,n} \,.\, v = \begin{bmatrix} 0 \\ \dots \\ Z_{obj} \end{bmatrix}_{m+1,1} \tag{4.10}$$

$$v_{min} \leq v \leq v_{max} \qquad for\ i = 1, 2, \dots, n \tag{4.11}$$

The optimization is performed by using the Academic Version of IBM ILOG CPLEX Optimizer in MATLAB (R2011b) with quadratic programming.

Resting condition flux distribution, *v*, found by two consecutive optimizations, is consistent with literature-reported findings. Values are listed in Table 4.1 comparatively. Thus, it is verified that the improved reaction set can be used in the modeling of brain metabolism.

Table 4.1. Predicted flux results in this study, Çakır et al. (2007), and experiments in resting (healthy) state

% Flux Ratio	**Çakır et al. (2007)**	**This Study**	**Experimental***	**Reference**
% Lactate release flux (r_{11}) with respect to CMR_{glc}	4.5	7.2	3–9	[94–97]
% Glutamate/Glutamine cycle flux (r_{95}) with respect to CMR_{glc}	68.0	73.1	40–80	[98–100]
$r_{TCA,A}/r_{TCA,total}$, $r_{25}/(r_{25} + r_{69})$ (percent relative oxidative metabolism of astrocytes)	35.0	33.9	30	[98,101,102]
% Total lipid synthesis with respect to CMR_{glc}	2.8	3.1	2	[103]
% Total PPP flux with respect to CMR_{glc}	5.6	5.5	3–6	[104,105]
% pyruvate carboxylase flux (r_{12}) with respect to CMR_{glc}	11.7	11.1	10	[98,101,106]

The advantages of the new developed brain model over Çakır model are:

- more detailed description of the brain metabolism.
- computational flux predictions for more reactions.
- integration of brain metabolic model with the transcriptome data.

4.2. Hypoxia

Hypoxia is the lack of oxygen level in the whole body or specific tissue of the body.

4.2.1. Cerebral Hypoxia

Cerebral hypoxia is the reduction in oxygen supply in the brain. Oxygen plays an important role in many metabolic reactions; therefore, decrease in the oxygen uptake rate of the brain brings about the change in metabolism. Experimental studies of the changes due to decline in oxygen level in the brain metabolism are time consuming and expensive, making simulation studies valuable tools. Resting state fluxes for the reactions investigated in hypoxia condition are given in Table 4.2.

4.2.1.1. MOMA Approach: Computational programs are an alternative to estimate change in the metabolism. MOMA is already used to simulate hypoxia in brain (Çakır et al, 2007) [6]. In the present study, hypoxia simulations by MOMA is repeated by the newly developed model to predict the changes in cerebral hypoxia, with the overall aim of comparing the consistency of results with the results reported in Çakır et al., 2007 [6]. In the computation, oxygen uptakes of both astrocytes and neurons are gradually decreased from resting condition level to cerebral anoxia level – the complete lack of oxygen in the brain. The results are given in Figure 4.2 and 4.3 for the original Çakır model and for the currently developed model, respectively.

Table 4.2. Resting state fluxes for the reactions investigated in hypoxia condition

Investigated Reaction	**Reaction No in Çakır Model**	**Reaction No in This Model**	**Resting State Flux (µmole/g/min)**
Glutamate transport from neurons to astrocytes	R75	R91	0.072
Glutamine transport from astrocytes to neurons	R78	R95	0.164
ATP production by astrocytes	R37	R45	1.768
ATP production by neurons	R73	R88	3.379
TCA Cycle activity in astrocytes	R22	R25	0.164
TCA Cycle activity in neurons	R58	R69	0.321
Lactate production by astrocytes	R11	R11	0.046
Lactate production by neurons	R48	R56	0
Malate Shuttle in neurons	R68	R81	0.300
GABA transport from neurons to astrocytes	R81	R98	0.058
Aspartate transport from neurons to astrocytes	R87	R104	0.093
Leucine transport from neurons to astrocytes	R106	R131	0.064
Glucose uptake by astrocytes	R1	R1	0.160
Glucose uptake by neurons	R38	R46	0.160
Glycogen uptake	R183	R436	0

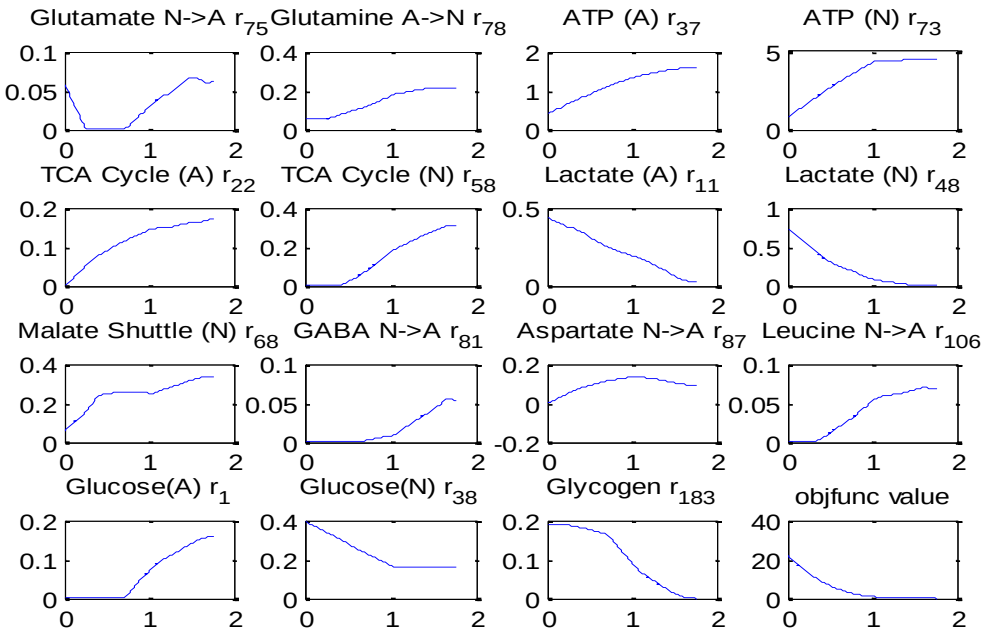

Figure 4.2. Cerebral hypoxia results by using MOMA approach for Çakır model [6] including 217 metabolic reactions in the brain metabolism. All x-axes represent oxygen uptake flux (µmole/g/min) and all y-axes show metabolic fluxes (µmole/g/min) of stated metabolites. The resting condition is the rightmost point on the plots stating 1.760 µmole/g/min oxygen uptake flux.

As seen from Figure 4.2 and 4.3, computational study of cerebral hypoxia demonstrates decreased activity of TCA cycle and ATP synthesis and increased lactate production in neurons and astrocytes as in Çakır et al. (2007). Oxygen limitation directly decreases the activity of oxidative phosphorylation resulting in less demand of NADH and FADH2 from TCA cycle reactions. Increase in the lactate fluxes depicts activation of anaerobic conditions in neurons and astrocytes. Activation of anaerobic condition brings about decline in ATP production as predicted computationally due to less energy requirement. Glucose uptake by neurons remains almost the same. However, in astrocytes, glucose uptake is decreased due to glycogen uptake. These results are also related with the fact that less energy is produced with the same amount of glucose in hypoxia due to activation of anaerobic condition. Transport of neurotransmitters between the neurons and astrocytes are also affected by hypoxia.

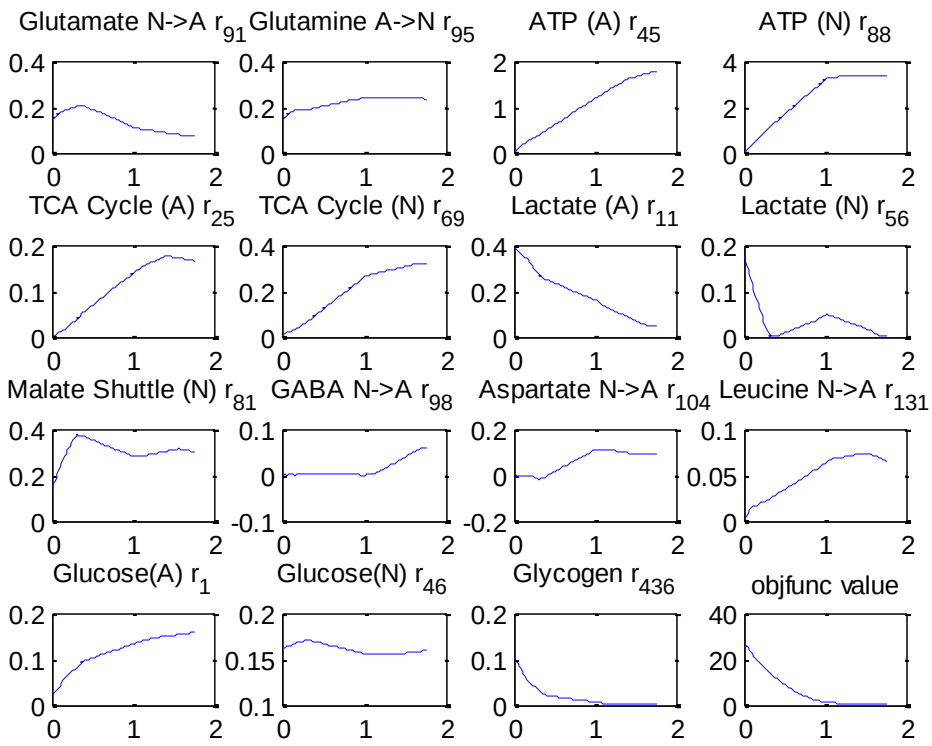

Figure 4.3. Cerebral hypoxia results by using MOMA approach for the present study covering 630 metabolic reactions in the brain metabolism demonstrating most of the predictions in the newly developed model have similar tendency as in Çakır model. All x-axes represent oxygen uptake flux (µmole/g/min) and all y-axes show metabolic fluxes (µmole/g/min) of stated metabolites. The resting condition is the rightmost point on the plots stating 1.760 µmole/g/min oxygen uptake flux.

According to simulations of the transfer reaction between astrocytes and neurons in Figure 4.2 and 4.3, neurotransmitters GABA and aspartate transport are decreased and does not takes place in cerebral anoxia condition. Branched chain amino acid leucine transfer from neurons to astrocytes also declines considerably. As expected, this result states that there is less interactions in hypoxic condition than those in healthy condition. Both model predictions give a slight reduction in glutamine transport from astrocytes to neurons. However, they predict the glutamate transfer from neurons to astrocytes differently. In contrast to Çakır model, transport of glutamate slightly increases due to addition of new glutamate producing reactions in arginine metabolism.

4.2.1.2. ROOM Approach: In addition to MOMA analysis, to test the power of the developed brain model and compare results with Çakır model, cerebral hypoxia computations are also performed by using ROOM approach for the newly developed brain model in this study. The results of computational predictions are given in Figure 4.4. According to ROOM computation in cerebral hypoxia, ATP synthesis and TCA cycle are declined in neurons and astrocytes consistent with MOMA results. In addition, GABA, aspartate, and leucine transport from neuron to astrocyte are also declined in cerebral hypoxia. In contrast to increase in glycogen uptake in MOMA, ROOM predicts no change (zero) in glycogen uptake due to oxygen limitation. Another important point necessary to state is that the prediction obtained from ROOM approach oscillates due to multiple optima as seen in Figure 4.4. However, tendency of the plotted points gives the general behavior of the computational results.

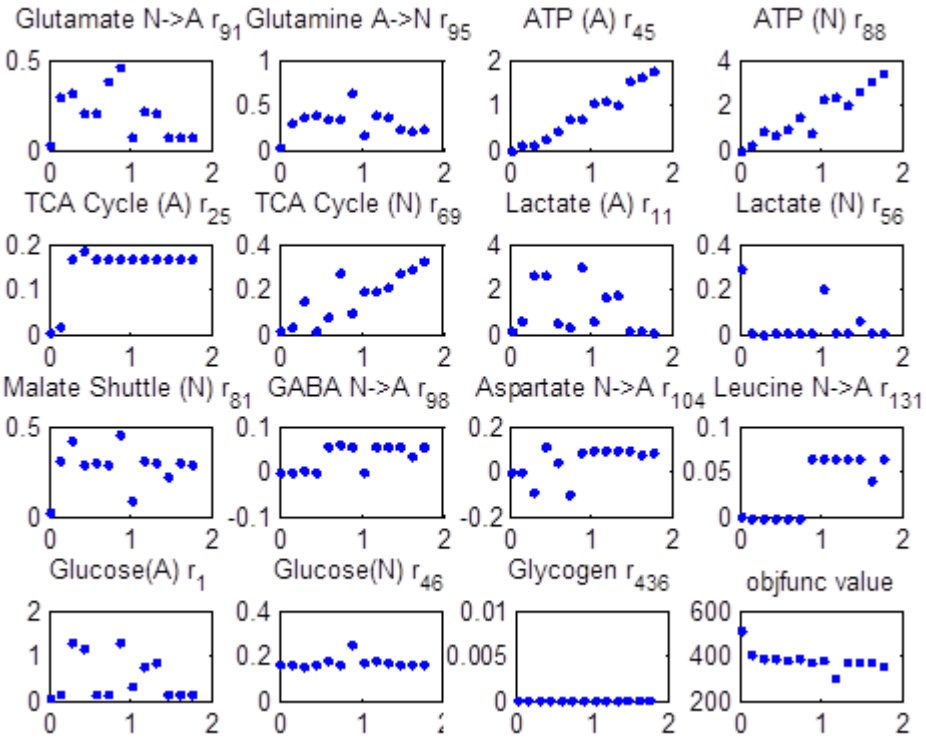

Figure 4.4. Cerebral hypoxia results by using ROOM approach for the present study covering 630 metabolic reactions in the brain metabolism. All x-axes represent oxygen uptake flux (µmole/g/min) and all y-axes show metabolic fluxes (µmole/g/min) of stated metabolites. The resting condition is the rightmost point on the plots stating 1.760 µmole/g/min oxygen uptake flux.

4.2.2. Astrocytic Hypoxia

Another type of hypoxia taking place in brain metabolism is astrocytic hypoxia which is the decline in oxygen level only in astrocytes. In this perturbed condition, although the decrease in the oxygen concentration occurs in astrocytes, it affects whole brain metabolism due to metabolic interactions of astrocytes and neurons. Computational prediction of metabolic changes due to astrocytic hypoxia is also performed for the new reaction set by gradual decreasing of oxygen level only in astrocytes.

4.2.2.1. MOMA Approach: MOMA is used in the computational flux analysis as in Çakır model (2007). The results of Çakır model and present study are seen in Figure 4.5 and 4.6, respectively.

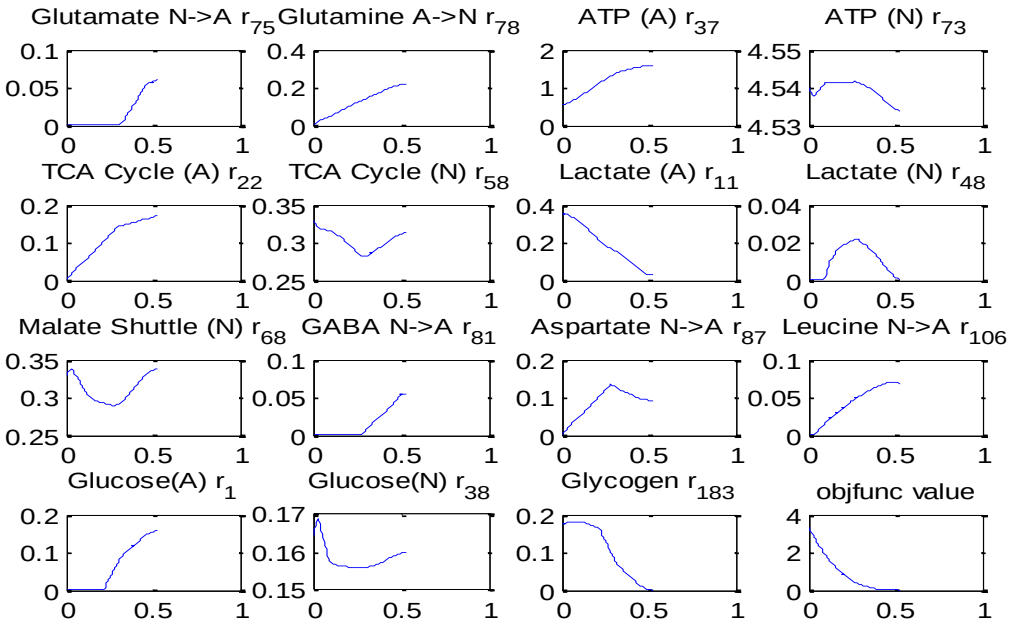

Figure 4.5. Astrocytic hypoxia results by using MOMA approach for Çakır model including 217 metabolic reactions in the brain metabolism. All x-axes represent oxygen uptake flux (µmole/g/min) by astrocytes and all y-axes show metabolic fluxes (µmole/g/min) of stated metabolites. The resting condition is the rightmost point on the plots stating 0.530 µmole/g/min oxygen uptake flux.

Despite the high number of interactions between reactions in neurons and astrocytes, astrocytic metabolism is perturbed more than neurons because of hypoxia in astrocytes.

Simulations of astrocytic hypoxia for the two discussed model show that TCA cycle and ATP synthesis are decreased only in astrocytes due to oxygen limitation. Lactate production, meaning activation of anaerobic condition, increases in astrocytes accordingly. During the astrocytic hypoxia, TCA cycle, ATP and lactate production in neurons almost remain the same as in healthy case. GABA, aspartate, and leucine transport from neurons to astrocytes decline and reach to zero in astrocytic hypoxia. Therefore similar to predictions for cerebral hypoxia, the trafficking between the astrocytes and neurons decreases.

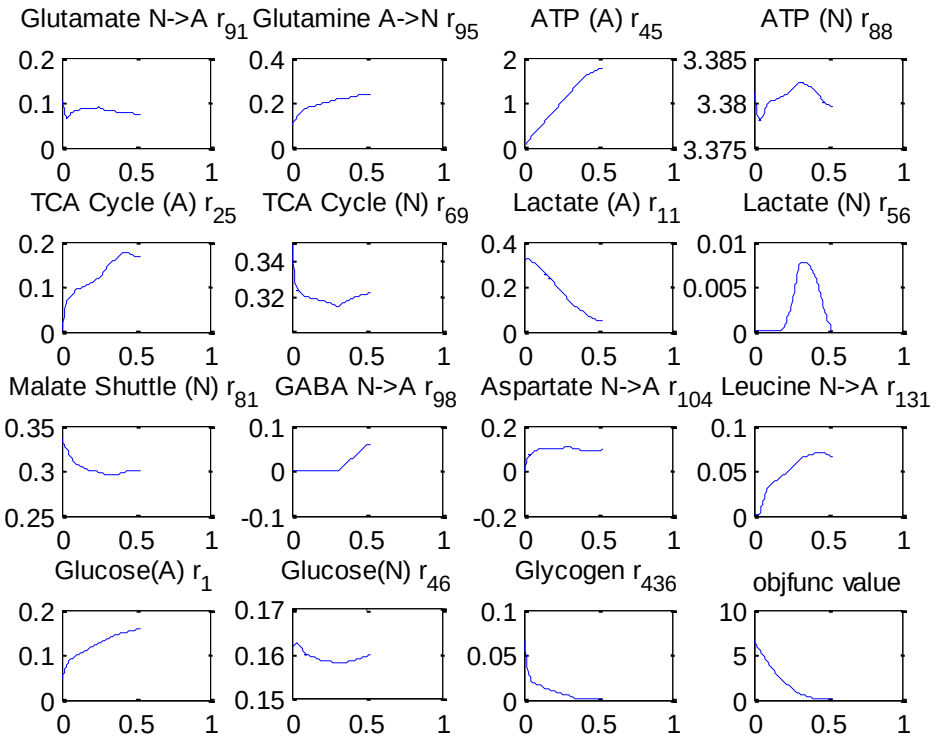

Figure 4.6. Astrocytic hypoxia results by using MOMA approach for the present study including 630 metabolic reactions in the brain metabolism indicating most of the predictions by using newly developed model are consistent with Çakır model. All x-axes represent oxygen uptake flux (µmole/g/min) by astrocytes and all y-axes show metabolic fluxes (µmole/g/min) of stated metabolites. The resting condition is the rightmost point on the plots stating 0.530 µmole/g/min oxygen uptake flux.

4.2.2.2. ROOM Approach: As done in predictions of fluxes in cerebral hypoxia, ROOM approach is used in astrocytic hypoxia calculations as a second technique. The results of

the ROOM computation for this type of hypoxia are given in Figure 4.7 and demonstrate that ATP synthesis decreases to zero only in astrocytes. GABA, aspartate, and leucine transfer from neurons to astrocytes declines due to lack of oxygen in astrocytes in accordance with MOMA results. Glucose uptake for astrocytes is increased by ROOM simulation in contrast to decreased glucose uptake predicted by MOMA.

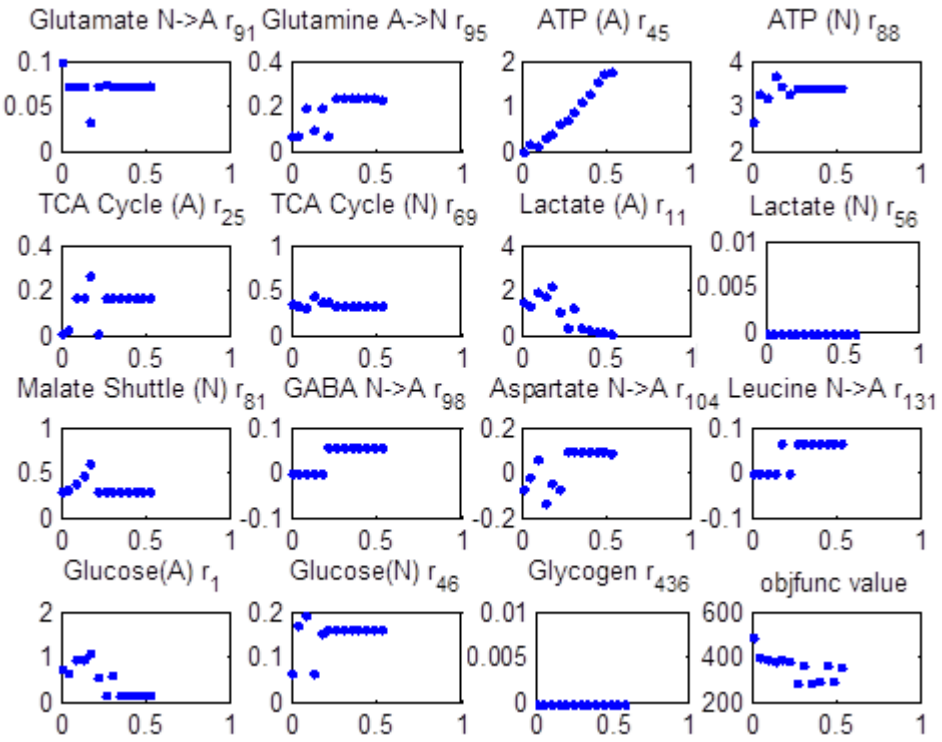

Figure 4.7. Astrocytic hypoxia results by using ROOM approach for the present study with 630 metabolic reactions in the brain metabolism. All x-axes represent oxygen uptake flux (µmole/g/min) by astrocytes and all y-axes show metabolic fluxes (µmole/g/min) of stated metabolites. The resting condition is the rightmost point on the plots stating 0.530 µmole/g/min oxygen uptake flux.

4.3. Parkinson Disease Modeling by Using Low Gene Expression Value

Parkinson's disease gene expression datasets from Gene Expression Omnibus (GSE20292 and GSE26927) are used in the prediction of metabolic fluxes in disease state. Two different Parkinson's disease datasets are investigated separately to demonstrate the consistency between different datasets. GSE20292 dataset includes transcriptional analysis

of substantia nigra with 29 samples in Parkinson's disease by using Affymetrix Human Genome U133A Array (GPL96). GSE26927 dataset covers the gene expression profiling of common neurological diseases, including Parkinson’s disease with 20 samples. For this dataset, Parkinson’s disease data, belonging to substantia nigra part of the brain, is used in flux balance analysis. The commercial microarray for this dataset is Illumina humanRef-8 v2.0 expression beadchip (GPL6255).

It is assumed that the genes which have low expression value in Parkinson case are not active in disease state. Within this scope, expression levels of 50 and 20 are selected as cut-off for GSE20292 and GSE26927 respectively to estimate inactive genes in the disease state. The idea behind the different cut-off values is that commercial microarrays of these datasets are different, and, so, their corresponding GPL codes are not the same. Therefore, the numerical values of intensities of gene expression have slightly different magnitudes on average. Here, it is aimed that the percentage of lowly expressed genes should be close to each other in the two datasets. When lowly expressed genes are extracted from the transcription datasets before matching with the model genes, these percentages are comparable, with 29.4% and 31.5% for GSE20292 and GSE26947, respectively.

If the expression value of any gene is less than the cut-off, the related gene is assumed to be inactive in the disease state. The genes having the expression values of less than the cut-off in most of the disease-case transcriptome data samples (more than 60%) are given in Tables 4.3 and 4.4 with corresponding reaction numbers for GSE20292 and GSE26947, respectively. One should note that a gene may control more than one reaction. That is why there are more than one reaction numbers associated with each of the lowly expressed genes.

Table 4.3. Lowly expressed genes in Parkinson's disease and corresponding reaction numbers for GSE20292.

Gene Symbols	**Reaction Number in the Model**
AASS	R154, R155
ACADSB	R134, R147
ACSL4	R288, R333
ANPEP	R428
AOC3	R470, R473
ARG1	R447, R458
ATP1B4	R506, R542
ATP6V1B1	R506, R542
CA3	R287, R332
CTH	R186, R194
DGKB	R397, R411
DGKE	R397, R411
EHHADH	R135, R148
ETNK1	R348, R354
INPP4B	R401, R415
LDHAL6B	R11, R56
PAH	R165
PCK1	R14, R58
PGK2	R7, R52
PSPH	R114
SLC27A2	R288, R333
TPH1	R174

Table 4.4. Low expressed genes in Parkinson's disease and corresponding reaction numbers for GSE26927.

Gene Symbols	**Reaction Number in the Model**
AANAT	R176
ASMT	R177
ATP12A	R506, R542
ATP1B4	R506, R542
ATP4B	R506, R542
ATP6V1C2	R506, R542
CA3	R287, R332
DBH	R170
DGKH	R397, R411
DGKK	R397, R411
GAPDHS	R6, R51
GPX6	R422, R432
IDI2	R207
LDHAL6A	R11, R56
LDHAL6B	R11, R56
MAT1A	R182, R190
NOS1	R455
NT5C1A	R505, R541
NT5C1B	R505, R541
PLCZ1	R393, R407
TKTL1	R22, R24, R66, R68
TKTL2	R22, R24, R66, R68
TPH1	R174
TPH2	R174

If the reaction is controlled by more than one gene and one of the genes has expression value of more than cut-off, this reaction is assumed to be active. In other words, all genes for a reaction should have expression value of less than cut-off to inactivate the related reaction in Parkinson's disease. The inactivated reactions satisfying stated criteria are listed in Tables 4.5 and 4.6 for GSE20292 and GSE26947, respectively. As seen, different reactions are found to be inactivated by using the two different datasets for the same brain region due to different commercial microchips. The only reaction, predicted to be inactivated in both datasets, is "R174" controlled by TPH1 and TPH2 enzyme.

When comparing the inactivated reactions in GSE20292 dataset for Parkinson's disease, the reactions are found to be in various pathways including lysine, isoleucine, methionine, phenylalanine-tyrosine, glycine-serine, and tryptophan metabolisms. However, the inactivated reactions are in phenylalanine-tyrosine and tryptophan metabolisms for GSE26927. Investigation of GSE26927 dataset by stated technique demonstrates inactivation of dopamine-beta-hydroxylase (DBH) being responsible for conversion of dopamine to norepinephrine consistent with Hurst et al (1985). This may results from degeneration of dopamine producing neurons. This outcome is expected due to decrease in the dopamine level in Parkinson's disease.

Computation is performed by adjusting upper and lower bounds of the reactions which are controlled by these genes to zero. This adjustment means the inactivation of the lowly expressed genes. MOMA approach which aims to calculate a deficient flux distribution as close as possible to the resting condition, and ROOM approach, minimizing the number of significant fluxes changing in the perturbed condition, are used to calculate Parkinson disease flux distribution. Results are computed as done in resting state and compared in Tables 4.7 and 4.8 for GSE20292 and GSE26947, respectively.

Table 4.5. Inactivated reactions due to low expression in Parkinson's disease for GSE20292.

Reaction Number in the Model	**Gene Symbols**	**Corresponding Reaction in the Model**
R154	AASS	Lysine_N + alpha-ketoglutarate_N + NADPH_N -> Saccharopine_N + NADP_N
R147	ACADSB	Methylbutyryl-CoA_A + FAD_AM -> FADH2_AM + E-2-methylcrotonoyl-CoA_A
R186	CTH	L-cystathionine_A -> NH3_A + 2-oxobutanoate_A + Cysteine_A
R194	CTH	L-cystathionine_N -> NH3_N + 2-oxobutanoate_N + Cysteine_N
R165	PAH	Phenylalanine_N + Tetrahydrobiopterin_N + O2_N -> Tyrosine_N + 4-alpha-hydroxy-tetrahydrobiopterin_N
R114*	PSPH	3_phospho_serine_A -> Serine_A
R174**	TPH1	Tryptophan_N + Tetrahydrobiopterin_N + O2_N -> 5-hydroxytryptophan_N + 4-alpha-hydroxy-tetrahydrobiopterin_N

* There is not probe ID for PSPHL in GSE20292 dataset so R114 is assumed to be inactivated since PSPH is found to be lowly expressed.

** There is not probe ID for TPH2 in GSE20292 dataset so R174 is assumed to be inactivated since TPH1 is found to be lowly expressed.

Table 4.6. Inactivated reactions due to low expression in Parkinson's disease for GSE26927.

Reaction Number in the Model	**Gene Symbols**	**Corresponding Reaction in the Model**
R176	AANAT	Seratonin_N + Acetyl-CoA_N -> N-acetyl-serotonin_N
R177	ASMT	N-acetyl-serotonin_N + S-adenosyl-L-methionine_N -> S-adenosyl-L-homocysteine_N + Melatonin_N
R170	DBH	Dopamine_N + O2_N -> Norepinephrine_N
R173	DBH	Dopamine_A + O2_A -> Norepinephrine_A
R174	TPH1	Tryptophan_N + Tetrahydrobiopterin_N + O2_N -> 5-hydroxytryptophan_N + 4-alpha-hydroxy-tetrahydrobiopterin_N
R174	TPH2	Tryptophan_N + Tetrahydrobiopterin_N + O2_N -> 5-hydroxytryptophan_N + 4-alpha-hydroxy-tetrahydrobiopterin_N

Table 4.7. Results of estimated fluxes for resting condition and Parkinson's disease by inactivating related reactions of lowly expressed genes for GSE20292.

% Flux Ratio	**Resting Condition**	**Parkinson Disease (MOMA)**	**Parkinson Disease (ROOM)**
% Lactate release flux (r_{11}) with respect to CMR_{glc}	7.2	0	10.1
% Glutamate/Glutamine cycle flux (r_{95}) with respect to CMR_{glc}	73.1	68.2	72.8
$r_{TCA,A}/r_{TCA,total}$, $r_{25}/(r_{25} + r_{69})$ (percent relative oxidative metabolism of astrocytes)	33.9	37.4	34.4
% Total lipid synthesis with respect to CMR_{glc}	3.1	2.1	3.3
% Total PPP flux with respect to CMR_{glc}	5.5	2.5	7.8
% pyruvate carboxylase flux (r_{12}) with respect to CMR_{glc}	11.1	10.7	11.4

Using GSE20292 results, computational approaches give different results. MOMA and ROOM predict the inactivated and increased lactate release in Parkinson's disease, respectively. Both methods state a slight decline in Glutamate-Glutamine flux. Total lipid

synthesis and pentose phosphate pathway flux are declined by MOMA and increased by ROOM approach. Pyruvate carboxylase flux remains almost same in both approaches. Predictions of pentose phosphate pathway (PPP) fluxes are highly different by using these two approaches in Parkinson disease. MOMA calculates a lower PPP flux than that in resting condition; however, ROOM computes a higher PPP flux than that in resting state.

Using GSE26927 results, computational approaches give almost similar results. MOMA and ROOM predict the same lactate release and Glutamate-Glutamine flux in Parkinson's disease as in healthy condition. MOMA computes the same total lipid synthesis and pyruvate carboxylase flux and ROOM calculates a slight increase in these parameters. MOMA calculates the same PPP flux as in resting condition; however, ROOM computes a higher PPP flux than that in resting state.

Table 4.8. Results of estimated fluxes for resting condition and Parkinson's disease by inactivating related reactions of lowly expressed genes for GSE26927.

% Flux Ratio	**Resting Condition**	**Parkinson Disease (MOMA)**	**Parkinson Disease (ROOM)**
% Lactate release flux (r_{11}) with respect to CMR_{glc}	7.2	7.2	7.2
% Glutamate/Glutamine cycle flux (r_{95}) with respect to CMR_{glc}	73.1	73.1	73.1
$r_{TCA,A}/r_{TCA,total}$, $r_{25}/(r_{25} + r_{69})$ (percent relative oxidative metabolism of astrocytes)	33.9	33.9	33.5
% Total lipid synthesis with respect to CMR_{glc}	3.1	3.1	3.4
% Total PPP flux with respect to CMR_{glc}	5.5	5.5	8.9
% pyruvate carboxylase flux (r_{12}) with respect to CMR_{glc}	11.1	11.1	11.2

5. INTEGRATIVE MODELING OF TRANSCRIPTOMA DATA AND BRAIN METABOLISM FOR NEURODEGENERATIVE DISEASES

In this chapter, the developed brain model in the present study is integrated with the transcriptome data for neurological diseases. This integration is possible since the model includes the information on genes controlling the reactions.

In the integrative modeling, 4 different GSE datasets are used for a comprehensive examination of Parkinson's disease (PD) as detailed in Table 5.1. In order to compare the effect of Parkinson's disease on brain metabolism to the changes induced by other neurological diseases, transcriptiome data for 5 other common neurological diseases are also analysed. The ideas behind the use of different datasets are:

(i) comparing effects of PD in different brain regions.
(ii) comparing PD results obtained from different commercial microarrays.
(iii) comparing effect of PD with the effect of different neurological diseases on brain metabolism.

The results obtained from the investigation of GSE20168, GSE20291, and GSE20292 lead to the comparison of Parkinson's disease in various regions due to the same experimental design excluding region of interest. The effect of the different commercial microarrays used in the experiments on the same disease, namely Parkinson's disease, is elucidated by comparing the results of GSE20292 and Parkinson's disease samples of GSE26927. The comparison of effects of Parkinson's disease with other common neurological diseases on the brain metabolism is performed by using GSE26927 since this dataset includes the gene expression data for different diseases including Alzheimer's disease, amyotrophic lateral sclerosis, Huntington's disease, multiple sclerosis, Parkinson's disease and schizophrenia.

Table 5.1. Detailed information of GSE datasets used in integrative modeling.

GSE Code	GPL Code	Disease	Brain Region	Commercial Microarray
20168	96	PD	Prefrontal cortex area 9	Affymetrix Human Genome U133A Array
20291	96	PD	Putamen	Affymetrix Human Genome U133A Array
20292	96	PD	Substantia nigra	Affymetrix Human Genome U133A Array
26927	6255	AD	Entorhinal cortex	Illumina humanRef-8 v2.0 expression beadchip
		ALS	Cervical spinal cord	
		HD	Ventral head of the caudate nucleus	
		MS	Subpial grey matter lesions from the frontal gyri	
		PD	Substantia nigra	
		SCH	Grey matter in Brodmann area	

When matching the genes in the developed brain model with the investigated GSE datasets, the numbers of the matched genes are different for different commercial microarrays, as tabulated in Table 5.2. Different GPL codes imply different commercial microarrays. As seen, although the total number of the probe IDs in GPL96 is higher than that in GPL6255, the number of the unique genes in GPL96 is less than that in GPL6255 on account of the fact that there are more than one probe IDs representing the same gene name in microarrays. Developed brain model have 670 genes with 630 reactions. Some of the reactions are controlled by one or more genes and some of the reactions do not have gene information. Therefore, the number of reactions and genes are not necessarily the same. The numbers of the matched genes are 468 (70%) and 496 (74%) for GPL96 and GPL6255, respectively. Since the total numbers of the matched genes are different for these two microarrays, the matched genes cover 447 and 448 of 571 internal reactions for GPL6255 and GPL96, respectively.

Table 5.2. Comparison of the total number of the genes and the number of genes that matched to the developed brain metabolic model for GPL6255 and GPL96.

Commercial Microarray Name	GPL Code	Probe IDs (or Genes)	Unique Genes	Matched Genes	Percentage of Matched Genes
Affymetrix Human Genome U133A Array	96	22283	13212	468	70%
Illumina humanRef-8 v2.0 expression beadchip	6255	20589	18190	496	74%

5.1. Reporter Metabolite Analysis

Reporter metabolites are the metabolites having the most significant transcriptional changes around. Reporter metabolite analysis (RMA) is applied as detailed in Appendix C. For RMA analysis p-value of 0.05 is selected as cut-off. This means that if p-value of any metabolite is less than 0.05, the related metabolite is determined as reporter metabolite and there are significant transcriptional changes around it due to perturbation (disease). Another important criterion applied in the determination of reporter metabolites is the number of genes (neighbors) used in the computation for each metabolite. In RMA, only metabolites whose p-value calculation includes more than 1 gene (neighbor) are considered. In other words, if a metabolite has a significant p-value, but only has a single gene neighbor, the related metabolite is not considered as a reporter metabolite because of the fact that the primary idea behind this analysis is to take many genes in the cellular network into account.

5.1.1. Parkinson's Disease

GSE20168, GSE20291, GSE20292 and GSE26927 are investigated for the effect of the Parkinson’s disease on brain metabolism. The results of the reporter metabolite analysis for these datasets are comparatively given in Tables 5.3 and 5.4. Platforms GSE20168, GSE20291, GSE20292 all represent three different regions in the brain, for the same type of commercial microarray (Affymetrix). GSE20292 and GSE26927, on the other hand, represent data for the same brain region (substantia nigra), but for different

commercial microarrays. Therefore, by using these 4 datasets it is possible to elucidate (i) effect of Parkinson's disease on different brain regions and (ii) compare the Parkinson's disease results obtained from different commercial microarrays for substantia nigra region. In Table 5.3, "+" sign states a significant change for the corresponding metabolite, i.e. p-value less than 0.05. That is, these are reporter metabolites. "-" sign represents a non-significant change, with p-value higher than 0.05.

Table 5.3. Reporter metabolite analysis results in different brain regions due to Parkinson's disease.

Metabolite	**20168**	**20291**	**20292**	**26927**
ATP_A	-	+	+	+
ADP_A	-	-	+	+
NAD_AM	+	-	-	-
NADH_AM	+	-	-	-
NAD_NM	+	+	-	+
NADH_NM	+	+	-	+
ATP_N	+	+	+	+
Histamine_N	+	-	-	-
KIV_A	+	-	-	+
KMV_A	+	-	-	+
methionine_A	+	+	-	-
L-homocysteine_A	+	-	-	-
adenosine_A	-	+	+	-
methionine_N	+	+	-	-
L-homocysteine_N	+	-	-	-
adenosine_N	-	+	+	-
lanosterol_A	+	-	-	-
desmosterol_A	-	-	+	-
Cholesterol_A	-	-	+	-
Palmitate_A	-	-	+	-
AMP_A	+	+	+	-

Table 5.3. Reporter metabolite analysis results in different brain regions due to Parkinson's disease (cont.).

Metabolite	20168	20291	20292	26927
Palmitate_N	-	-	+	-
ADP_N	-	+	+	+
Phosphatidate_A	+	-	+	-
Phosphatidate_N	+	-	+	-
phosphatidyl-1D-myo-inositol-4-phosphate_A	-	-	+	-
phosphatidyl-1D-myo-inositol-4-5-bisphosphate_A	-	-	+	+
myo-inositol-(1-4-5)-trisphosphate_A	+	+	-	+
myo-inositol-(1-3-4-5)-tetrakisphosphate_A	+	+	-	+
phosphatidyl-1D-myo-inositol-4-phosphate_N	-	-	+	-
phosphatidyl-1D-myo-inositol-4-5-bisphosphate_N	-	-	+	+
myo-inositol-(1-4-5)-trisphosphate_N	+	+	-	+
Ubiquinone_A	+	+	-	+
Ubiquinol_A	+	+	-	+
Hc_A	+	+	+	+
myo-inositol-(1-3-4-5)-tetrakisphosphate_N	+	+	-	+
CytCox_A	+	+	-	+
CytCred_A	+	+	-	+
2-phosphoglycerate_N	+	-	-	-
2-phosphoglycerate_A	+	-	-	-
Ubiquinone_N	+	+	-	+
Ubiquinol_N	+	+	-	+
Hc_N	+	+	+	+
CytCox_N	+	+	-	+
CytCred_N	+	+	-	+
Pyruvate_A	-	-	-	+
Pyruvate_N	-	-	-	+
Serine_A	-	-	-	+
Serine_N	-	-	-	+

Table 5.3. Reporter metabolite analysis results in different brain regions due to Parkinson's disease (cont.).

Metabolite	20168	20291	20292	26927
GTP_A	-	-	-	+
Palmitoyl-CoA_A	-	-	-	+
Palmitoyl-CoA_N	-	-	-	+
Malate_A	-	-	-	+
myo-inositol-(1-4)-bisphosphate_A	-	-	-	+
myo-inositol-(4)-monophosphate_A	-	-	-	+
myo-inositol-(1-3-4)-trisphosphate_A	-	-	-	+
myo-inositol-(1-4)-bisphosphate_N	-	-	-	+
myo-inositol-(4)-monophosphate_N	-	-	-	+
myo-inositol-(1-3-4)-trisphosphate_N	-	-	-	+
GTP_N	-	-	-	+
Malate_N	-	-	-	+

+: Reporter Metabolites

Table 5.4. Number of reporter metabolites in different Parkinson's disease datasets.

Data Set	Number of Reporter Metabolites
GSE20168	32
GSE20291	24
GSE20292	19
GSE 26927	40

When comparing the results in Table 5.3 and 5.4 for GSE20168, GSE20291, and GSE20292, it is clearly seen that various metabolites are found to be reporter metabolites in different parts of the brain due to Parkinson's disease. L-homocysteine, 2-phosphoglycerate, and histamine are found to be reporter metabolites only in prefrontal cortex area 9. Methionine has significant transcriptional changes around in prefrontal cortex area 9 and putamen. Desmosterol, cholesterol, palmitate phosphatidyl-1D-myo-inositol-4-phosphate, and phosphatidyl-1D-myo-inositol-4-5-bisphosphate are defined as

reporter metabolite in substantia nigra region. Phosphatidate is a reporter metabolite in Parkinson disease in prefrontal cortex area 9 as well as in substantia nigra. The detailed distribution of the common reporter metabolites is illustrated with venn diagram in Figure 5.1. As indicated, all reporter metabolites found for putamen region are shared with prefrontal cortex area 9 and substantia nigra regions. There are 4 common reporter metabolites (ATP_N, AMP_A, Hc_A, and Hc_N) detected in all investigated regions of the brain.

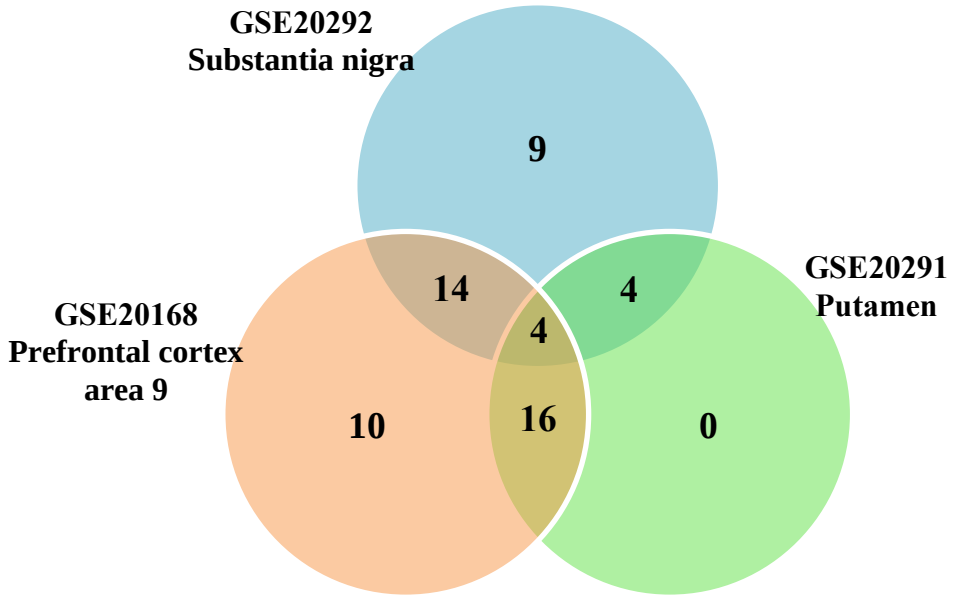

Figure 5.1. Distributions of the common reporter metabolites for GSE20292, GSE20168, and GSE20291.

The investigation of the reporter metabolite analysis results of GSE20292 and GSE26927, both of which belong to Parkinson's disease and substantia nigra region, demonstrates that different commercial microarray platforms do not predict exactly same results. The metabolites that are found to be reporter metabolites in both datasets are ATP, ADP, phosphatidyl-1D-myo-inositol-4-5-bisphosphate, phosphatidyl-1D-myo-inositol-4-5-bisphosphate, and Hc (hydrogen). As tabulated in Table 5.3, the number of reporter metabolites found by the analysis of GSE20292 and GSE26927 are 19 and 40. The distribution of these reporter metabolites is given in a venn diagram in Figure 5.2. As seen, the number of common reporter metabolites determined in both GSE20292 and GSE26927 is only 8.

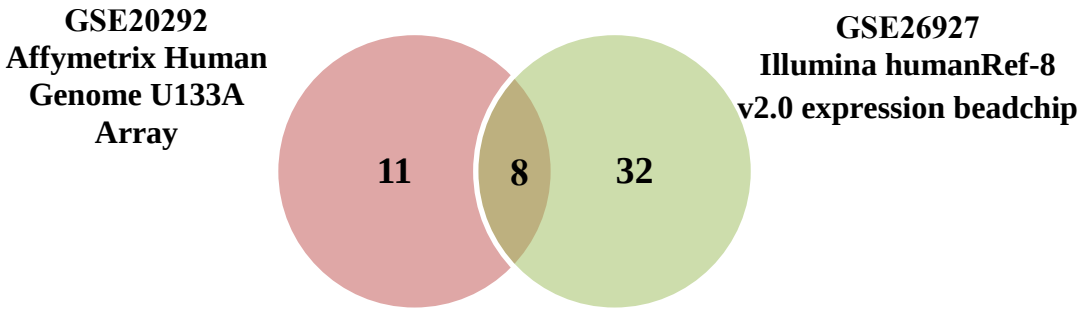

Figure 5.2. Distributions of the common reporter metabolites for GSE20292 and GSE26927.

5.1.2. Other Neurological Diseases

GSE26927 is investigated to see whether the effect of Parkinson's disease (PD) on brain metabolism is similar to the effect induced by the other neurological diseases including Alzheimer's disease (AD), amyotrophic lateral sclerosis (ALS), Huntington's disease (HD), multiple sclerosis (MS), and schizophrenia (SCH) on brain metabolism. The brain regions available at these datasets and listed in Table 5.1 are the most affected parts due to corresponding diseases. The results of the reporter metabolite analysis for this dataset are given in Table 5.5 in comparison with each other. In Table 5.5 "+" sign states significant changes (p-values less than 0.05). "-" sign represents p-values higher than 0.05. The comparison of the number of common reporter metabolites for these 6 diseases is tabulated in Figure 5.3. The diagonal cells in this figure represent total number of reporter metabolites for corresponding neurological diseases.

5.1.2.1. Reporter metabolites specific to a disease: The outcomes of the Table 5.5 and Figure 5.3 demonstrate that the number of reporter metabolites is the highest in Parkinson disease compared to other neurological diseases. KIV, KMV, palmitoyl-CoA, and malate are found to be reporter metabolite only in Parkinson's disease. Succinate and dimethylallyl_diphosphate have significant transcriptional changes around only in Alzheimer's disease. S-3-hydroxy-isobutyrate and propionyl-CoA satisfy the reporter metabolites criteria only in amyotrophic lateral sclerosis. The reporter metabolite specific to Huntington's disease is 3-phosphohydroxypyruvate. The transcriptional changes only in multiple sclerosis occur around lanosterol, 5alpha-cholesta-7-24-dien-3beta-ol, desmosterol, cholesterol, 24-25-dihydrolanosterol, and acetamidobutanal significantly.

Fumarate and phosphoenol-pyruvate are reporter metabolites solely in schizophrenia. When looking at ATP deeply, ATP in neurons is found to be a reporter metabolite in all investigated neurological diseases. However, ATP in astrocytes is determined as a reporter metabolite in 4 diseases including Parkinson's disease, Alzheimer's disease, Huntington's disease, and multiple sclerosis (MS). The reason underlying this outcome stems from the fact that the reactions having ATP are not the same in astrocytes and neurons. There are ATP related reactions specific to only neurons or astrocytes. The other metabolites obeying this description are ADP, AMP, bicarbonate, NAD, NADH, NADP, NADPH, pyruvate, and serine. Hc is found to be reporter metabolite in all investigated neurological diseases.

Table 5.5. Reporter metabolite analysis results in different neurological diseases for GSE26927.

Metabolite	**PD**	**AD**	**ALS**	**HD**	**MS**	**SCH**
ATP_A	+	+	-	+	+	-
ADP_A	+	+	-	+	+	-
Phosphoenol-pyruvate_A	-	-	-	-	-	+
Pyruvate_A	+	-	-	-	-	-
NAD_AM	-	-	-	+	-	-
NADH_AM	-	-	-	+	-	-
Succinate_A	-	+	-	-	-	-
NAD_NM	+	-	-	-	-	-
NADH_NM	+	-	-	-	-	-
Succinate_N	-	+	-	-	-	-
ATP_N	+	+	+	+	+	+
AMP_N	-	-	-	-	-	+
Pyruvate_N	+	-	-	+	-	+
3-phosphohydroxypyruvate_A	-	-	-	+	-	-
Serine_A	+	-	+	-	-	-
Serine_N	+	-	-	-	-	-
Bicarbonate_A	-	-	+	-	-	-
KIV_A	+	-	-	-	-	-
S-3-hydroxy-isobutyrate_A	-	-	+	-	-	-
Propionyl-CoA_A	-	-	+	-	-	-

Table 5.5. Reporter metabolite analysis results in different neurological diseases for GSE26927 (cont.).

Metabolite	PD	AD	ALS	HD	MS	SCH
GTP_A	+	-	-	-	-	+
KMV_A	+	-	-	-	-	-
NADP_A	-	-	-	-	+	-
NADPH_A	-	-	-	-	+	-
dimethylallyl_diphosphate_A	-	+	-	-	-	-
lanosterol_A	-	-	-	-	+	-
5alpha-cholesta-7-24-dien-3beta-ol_A	-	-	-	-	+	-
desmosterol_A	-	-	-	-	+	-
Cholesterol_A	-	-	-	-	+	-
lathosterol_A	-	-	-	-	+	-
24-25-dihydrolanosterol_A	-	-	-	-	+	-
Palmitoyl-CoA_A	+	-	-	-	-	-
AMP_A	-	-	-	+	-	+
ADP_N	+	+	+	+	+	+
Bicarbonate_N	-	+	+	-	-	-
Palmitoyl-CoA_N	+	-	-	-	-	-
Malate_A	+	-	-	-	-	-
FattyAcid_A	-	+	-	-	-	+
1-acyl-sn-glycerol-3-phosphate_A	-	+	-	-	-	+
FattyAcid_N	-	+	-	-	-	+
1-acyl-sn-glycerol-3-phosphate_N	-	+	-	-	-	+
phosphatidyl-1D-myo-inositol-4-5-bisphosphate_A	+	+	-	-	-	-
myo-inositol-(1-4-5)-trisphosphate_A	+	-	-	+	+	-
myo-inositol-(1-4)-bisphosphate_A	+	-	-	-	-	-
myo-inositol-(4)-monophosphate_A	+	-	-	-	-	-
myo-inositol-(1-3-4-5)-tetrakisphosphate_A	+	-	-	+	+	-
myo-inositol-(1-3-4)-trisphosphate_A	+	-	-	-	-	-
phosphatidyl-1D-myo-inositol-4-5-bisphosphate_N	+	+	-	-	-	-

Table 5.5. Reporter metabolite analysis results in different neurological diseases for GSE26927 (cont.).

Metabolite	PD	AD	ALS	HD	MS	SCH
myo-inositol-(1-4-5)-trisphosphate_N	+	-	-	+	+	-
myo-inositol-(1-4)-bisphosphate_N	+	-	-	-	-	-
myo-inositol-(4)-monophosphate_N	+	-	-	-	-	-
Ubiquinone_A	+	+	+	-	-	-
Ubiquinol_A	+	+	+	-	-	-
Hc_A	+	+	+	+	+	+
myo-inositol-(1-3-4-5)-tetrakisphosphate_N	+	-	-	+	+	-
myo-inositol-(1-3-4)-trisphosphate_N	+	-	-	-	-	-
CytCox_A	+	+	+	+	+	-
CytCred_A	+	+	+	+	+	-
ReducedGlutathione_A	-	-	-	-	-	+
OxidizedGlutathione_A	-	-	-	-	-	+
ReducedGlutathione_N	-	-	-	-	-	+
OxidizedGlutathione_N	-	-	-	-	-	+
NADP_NM	-	-	-	-	-	+
NADPH_NM	-	-	-	-	-	+
Fumarate_N	-	-	-	-	-	+
Acetamidobutanal_A	-	-	-	-	+	-
5-amino-levulinate_A	-	+	-	-	-	-
5-amino-levulinate_N	-	+	-	-	-	-
2-phosphoglycerate_N	-	+	-	-	-	+
Phosphoenol-pyruvate_N	-	-	-	-	-	+
GTP_N	+	-	-	-	-	+
Malate_N	+	-	-	-	-	-
2-phosphoglycerate_A	-	+	-	-	-	+
Ubiquinone_N	+	+	+	-	-	-
Ubiquinol_N	+	+	+	-	-	-
Hc_N	+	+	+	+	+	+
CytCox_N	+	+	+	+	+	-
CytCred_N	+	+	+	+	+	-

+: Repoerter Metablite

PD	40					
AD	16	28				
ALS	13	13	17			
HD	15	10	8	19		
MS	14	10	8	14	23	
SCH	7	10	4	6	4	24
	PD	**AD**	**ALS**	**HD**	**MS**	**SCH**

Figure 5.3. Distributions of the common reporter metabolites for neurological diseases available at GSE26927 dataset.

5.1.2.2. Reporter metabolites common among diseases: Comparison of the common reporter metabolites in different neurological diseases (Figure 5.3) elucidates the effect of the transcriptional changes on brain metabolism due to different kinds of perturbations. As seen, Parkinson's disease has the highest number of reporter metabolites (40) with respect to the other neurological diseases. The lowest number of the reporter metabolites is 17 and found in amyotrophic lateral sclerosis. The highest number of common reporter metabolites is 16 between Parkinson's disease and Alzheimer's disease. Parkinson's disease has the lowest number of shared reporter metabolites with schizophrenia (7). The results indicate that transcriptional changes taking place in Parkinson's disease are quite different from other diseases. Especially, many metabolites in inositol metabolism are found to be reporter metabolites in Parkinson's disease. When comparing reporter metabolites of Parkinson's disease, Alzheimer's disease, and amyotrophic lateral sclerosis, most of them are found in oxidative phosphorylation metabolism. Among the 15 common reporter metabolites between Parkinson's and Huntington's disease, many of them are in oxidative phosphorylation metabolism and inositol metabolism. The similar relationship exists between Parkinson's disease and multiple sclerosis. Pyruvate, GTP and hydrogen

(Hc) are among the common reporter metabolites between Parkinson disease and schizophrenia.

Although our focus is to compare Parkinson's disease with the other neurological diseases, a brief comparison of other neurological diseases among each other can also be made based on Figure 5.3. The lowest number of common reporter metabolites is 4 and exists between multiple sclerosis and schizophrenia. When looking at the last row standing for the common reporter metabolites between schizophrenia and other neurological diseases, it is obviously seen that schizophrenia has the lowest number of common reporter metabolites with other diseases. Despite considerably high number of reporter metabolites in schizophrenia, this means the transcriptional changes taking place in this disease are quite different from other diseases. Comparison of reporter metabolites in Huntington's disease and multiple sclerosis reveals a considerable number of reporter metabolites in inositol metabolism.

5.2. Reporter Pathway Analysis

To elucidate the pathways significantly changed in perturbed (disease) state, a new approach named as reporter pathway analysis (RPA) is performed, which is derived from the principles of RMA. P-values of each metabolite calculated from reporter metabolite analysis (RMA) are used for RPA in Parkinson's disease and other common neurological diseases as prescribed in Appendix D.

In RMA, p-values of metabolites are computed from the p-values of genes. Similarly, in RPA, p-values of pathways are calculated from the p-values of metabolites in pathways. The pathways having p-value of less than 0.05 are defined as reporter pathways and they involve significant change due to disease condition.

5.2.1. Parkinson's Disease

The investigation of the reporter pathways in Parkinson's disease is performed by using GSE20168, GSE20291, GSE20292 and GSE26927 as in the reporter metabolite analysis. The result of this examination is tabulated in Table 5.6 with the "+" sign representing reporter metabolites.

Comparison of GSE20168, GSE20291, and GSE20292 results reveals the effect of Parkinson's disease on the different parts of the brain. According to the results, isoleucine, oxidative phosphorylation and ATPase metabolisms are significantly changed due to Parkinson's disease in the investigated three different regions including substantia nigra, putamen, and prefrontal cortex area 9. Experimental study of Parkinson's disease shows that oxidative phosphorylation does not function properly due to reduced activity of NADH-ubiquinone reductase (Complex I) and NADH cytochrome c reductase [107]. Aspartate metabolism, cholesterol synthesis, TCA cycle, alanine metabolism and phosphatidylcholine metabolism are reporter pathways only in putamen region. The alteration in TCA cycle found by RPA is in agreement with the studies showing decrease in the α-ketoglutarate dehydrogenase complex enzyme due to Parkinson's disease [108,109]. Histamine metabolism, leucine metabolism and GABA cycle are significantly changed pathways only in prefrontal cortex area 9 due to Parkinson's disease. The reporter pathways only in substantia nigra are fatty acid synthesis and CDP-diacylglycerol biosynthesis. Consequently, the reporter pathways in different regions of the brain are quite different despite some similarities.

The experiments of GSE20292 and GSE26927 are based on different microarrays: Affymetrix Human Genome U133A Array and Illumina humanRef-8 v2.0 expression beadchip respectively. Therefore, comparison of these two microarrays shows the consistency between the different commercial microarrays in Parkinson's disease and substantia nigra part of the brain. As given in Table 5.6, the total numbers of significantly changed pathways are 6 and 16 for GSE20292 and GSE26927, respectively. Among the all pathways, 4 of them are found to be reporter pathways in both datasets. These pathways include glycolysis, oxidative phosphorylation and ATPase, isoleucine metabolism, and methionine metabolism. In accord with this finding, plasma analysis of L-Dopa treated Parkinson's patients demostrates significantly decreased level of methionine and increased level of homocysteine in methionine metabolism [110].

Table 5.6. Reporter pathway analysis results in different brain regions due to Parkinson's disease.

Pathway	20168	20291	20292	26927
Glycolysis	+	-	+	+
TCA_Cycle	-	+	-	+
Oxidative_Phosphorylation_and_ATPase	+	+	+	+
Glutamate_-_Glutamine_Cycle	-	-	-	+
GABA_Cycle	+	-	-	+
Aspartate_Metabolism	-	+	-	-
Histamine_Metabolism	+	-	-	-
Alanine_Metabolism	-	+	-	+
Glycine-Serine_Metabolism	-	-	-	+
Leucine_Metabolism	+	-	-	+
Ketone_Body_Metabolism	+	+	-	+
Valine_Metabolism	+	+	-	+
Isoleucine_Metabolism	+	+	+	+
Methionine_Metabolism	+	-	+	+
Cholesterol_Synthesis	-	+	-	-
Fatty_Acid_Synthesis	-	-	+	-
Phosphatidylcholine_Metabolism	-	+	-	-
Sphingomyelin_Metabolism	-	-	-	+
CDP-Diacylglycerol_Biosynthesis	-	-	+	-
Inositol_Metabolism	+	+	-	+
Purine_Nucleoside_Metabolism	+	+	-	+
Pirimidine_Nucleoside_Metabolism	-	-	-	+

+: Reporter Pathway

5.2.2. Other Neurological Diseases

GSE26927 includes the gene expression data for Parkinson's disease and 5 other neurological diseases. The examination of this dataset leads to analysis of reporter

pathways in different neurological diseases and allows comparison of the results with the Parkinson's disease, the disease of main focus in the present study. The outcomes of this analysis are given in Table 5.7 with the "+" sign representing reporter pathways. According to these results, purine nucleoside metabolism, oxidative phosphorylation and ATPase pathways are found to be reporter pathways in all neurological diseases. There is significant change in sphingomyelin and methionine metabolism only in Parkinson disease. In PD, sphingolipid structures are altered due to interactions with alpha-synuclein protein [111]. In Alzheimer's disease, fatty acid synthesis, phosphotidylcholine metabolism, CDP-diacylglycerol biosynthesis, and inositol metabolism are determined as significantly altered metabolisms by RPA. Identification of inositol metabolism as reporter pathway in AD is in accordance with literature finding stating altered level of inositol-related compunds [112,113]. In amyotrophic lateral sclerosis (ALS), inositol is the only reporter pathway among the lipid metabolism. This result is in accordance with experimental study showing altered composition of inositol due to this disease [114]. Cholesterol synthesis is influenced only in multiple sclerosis. This finding is in agreement with study performed by Teunissen et al. (2003) [115], demonstrating decline in cholesterol, lathosterol, desmosterol and lanosterol in multiple sclerosis. Despite some similarities, the effects of the different neurological diseases are different in pathway level in the brain.

5.2.2.1. Reporter pathway common among diseases: Comparison of the common reporter pathways are given in Figure 5.4 for different neurological diseases available at GSE26927. The results help to elucidate the effect of the transcriptional changes on brain metabolism due to different neurological diseases. As seen, Parkinson's disease has the second highest number of 16 reporter pathways after Huntington's diseases. The lowest number of the reporter pathways is 11 and found in schizophrenia. The highest number of common reporter pathways is 12 which is found between Parkinson's disease and Huntington's disease. Parkinson's disease has the lowest number of common reporter pathways with Alzheimer's disease. RPA identified alterations in alanine, valine, leucine, and isoleucine metabolisms due to Parkinson's disease. CSF studies support this finding since these amino acids, among others, were reported to be changed [116]. In case of Huntington's disease, results of our reporter pathway and reporter metabolite analyses are in accord with the literature findings indicating increased level of alanine, isoleucine, and glutamate [117,118]. Alteration in valine metabolism in multiple sclerosis indicated by

Table 5.7. Reporter pathway analysis results in different neurological diseases for GSE26927.

Pathway	PD	AD	ALS	HD	MS	SCH
Glycolysis	+	+	+	+	-	+
Pentose_Phosphate_Pathway	-	-	+	-	-	-
TCA_Cycle	+	+	-	+	+	+
Oxidative_Phosphorylation_and_ATPase	+	+	+	+	+	+
Glutamate_-_Glutamine_Cycle	+	-	-	+	+	+
GABA_Cycle	+	+	+	+	-	-
Aspartate_Metabolism	-	-	-	-	+	-
Asparagine_Metabolism	-	+	-	+	+	+
Alanine_Metabolism	+	-	+	+	-	+
Glycine-Serine_Metabolism	+	-	+	-	-	-
Leucine_Metabolism	+	-	+	+	-	+
Ketone_Body_Metabolism	+	-	+	+	-	+
Valine_Metabolism	+	-	+	+	+	-
Isoleucine_Metabolism	+	-	+	+	+	-
Methionine_Metabolism	+	-	-	-	-	-
Cholesterol_Synthesis	-	-	-	-	+	-
Fatty_Acid_Synthesis	-	+	-	+	-	-
Phosphatidylethanolamine_Metabolism	-	-	-	+	-	-
Phosphatidylcholine_Metabolism	-	+	-	+	+	-
Sphingomyelin_Metabolism	+	-	-	-	-	-
CDP-Diacylglycerol_Biosynthesis	-	+	-	-	-	-
Inositol_Metabolism	+	+	+	+	+	-
Reactive_Oxygen_Species_Pathway	-	+	-	+	+	+
Creatine_Metabolism	-	+	+	-	+	+
Purine_Nucleoside_Metabolism	+	+	+	+	+	+
Pirimidine_Nucleoside_Metabolism	+	+	-	-	+	-

+: Reporter Pathway

RPA is supported by experimental study which reports a change in the related metabolite [119]. The study also reports a change in eg. tryptophan, but this is not captured in our analysis. In schizophrenia, significant changes observed in leucine and glutamate metabolisms by RPA can be linked to the literature studies reporting alterations in the levels of these amino acids, among others [118,120]. When comparing total number of reporter metabolites and reporter pathways for Parkinson's and Huntington's diseases, although the number of the reporter metabolites in Parkinson disease is considerably higher than that in Huntington's disease, total number of reporter pathways in Huntington's disease is higher than that in Parkinson disease.

A brief comparison of neurological diseases apart from Parkinson's disease indicates that fatty acid synthesis is changed in both Alzheimer's disease and Huntington's disease significantly. Phosphatidylcholine metabolism is affected in Alzheimer's disease, Huntington's disease, and multiple sclerosis. Creatine metabolism is found to be significantly changed in Alzheimer's disease, amyotrophic lateral sclerosis, multiple sclerosis, and schizophrenia. There are some studies pointing to creatine supplementation as a potential therapeutic in neurological diseases for energy homeostasis [121–123]. Similar to creatine, ketone body metabolism, another reporter pathway for some of the investigated diseases, is also used in therapeutic strategies to provide energy [124].

	PD	AD	ALS	HD	MS	SCH
PD	16					
AD	7	13				
ALS	11	6	13			
HD	12	10	10	17		
MS	8	9	6	10	14	
SCH	8	7	7	10	7	11

Figure 5.4. Distributions of the common reporter pathways for neurological diseases available at GSE26927 dataset.

5.3. Computational Binding Site Analysis

In computation of the binding site analysis, reporter metabolites of Parkinson's disease are used. The main idea behind this analysis is to elucidate over-represented transcription factor motifs from the genes of reporter metabolite. That is, it is checked whether genes in the neighbor of a reporter metabolite are regulated by a common transcription factor. Genes of each reporter metabolite are divided into two groups by taking fold change of control and disease gene expression value. Fold change states the ratio of mean expression value of disease condition to control case. If fold change is higher than 1, the corresponding gene is upregulated due to Parkinson disease. In case of less than 1, the gene is downregulated.

Reporter metabolites obtained from GSE26927 dataset for Parkinson's disease are used in this analysis. In order to perform this analysis, investigated reporter metabolite should have minimum 4 up regulated or down regulated gene. This cut-off is used to ensure trustability of identified transcription factors. The reporter metabolites satisfying this criterion are tabulated in Table 5.8 with the related up- and downregulated genes. If there are minimum 4 genes only for upregulation or downregulation, the analysis is performed only for the satisfied regulation. For example, Hc_A, Hc_N, NADH_NM, NAD_NM, pyruvate_A, and pyruvate_N reporter metabolites do not have minimum 4 genes for up-regulation, so this analysis is applied for only down-regulation for these reporter metabolites. The reverse case is valid for serine_A and serine_N.

Over-represented transcription factor binding site motif analysis is performed by using internet-based software Pscan [41]. The computation is carried out for each up or down regulated genes separately by using the accession numbers which is unique identification number for a DNA sequence. The accession of each gene is extracted from GPL data. The region in the DNA sequence is selected between -950 and +50. As a transcription factor descriptor database JASPAR is chosen due to being open-access for users. Transcription factor motifs that match with a p-value of less than 0.05 are considered to be significantly enriched and the results are given in Table 5.8.

According to the results, up-regulated genes of ATP are enriched with the binding sites of Mycn, Myb, Myc, Zfp423, IRF1 and some others. Down-regulated genes for the same reporter metabolite are enriched with Sox17, FOXF2, PBX1, E2F1, Klf4, and FOXO3. Genes of the pyruvate are found to be down-regulated and in this type of regulation motifs of TAL1::TCF3, Sox2, AP1, and Sox5 are over-represented in neighbor genes of pyruvate. Gene of reporter metabolite serine satisfy up-regulated criterion. Up-regulated gene of serine are enriched by NFYA, Zfx, PLAG1, and RORA_2.

Table 5.8. List of up-regulated genes, down-regulated genes, over-represented motifs in upregulation and downregulation with the corresponding reporter metabolites.

Reporter Metabolite	**Up-regulated Genes**	**Down-regulated Genes**	**Over-represented Motifs in Upregulation**	**Over-represented Motifs in Downregulation**
ADP_A	GUK1; MVD MVK; PC; ENTPD1; ACACB; MCCC2; UCKL1; CHKA	PIP5K1B; NME5; ITPKC; ATP6V1C1; DGKI; PFKM; ETNK1; PKM2; HK1; GLUL SUCLA2; C9orf98; GSS; ATP5B; ADK; PGK1; ACLY; PMVK; CKB; PI4KII; GCLM; PCCA	Mycn MYC::MAX Myc NFYA MAX Esrrb USF1 IRF1 Arnt REST Myb TP53	Sox17 FOXF2 PBX1 Sox2 Zfx Klf4 FOXO3 E2F1
ADP_N	GUK1; ENTPD1; ACACB; UCKL1; CHKA	PIP5K1B; NME5; ITPKC; ATP6V1C1; DGKI; PFKM; ETNK1; PKM2; HK1; SUCLA2; C9orf98; GSS; ATP5B; ADK; PGK1; ACLY; CKB; PI4KII; GCLM	REST znf143 IRF1 Mycn NFIL3 Myb MYC::MAX	FOXF2 NFYA Sox17 FOXO3 PBX1

Table 5.8. List of up-regulated genes, down-regulated genes, over-represented motifs in upregulation and downregulation with the corresponding reporter metabolites (cont.).

Reporter Metabolite	Up-regulated Genes	Down-regulated Genes	Over-represented Motifs in Upregulation	Over-represented Motifs in Downregulation
ATP_A	GUK1; MVD; MVK; PC; ENTPD1; ACACB; MAT2A; MCCC2; UCKL1; ACSL1; CHKA	PIP5K1B; NME5; ITPKC; ATP6V1C1; DGKI; PFKM; ETNK1; PKM2; HK1; GLUL; SUCLA2; C9orf98; GSS; PRPS1; ATP5B; ADK; PGK1; ACLY PMVK; CKB; PI4KII; GCLM; PCCA	Mycn Myc MYC::MAX NFYA MAX Myb IRF1 Zfp423 USF1 TP53 Arnt Klf4	Sox17 FOXF2 PBX1 E2F1 Klf4 FOXO3 Sox2
ATP_N	GUK1; ENTPD1; ACACB; MAT2A; UCKL1; ACSL1; CHKA	PIP5K1B; NME5; ITPKC; ATP6V1C1; DGKI; PFKM; ETNK1; PKM2; HK1; SUCLA2; C9orf98; GSS; PRPS1; ATP5B; ADK; PGK1; ACLY; CKB; PI4KII; ASNS; GCLM	Myb REST Mycn SP1 Myc Zfp423 IRF1 znf143 NFIL3	Sox17 FOXF2 FOXO3 Pax6 E2F1 NFYA PBX1 SOX9 Klf4
Hc_A	-	ATP5B; COX7B; NDUFA5; UQCRH	-	Ddit3::Cebpa RORA_2 ELF5 SRF
Hc_N	-	ATP5B; COX7B; NDUFA5; UQCRH	-	Ddit3::Cebpa RORA_2 ELF5 SRF

Table 5.8. List of up-regulated genes, down-regulated genes, over-represented motifs in upregulation and downregulation with the corresponding reporter metabolites (cont.).

Reporter Metabolite	Up-regulated Genes	Down-regulated Genes	Over-represented Motifs in Upregulation	Over-represented Motifs in Downregulation
NAD_NM	BDH2	NDUFA5; DLD; DLAT; MDH1; ALDH5A1; IDH3G; GLUD1; NNT	-	Pax2 TEAD1 SPIB
NADH_NM	BDH2	NDUFA5; DLD; DLAT; MDH1; ALDH5A1; IDH3G; GLUD1; NNT	-	Pax2 TEAD1 SPIB
Pyruvate_A	PC; GPT	SDSL; ME1; DLAT; PKM2; LDHB	-	AP1 TAL1::TCF3 Sox2 Sox5 Arnt::Ahr
Pyruvate_N	GPT	ME1; DLAT; PKM2; LDHB	-	TAL1::TCF3 Sox2 Sox17 AP1 Sox5 SOX9
Serine_A	PTDSS2; SHMT1; CBS; PSPH; SPTLC2	SDSL	NFYA Zfx PLAG1 Gfi Esrrb	-
Serine_N	CBS; PTDSS2; SHMT1; SPTLC2;	-	NFYA RORA_2	-

6. CONCLUSION AND RECOMMENDATIONS

6.1. Conclusions

Investigation of the brain metabolism by using a computational systems biology approach is performed in the present study. The following conclusions can be drawn on the basis of the results.

- Brain metabolism can be modeled with the set of 630 reactions (571 internal, 59 exchange) and 524 metabolites (465 internal, 59 external) based on the metabolic interactions in/between the astrocytes and neurons as well as exchange reaction through blood-brain-barrier.
- Since flux balance analysis results of healthy-case brain metabolism developed in this study are consistent with the experimental results, the current extended brain model can be used for further detailed computational predictions.
- Two constraint-based computational methods, MOMA and ROOM, can be used in the prediction of flux changes in perturbed (disease) condition by taking resting (healthy) state into account.
- Integration of the transcriptome data with the brain model is achieved on account of availability of the gene information in the developed brain model.
- Despite some common metabolites, transcriptional changes in Parkinson's disease occur around different metabolites in the different parts of the brain. Among three investigated regions, desmosterol, cholesterol, palmitate phosphatidyl-1D-myo-inositol-4-phosphate, and phosphatidyl-1D-myo-inositol-4-5-bisphosphate are defined as reporter metabolite in substantia nigra region.
- Parkinson's disease brings about the highest number of reporter metabolites among the investigated six common neurological diseases. KIV, KMV, palmitoyl-CoA, and malate are found to be reporter metabolite only in Parkinson's disease.
- In Parkinson's disease oxidative phosphorylation pathway and methionine metabolism are predicted to be significantly affected pathway in agreement with the literature findings.

- Computational transcriptional binding site analysis enables to identify possible transcriptional factors for up-regulated and down-regulated set of genes in Parkinson disease.
- SOX17, FOXF2, PBX1, Mycn, and Myb are identified as over-represented transcription factors with a high frequency among many others, pointing to these transcription factors as putative regulators of Parkinson's disease.

6.2. Recommendations

Brain has different regions such as substantia nigra, striatum, frontal cortex, and cerebellum. In the current study, brain metabolism is considered as a whole regardless of different regions of the brain. However, one reaction or gene may be active in one region of the brain and may not be active on the other region. Therefore, the idealized case would be the construction metabolic networks for each brain region separately.

The transcriptome datasets used in this study are not neuron and astrocytes specific. But the model includes compartmentalization of the brain cells as astrocytes and neurons. The use of separate transcriptome datasets for astrocytes and neurons datasets would provide prediction of more reactions specific to each cell type and integration of the transcriptome data with corresponding reactions in a higher consistency.

APPENDIX A: GENE EXPRESSION OMNIBUS

Experiments in transcriptome and proteome analysis are expensive. Therefore, it is better to share experimental results obtained by a research group in order to be used by other researchers globally. Within this scope, Gene Expression Omnibus (GEO) is the database storing microarray experimental data set served by National Center for Biotechnology Information (NCBI) (www.ncbi.nlm.nih.gov/geo). Data stored in GEO database includes four types of formats: GEO Platform (GPL), GEO Sample (GSM), GEO Series (GSE) and curated GEO DataSet (GDS). The following table gives the explanation of each data format.

Table A.1. Explanations of GEO database format.

Data Format	**Abbreviation**	**Explanation**	**Example**
Platform	GPL	list of elements on the array to match probe ID (gene-specific region on microarray) with gene names used in the experiment	GPL96
Sample	GSM	individual results of each experimental sample (array) used in the experiment with probe ID reference and corresponding detection value	GSM508708 GSM508710 GSM508711 GSM508717
Series	GSE	a group of related Sample (GSM) data for whole study	GSE20292
Curated Dataset	GDS	curated collection of comparable GEO Samples	GDS2821

When the data is uploaded to GEO database, a unique number is assigned to it. For example in the Table A.1, GSE20292 is a group of 29 samples obtained for normal case and Parkinson's disease in substantia nigra region of the brain [125]. GSM codes of only four of those samples are given in the table for two normal cases and two Parkinson diseases. The platform file for this sample is GPL96 which belongs to Affymetrix Human

Genome U133A Array. The example of the curated dataset stated in the table belongs to another study performed by Lesnick *et. al*., (2007) [126], and named as GDS2821 which compares the normal and disease conditions based on the microarray data. GDS format is not available for many datasets. Instead, the interested user must curate the data. An example of this is detailed below.

A.1. Example of MATLAB Code used in This Study

Data analysis obtained by high-throughput techniques which allows simultaneous determination of the levels of hundreds of biomolecules in one experiment, requires computational programs compatible with the data format. MATLAB is one of the commonly used computer programs to perform the analysis of microarray data due to its user-friendly toolboxes. Matlab's Bioinformatics Toolbox has specific functions which enable researchers to download GEO Data from GEO website and process it to make it suitable for data analysis. Procedure used in this study is stated below.

A.1.1. Downloading GEO Data from GEO Website

The first step is to get the GSE code from the related publication due to the fact that it stores the experimental results of all microarray samples entitled GSM code, and the information of GPL code corresponding to commercial microarray. Since it is aimed to investigate neurological diseases in this study, GSE codes, available in the literature, are found for Parkinson's diseases. In here, investigation of only one GSE code is given to show the computation steps in detail. Within this scope, GSE20292 which is used by Zhang *et. al.*, (2005) [125] for the analysis of expression data of substantia nigra in Parkinson's disease patients is selected. Then, it is required to get data from the GEO by using *getgeodata* command in Matlab. It is also possible to save the data for later use. GSE20292 is downloaded and saved as GSE20292.txt by the following *getgeodata* command.

```
a=getgeodata('GSE20292', 'ToFile', 'GSE20292.txt')

    Header: [1x1 struct]
    Data: [22283x29 bioma.data.DataMatrix]
```

Once the data has been downloaded from GEO Database, it is possible to call it by geoseriesread command for later use.

```
a= geoseriesread('GSE20292.txt')

    Header: [1x1 struct]
    Data: [22283x29 bioma.data.DataMatrix]
```

Data downloaded contains Header and Data fields which respectively correspond to metadata and matrix data of Series. Any data in the Data field can be written on the command window with the probe ID and GSM number.

```
a.Data(1:3,[1 9 2 3])
```

	GSM508708	GSM508717	GSM508710	GSM508711
1007_s_at	11.286	11.637	11.985	12.117
1053_at	5.8439	5.8289	5.8409	5.7939
117_at	7.3687	7.4564	7.3774	7.3197

The result gives the expression values of samples stated in the Table A.1 based on the first three probe IDs.

Header field contains two structures named as Series and Samples which give the detailed description of GSE files including submission date, contact information of researchers who performed the experiments, and GPL number.

```
a.Header

    Series:     [1x1 struct]
    Samples:    [1x1 struct]
```

```
 a.Header.Series

                    title  :  [1x73 char]
                geo_accession  :  'GSE20292'
                       status  :  'Public on Mar 12 2010'
              submission_date  :  'Feb 11 2010'
             last_update_date  :  'Mar 22 2012'
                    pubmed_id  :  '15965975
                               :  20926834'
                      summary  :  [1x115 char]
                overall_design  :  [1x162 char]
```

type	:	'Expression profiling by array'
contributor	:	[1x61 char]
sample_id	:	[1x290 char]
contact_name	:	'Frank,A,Middleton'
contact_email	:	'middletf@upstate.edu'
contact_phone	:	'315-464-7721'
contact_department	:	'Neuroscience and Physiology'
contact_institute	:	'SUNY Upstate Medical Univ'
contact_address	:	'750 East Adams St'
contact_city	:	'Syracuse'
contact_state	:	'NY'
contact_zip0x2Fpostal_code	:	'13210'
contact_country	:	'USA'
supplementary_file	:	[1x82 char]
platform_id	:	'GPL96'
platform_taxid	:	'9606'
sample_taxid	:	'9606'
relation	:	[1x80 char]

a.Header.Samples

title	:	{1x29 cell}
geo_accession	:	{1x29 cell}
status	:	{1x29 cell}
submission_date	:	{1x29 cell}
last_update_date	:	{1x29 cell}
type	:	{1x29 cell}
channel_count	:	{1x29 cell}
source_name_ch1	:	{1x29 cell}
organism_ch1	:	{1x29 cell}
characteristics_ch1	:	{4x29 cell}
molecule_ch1	:	{1x29 cell}
extract_protocol_ch1	:	{1x29 cell}
label_ch1	:	{1x29 cell}
label_protocol_ch1	:	{1x29 cell}
taxid_ch1	:	{1x29 cell}
hyb_protocol	:	{1x29 cell}
scan_protocol	:	{1x29 cell}
data_processing	:	{1x29 cell}
platform_id	:	{1x29 cell}
contact_name	:	{1x29 cell}
contact_email	:	{1x29 cell}
contact_phone	:	{1x29 cell}
contact_department	:	{1x29 cell}
contact_institute	:	{1x29 cell}

```
                contact_address  :  {1x29 cell}
                   contact_city  :  {1x29 cell}
                  contact_state  :  {1x29 cell}
contact_zip0x2Fpostal_code  :  {1x29 cell}
                contact_country  :  {1x29 cell}
              supplementary_file  :  {2x29 cell}
                 data_row_count  :  {1x29 cell}
```

A.1.2. Probe ID - Gene Name Match

Microarrays have thousands of regions and each specific region is labeled with a probe ID to detect target gene expression. GSE data format contains the experimental measurements with respect to probe IDs. Therefore, it is necessary to replace probe IDs with related gene names and this is why GPL data is required. There are various commercial microarray types. For example, microarrays for two different microorganisms will have different GPL files or even; a new version of microarray for the same microorganism is assigned updated probe IDs and different GPL codes listed in a.Header.Series field of the output of *getgeodata* or *getseriesdata*. Accordingly, for the GSE20292 mentioned above, the GPL code, named as Platform ID, is GPL96. Therefore, probe IDs in GSE20292 are required to be replaced with gene names in GPL96. The Data file for platform format can also be downloaded from GEO Database by *getgeodata* command.

```
c=getgeodata('GPL96', 'ToFile', 'GPL96.txt')
```

```
                Scope  :  'PLATFORM'
            Accession  :  'GPL96'
               Header  :  [1x1 struct]
  ColumnDescriptions  :  {16x1 cell}
          ColumnNames  :  {16x1 cell}
                 Data  :  {22283x16 cell}
```

Downloaded Platform file can be read by *geosoftread* command for later use.

```
d=geosoftread('GPL96.txt')
```

```
                Scope  :  'PLATFORM'
            Accession  :  'GPL96'
               Header  :  [1x1 struct]
```

```
ColumnDescriptions   :   {16x1 cell}
       ColumnNames   :   {16x1 cell}
              Data   :   {22283x16 cell}
```

It is aimed to retrieve the column that specifies the gene names in the Platform file. The column names in the Platform data are listed below including Gene Symbol that is required to change with probe IDs.

```
d.ColumnNames

    'ID'
    'GB_ACC'
    'SPOT_ID'
    'Species Scientific Name'
    'Annotation Date'
    'Sequence Type'
    'Sequence Source'
    'Target Description'
    'Representative Public ID'
    'Gene Title'
    'Gene Symbol'
    'ENTREZ_GENE_ID'
    'RefSeq Transcript ID'
    'Gene Ontology Biological Process'
    'Gene Ontology Cellular Component'
    'Gene Ontology Molecular Function'
```

Gene Symbol column is aimed to be inserted in place of probe ID column of GSE data. Therefore, a new variable named as GS below including Gene Symbol column in the GPL file is constituted; then, gene symbols are replaced with the probe IDs in the GSE data by the following codes.

```
GS = d.Data(:, strcmp(d.ColumnNames, 'Gene Symbol'));

a.Data = rownames(a.Data, ':', GS);
```

The new look of the GSE file becomes as follows:

```
a.Data(1:3,[1 9 2 3])

          GSM508708  GSM508717  GSM508710  GSM508711
DDR1      11.286     11.637     11.985     12.117
RFC2      5.8439     5.8289     5.8409     5.7939
HSPA6     7.3687     7.4564     7.3774     7.3197
```

A.1.3. Obtaining Required Gene Names and Expression Values

In this study, it is aimed to get expression values of genes included in the brain metabolic model. The model includes 670 different gene names. These gene names are mapped with manipulated GSE20292 dataset and it is found that 468 of the gene names are matched with the gene names stated in microarray analysis. Rest of them (202 gene names) is not matched due to absence of these genes in commercial Affymetrix Human Genome U133A Array.

Firstly, all gene names in the brain metabolic model are written in the text file and saved under the name of all_gene_in_once. Model gene names are imported by using *importdata* command irrespective of whether gene names in the model are included in the platform file. Then, exactly matched and nonexistent gene names with the GSE file are investigated and they are obtained as two separate character arrays. Lastly, *unique* command is used to rearrange the exactly matched and non-matched gene names since empty character arrays are defined to store them beforehand.

```
ModelGenes=importdata('all_gene_in_once.txt')
        for i=1:length(ModelGenes);
                x3 = strmatch(ModelGenes(i), GS, 'exact')

                if isempty(x3)
                        bb{1}='';
                        n=length(bb)+1;
                        p=1;
                        bb(n:p+n-1,1)= ModelGenes(i);
                else
                        for     j=1:length(x3)
                                C3(j,1)=GS(x3(j,1));
                        end
                aa{1}='';
                m=length(aa)+1;
                k=length(C3);
                aa(m:k+m-1,1)=C3;
                C3
                clear x3
                clear C3
                end
                i
        end
```

```
exactly_matched_genes = unique(aa(2:end))
exactly_non_matched_genes = unique(bb(2:end))
```

A.1.4. Obtaining the Genes Having Low Expression Values

GSE20292 which includes 29 samples of transcriptional analysis of whole substantia nigra in Parkinson disease and healthy condition is selected as example study for the below MATLAB code. Since microarray chip used in the experimental study covers all human genes, it is undoubted that different genes are active in different human tissues. Therefore, the genes which have expression value of less than 50 are assumed to be inactive due to low expression. This approach is applied to Parkinson's disease datasets. The MATLAB code used for this purpose is stated below for this condition.

Firstly, Series Data and Platform information are loaded by using *geoseriesread* and *geosoftread* commands, respectively. Then, probe IDs are replaced with the related gene names as detailed above by using MATLAB code below.

```
a= geoseriesread('GSE20292.txt');
d= geosoftread('GPL96.txt');
GS=d.Data(:, strcmp(d.ColumnNames, 'Gene Symbol'));
a.Data = rownames(a.Data, ':', GS);
B=GS(:,:);
```

Expression data for GSE20292 dataset is given in the form of log2; therefore, it is necessary to use *pow2* command for 2 raised to the power whole data excluding 3 samples for control case (GSM606624, GSM606625, and GSM606626) due to different data processing method. There are 11 samples for Parkinson's disease. However, 9 samples are used in computation since 2 samples (GSM508728 and GSM508732) are found to be outlier (See Appendix B). Since GSE20292 randomly covers the control and disease samples, 11 disease samples are distinguished by using exact matching of defined keyword in characteristics information of samples. Then, detected outlier arrays are excluded from computation by specifying their order in the manipulated data.

```
a.Data=pow2(a.Data);
Control_Disease=a.Header.Samples.characteristics_ch1(1,:)';
Disease=strmatch('disease state: Parkinsons disease', Control_Disease, 'exact')
```

```
Disease=Disease([1:8 10])';
```

An arbitrary cell matrix is defined to store lowly expressed genes and their order in the array. There are 30 columns in the arbitrary cell for 15 samples. (2n-1)th and (2n)th columns give the information of gene names and and their order in the array, respectively.

```
limit=50;
ccc{1,2*length(Disease)}='';
        for n=1:length(Disease)
        clear ff;
        ff=find(a.Data(:,Disease(n))<limit);
        g=size(ff,1);
        ccc(1:g,2*n-1)=B(ff);
        ccc(1:g,2*n)=num2cell(ff);
        end
clear ff;
clear n;
```

After the separation of lowly expressed data from the whole data, genes in the model are matched with the lowly expressed gene data to determine the lowly expressed model genes. Instead of model genes, previously matched genes with corresponding GPL code are loaded by load command under the name of “matched_genes_glp96” as a MATLAB file.

In the first step, exact matching is used. Secondly, unmatched genes are checked one by one because some genes are assigned with more than one symbols. Therefore, it is not possible to match exactly for these gene symbols. An additional cell under the name of nonexact_matched_genes is introduced for these cases.

```
load('matched_genes_glp96.mat')
mm{1,length(Disease)}='';
nn{1,length(Disease)}='';
pp{1,length(Disease)}='';
Genes{1000,2*length(Disease)}='';
aasize{1,length(Disease)}='';
        for u=1:length(Disease);
        fff{1000,1}='';
        clear aa;
        clear cc;
        aa{1}='';
        cc=0;
```

```
clear BB1;
clear BB2;
clear bb;
BB1=cell2mat(ccc(1:end,2*u));
BB2=ccc(1:end,2*u-1)        ;
        for i=1:length(matched_genes_glp96);
        x3 = strmatch(matched_genes_glp96(i), BB2(1:nnz(BB1)), 'exact');
                if isempty(x3);
                bb{1}='';
                n=length(bb)+1;
                bb(n,1)= matched_genes_glp96(i);
                else
                m1=length(cc)+1;
                k1=length(x3);
                cc(m1:k1+m1-1,1)=x3;
                        for j=1:length(x3)
                        C3(j,1)=BB1(x3(j,1));
                        end
                m=length(aa)+1;
                k=length(C3);
                aa(m:k+m-1,1)=num2cell(C3);
                clear x3
                clear C3
                end
        end
mm(1:size(aa(2:end),1),u)=aa(2:end);
nn(1:size(bb(2:end),1),u)=bb(2:end);
pp(1:size(aa(2:end),1),u)=num2cell(cc(2:end));
aasize(1,u)=num2cell(length(aa)-1);
fff(1:size(aa,1)-1,1)=num2cell(double(a.Data(BB1(cell2mat(pp(1:size(aa,1)-
1,u)),:),Disease(u))));
srt=length(B(cell2mat(mm(:,u))));
Genes(:,2*u)=fff;
Genes(1:srt,2*u-1)=B(cell2mat(mm(:,u)));
clear srt
clear fff
end
```

Up to this point, lowly expressed genes in our model are extracted from whole data. For next steps, it is necessary to determine whether the genes are lowly expressed in a high percentage of replicate samples. For this purpose, All the genes are rearranged in a cell by using unique command. The cell named unique_genes_control consists of the lowly expressed gene symbols only one time.

```
vv1{1}='';
for i=1:length(Disease);
```

```
clear vv;
vv=unique(Genes(1:nnz(cell2mat(Genes(1:cell2mat(aasize(1,i)),2*i))),2*i-1));
vv1((size(vv1,1)+1):(size(vv1,1)+size(vv,1)),1)=vv;
end
unique_genes_disease=unique(vv1(2:end,1));
```

In this step, for each sample (among 9) having each lowly expressed gene symbol is computed. Occurrence numbers in all samples are added to unique_genes_control cell as second column. If the gene is lowly expressed in more than 60% of the total number of samples, it is assumed to be low expressed. “INCLUDE” and “exclude” terms are assigned as a third column for stating whether the occurrence percentage of more than and less than 60, respectively. srt1 and srt2 cells also store these information in the same manner.

```
for i=1:size(unique_genes_disease,1);
clear mstf
clear mstf1
mstf=strmatch(char(unique_genes_disease(i)), vv1, 'exact');
mstf1=nnz(mstf);
unique_genes_disease(i,2)=num2cell(mstf1);
end

cut_off=0.6*length(Disease);

srt1{1}='';
srt2{1}='';
for i=1:size(unique_genes_disease,1);
        if cell2mat(unique_genes_disease(i,2))>=cut_off;
        srt1(size(srt1,1)+1,1)=unique_genes_disease(i,1);
        unique_genes_disease{i,3}='INCLUDE';
        else
        unique_genes_disease{i,3}='exclude';
        srt2(size(srt2,1)+1,1)=unique_genes_disease(i,1);
        end
clear mstf3
end
srt1=srt1(2:end);
srt2=srt2(2:end);
```

In the previous section lowly expressed genes are identified. In this part it is aimed to match lowly expressed genes with the model genes computationally. The code stated below gives which reactions are controlled by the lowly expressed genes. MATLAB file named reaction_list consists of six columns including Reaction Number, Reaction Name, EC Number, Enzyme Name, Gene Symbol, and Reaction. The result of this code is a cell

matrix called Delete_Gene_Control and includes Reaction Number, Reaction Name, and Gene Symbols.

```
load('reaction_list.mat')
aa1{1}='';
cc1=0;
for i=1:length(srt1)
x3=[];
ss=strfind(reaction_list(:,5),char(srt1(i)));
x3=find(cellfun(@isempty,ss)==0);

        if isempty(x3)
        bb1{1}='';
        n=length(bb1)+1;
        p=1;
        bb1(n:p+n-1,1)=srt1(i);
        else
        m1=length(cc1)+1;
        k1=length(x3);
        cc1(m1:k1+m1-1,1)=x3;
                for j=1:length(x3);
                C3(j,1)=reaction_list(x3(j,1));
                end
        m=length(aa1)+1;
        k=length(C3);
        aa1(m:k+m-1,1)=C3;
        clear x3;
        clear C3;
        end
end

mm1=(aa1(2:end));
pp1=cc1(2:end);
pp2=unique(cc1(2:end));

Delete_Gene_Reaction_List_Disease=reaction_list(pp1,[1 2 5]);
```

Another step is to check whether the genes have greater expression level of 50 because there may be more than one probe ID for the same gene. Therefore, it is necessary to check whether the genes found by using the above code have another expression data which is greater than 50 in more than 60% of the total number of samples. If so, these genes are assumed not to be lowly expressed.

```
aa2{1}='';
```

```
cc2=0;
for i=1:length(srt1);
x3 = strmatch(srt1(i), B, 'exact');
m1=length(cc2)+1;
k1=length(x3);
cc2(m1:k1+m1-1,1)=x3;
        for j=1:length(x3)
        C3(j,1)=B(x3(j,1));
        end
m=length(aa2)+1;
k=length(C3);
aa2(m:k+m-1,1)=C3;
clear x3
clear C3
end
mm2= unique(aa2(2:end));
pp2=cc2(2:end);
KLM1=a.Data(pp2',Disease);
Check_Deleted_Genes_Disease=[B(pp2',1) num2cell(double(KLM1))];
```

Up to here, the resulting data includes not only low expression of the genes of interest but also high expressions due to availability of multiple probe IDs for the same gene. Therefore, it is necessary to extract only low expressed.

```
all_gene_in_Check_Deleted_Genes=Check_Deleted_Genes_Disease(:,1);
for i=1:size(all_gene_in_Check_Deleted_Genes,1);
        if length(find(cell2mat(Check_Deleted_Genes_Disease(i,2:end))<limit))>cut_off
        all_gene_in_Check_Deleted_Genes(i,2)=num2cell(0);
        else
        all_gene_in_Check_Deleted_Genes(i,2)=num2cell(1);
        end
end
ee1{1}='';
ff1{1}='';
for i=1:size(mm2,1);
clear mstf
clear mstf1
mstf=strmatch(mm2(i), all_gene_in_Check_Deleted_Genes(:,1), 'exact');
mstf1=sum(cell2mat((all_gene_in_Check_Deleted_Genes(mstf',2))));
        if mstf1==0
        n=length(ee1)+1;
        p=1;
        ee1(n:p+n-1,1)=mm2(i);
        else
        n=length(ff1)+1;
        p=1;
        ff1(n:p+n-1,1)=mm2(i);
```

```
        end
end
only_low_expressed_genes=ee1(2:end)
low_and_high_expressed=ff1(2:end)
```

The last step is to assign lowly expressed genes to their corresponding reactions (in the model). If all genes of a reaction are found to have only low expression satisfying the criteria mentioned above, the corresponding reaction is inactivated in Parkinson's disease condition.

```
clear aa1
clear cc1
clear pp1
aa1{1}='';
cc1=0;
srt1=only_low_expressed_genes
        for i=1:length(srt1)
        x3=[];
        ss=strfind(reaction_list(:,5),char(srt1(i)));
        x3=find(cellfun(@isempty,ss)==0);
                if isempty(x3)
                bb1{1}='';
                n=length(bb1)+1;
                p=1;
                bb1(n:p+n-1,1)=srt1(i);
                else
                m1=length(cc1)+1;
                k1=length(x3);
                cc1(m1:k1+m1-1,1)=x3;
                        for j=1:length(x3);
                        C3(j,1)=reaction_list(x3(j,1));
                        end
                m=length(aa1)+1;
                k=length(C3);
                aa1(m:k+m-1,1)=C3;
                clear x3;
                clear C3;
                end
        end
mm1=(aa1(2:end));
pp1=cc1(2:end);
pp2=unique(cc1(2:end));
Only_Delete_Gene_Reaction_List_Disease=reaction_list(pp1,[1 2 5]);
```

APPENDIX B: ARRAY OUTLIER ANALYSIS

Sammon mapping is a dimension reduction method used for high dimensional data and it helps the identification of outliers [127,128]. In Sammon mapping, distance matrix between the arrays is used in place of original data matrix which is generally used in other methods. A new representation of the arrays in a lower-dimensional space is aimed by minimizing the total stress with reference to original one. This method is performed on MATLAB with the commands of '*pdist*' giving Euclidean distances between each pair of observations in the data matrix, and '*mdscale'* performing non-metric multidimensional scaling on the Euclidean distances.

When the results of Sammon mapping are plotted, it demonstrates the numerical data on the plot by taking similarity between the datasets into consideration. In this analysis, each point on the plot stands for a GSM sample dataset used in the computation. Any point far from the other grouped points for the same condition is defined as outlier and is not used in further calculation. By performing Sammon mapping, it is expected that outlier datasets in control and disease are distinguished by using the distance of each point on the plot. GSE20141 is selected as an example to be used in illustration of Sammon mapping. As seen Figure B.1, each point represents a GSM sample array results from Sammon mapping for GSE20141. Point a, representing Sammon mapping result for GSM503952, is an outlier from the rest because it is quite distant from other circular blue points in the same control condition. Star-shaped red points represent Parkinson disease case and they are all similar since they are not distant from each other.

The Sammon mapping analysis is performed again for the remaining datasets in the GSE20141, excluding GSM503952, and the result of the analysis is given in Figure B.2. As seen, represented points for the control condition and excluding GSM503952, are distributed closer than the previous case. This result shows that remaining 7 arrays are similar to each other and GSM503952 is different from them. Therefore, GSM503952 is disregarded in this study.

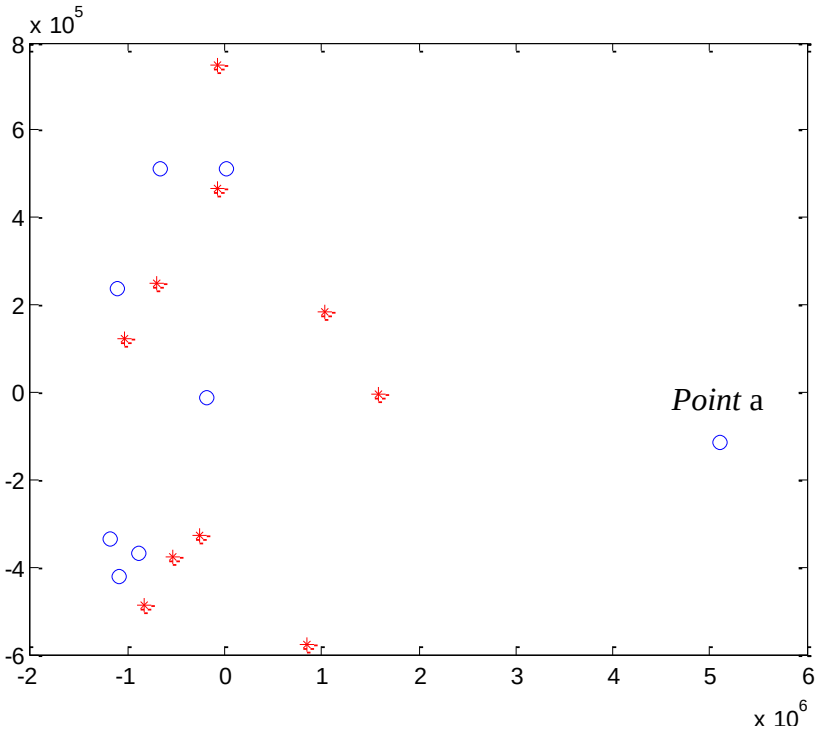

Figure B.1. Sammon mapping result for GSE20141 dataset to elucidate outlier array

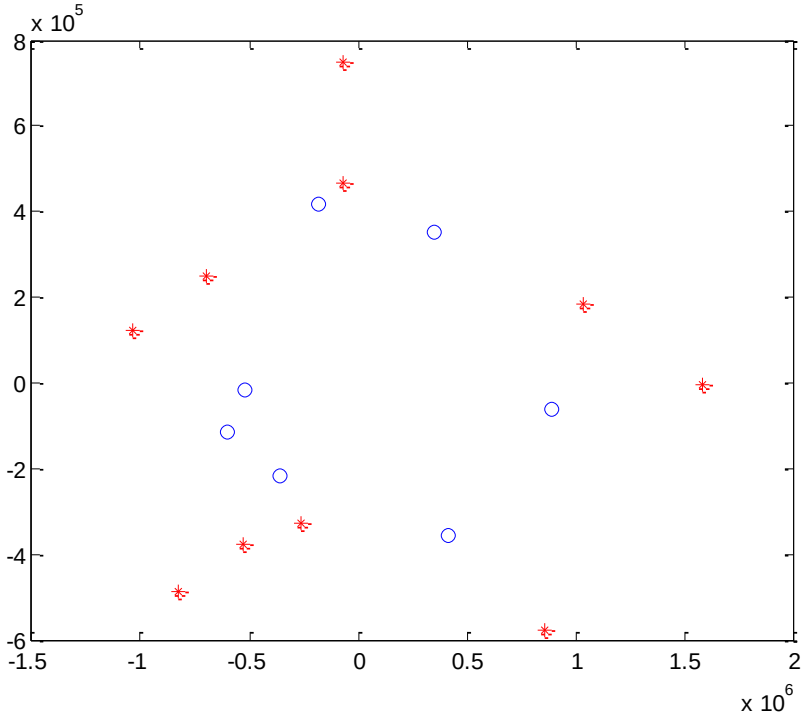

Figure B.2. Sammon mapping result for GSE20141 dataset excluding outlier array GSM503952

Array outlier analysis, explained above, is applied for all GSE datasets used in this study. The results of this analysis are tabulated in Table B.1 with disease and brain region information. As seen, some of the related GSE datasets have 1 or 2 outlier arrays which are not used in the computations.

Table B.1. Sammon mapping results for GSE20141 with the information of disease, brain region, and outlier array

GSE SET	**Disease**	**Brain Region**	**Number of Samples Used in Computation**		**Outlier Samples**	
			Healthy	**Disease**	**Healthy**	**Disease**
GSE20291	PD	Putamen	15	15	-	-
GSE20292	PD	Substantia Nigra	14	9	GSM508723	GSM508728 GSM508732
GSE20168	PD	Prefrontal cortex area 9	15	14	-	-
GSE26927	AD	Entorhinal cortex	7	11	-	-
GSE26927	ALS	Cervical spinal cord	10	10	-	-
GSE26927	HD	Ventral head of the caudate nucleus	10	9	-	GSM663064
GSE26927	MS	Subpial grey matter lesions from the frontal gyri	10	9	-	GSM663079
GSE26927	PD	Substantia nigra	8	12	-	-
GSE26927	SCH	Grey matter in Brodmann area	8	10	GSM663106 GSM663108	-

APPENDIX C: REPORTER METABOLITE ANALYSIS

Reporter Metabolite Analysis (RMA) is performed by using Reporter Features Online Toolbox (http://129.16.106.142/toolbox.php#reporterfeatures) on the webpage of Systems Biology Group at Chalmers University of Technology (http://www.sysbio.se). All files required for the computation should be prepared in accordance with the given instructions. There are 3 different files to load to online program with the information as follows:

(i) Gene names in the developed brain model with the corresponding p-values obtained from the transcription data.

(ii) Reactions and corresponding genes.

(iii) Metabolites and corresponding reactions.

The arrangement of these three files is performed by using a MATLAB code and summarized in Figure C.1. The steps are stated below.

(i) Probe IDs in GSE data are matched with related gene symbols stored in GPL data.

(ii) Genes available in the developed brain model are extracted from the transcription data to continue computation with the metabolic genes of interest rather than thousands of genes in the data set.

(iii) P-values of all genes in the model are calculated by using "*ttest2*" command in MatLab. In the transcription data, it is possible to have more than one probe IDs for a certain gene. In this case, it is necessary to use only one p-value raher than all p-values by specifying selection criterion. For Illumina microchips, p-value of the highest average expression value is considered. For Affymetrix microchips, there are 4 types of probe IDs ending with "_at", "_a_at", "_s_at", and "_x_at". Based on information on Affymetrix webpage (http://www.affymetrix.com/support/help/faqs/mouse_430/faq_8.jsp), the priorities of these 4 suffixes are used in the study as follows:

- _at
- _a_at

- _s_at
- _x_at
- If there are more than one expression value with the same suffix for a particular gene symbol, p-value of the highest average expression value is used as a p-value selection criterion.

By using the method stated above, p-values of all genes matched with the transcription data are calculated, and the required tab delimited text file with two columns including gene symbols and corresponding p-values is prepared.

(iv) In the arrangement of "reaction names and corresponding genes" file in the format of tab delimited text file with two columns, if the reaction is controlled by only one gene, related gene is specified for this reaction. However, in case of multiple genes being responsible for the same reaction, gene having the lowest p-value is defined for the related reaction to be used in computation [35].

(v) Lastly, tab delimited text file in the sif format covering metabolite names and corresponding reaction names is prepared for RMA. This file includes three columns where first, second and third columns represent metabolites, interaction types, and reactions, respectively. The second column is not used in the Reporter Metabolite Analysis. This format is preferred for the sake of being compatible with Cytoscape format (http://cytoscape.org).

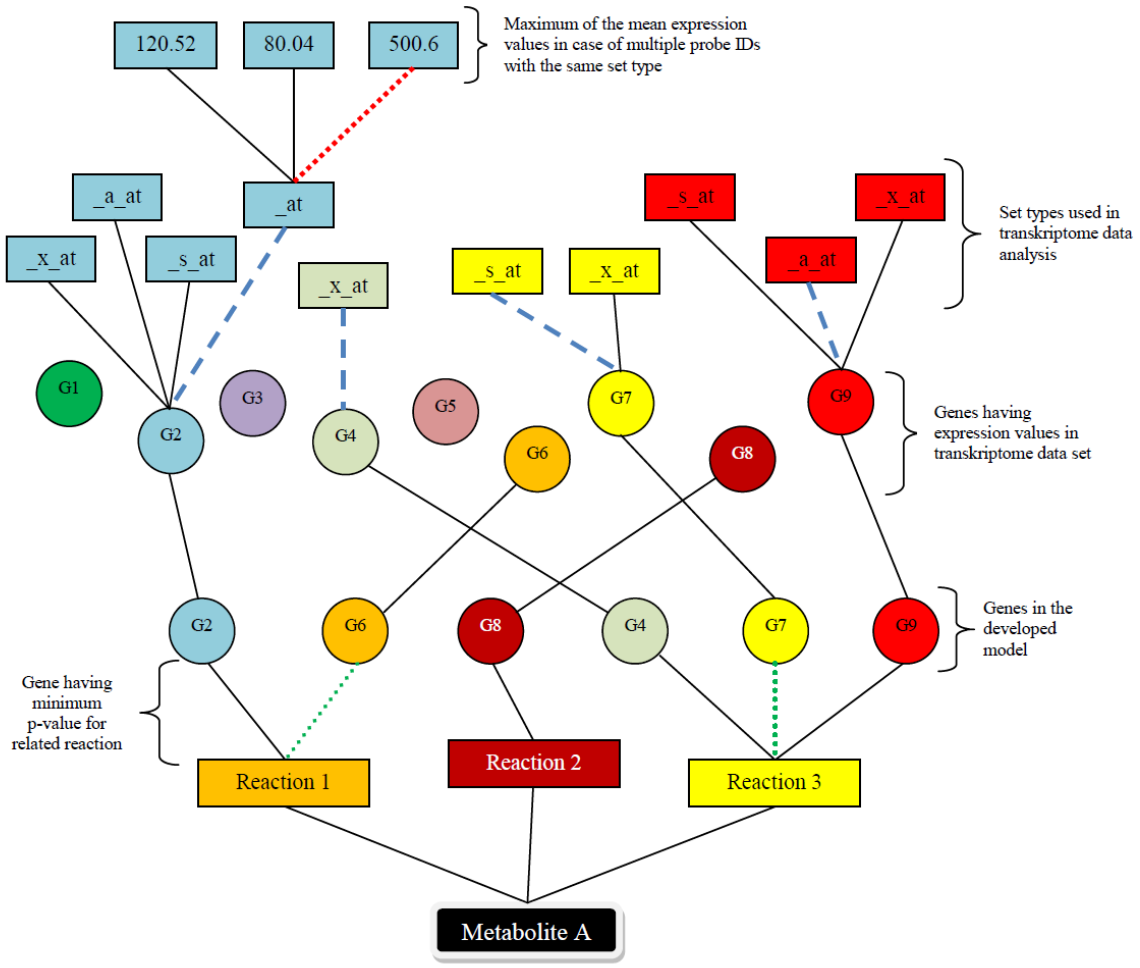

Figure C.1. Summary of methods used in integration of transcription data with the brain model genes for reporter metabolite analysis. Dashed lines represent selections used in computation for Affymetrix microchips in case of multiple options. Red dashed line: If there are more than one expression values with the same suffix for a particular gene symbol, p-value of the highest average expression value is used as a p-value selection criterion. Blue dashed line: In case of multiple suffixes, the priority used in computation is "_at", "_a_at", "_s_at", and "_x_at", respectively. Green round dotted line: In case of multiple gene controlling the same reaction, the gene with the lowest p-value is considered. Similarly, if there are multiple probe IDs for a single gene in Illumina microchips, probe ID with the highest average expression value is used in calculations.

APPENDIX D: REPORTER PATHWAY ANALYSIS

In this part of study, a new method is proposed in the prediction of significantly changed pathways. This method is similar to reporter metabolite analysis (RMA). In RMA, p-values of related genes are used in determination of reporter metabolites having the most significant transcriptional changes around. Similarly, in the present method, each pathway is scored with a p-value based on p-values of its metabolites calculated from RMA. Therefore, this new method is named as Reporter Pathway Analysis (RPA) specifying significance of change due to perturbation (disease). The pathways having p-value of less than the selected cut-off are defined as reporter pathways and they involve significant change due to perturbed condition. The procedure for the determination of p-value of a pathway is illustrated in Figure D.1 and explained below.

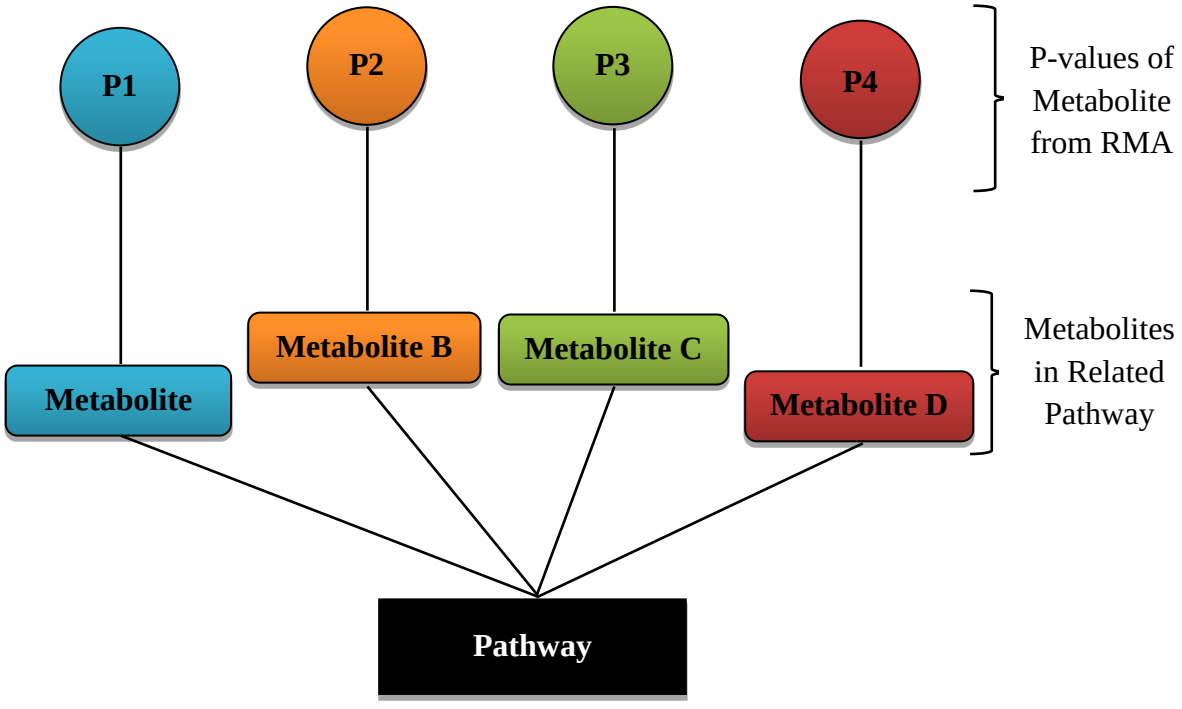

Figure D.1. Illustration of reporter pathway analysis computation by using reporter metabolite results

As done in RMA, RPA is also performed by using Reporter Features Online Toolbox (http://129.16.106.142/toolbox.php#reporterfeatures) on the webpage of Systems Biology

Group at Chalmers University of Technology (http://www.sysbio.se). To make input files compatible with this online toolbox, a specific term starting with “p” and continue with a number is defined for each metabolite. The idea underlying this arrangement is to link each metabolite with its p-value calculated from RMA. The 3 required files are arranged as follows:

(i) Metabolite-specific “p” terms with the corresponding p-values: This is a tab delimited text file with 2 columns. P-values in this file are obtained from the RMA.

(ii) Metabolites and corresponding specific “p” terms: This is also a tab delimited text file with 2 columns to connect each metabolite with its p-value.

(iii) Pathway names and corresponding metabolites: This is a tab delimited text file in the sif format covering pathways and corresponding metabolites. This file includes three columns: pathways, interaction types, and metabolites, respectively. The second column is not used in the Reporter Pathway Analysis. This format (known also as sif format) is selected for being compatible with Cytoscape format (http://cytoscape.org) by Online Toolbox.

APPENDIX E: METABOLIC REACTION MODEL OF BRAIN

Table E.1. Metabolic reactions and genes in the developed brain model.

Reaction No	Metabolism	Gene Symbol	Reaction
R1	Glycolysis	GCK; HK1; HK2; HK3; HKDC1; HS15971	Glucose_A + ATP_A -> Glucose-6-phosphate_A + ADP_A
R2	Glycolysis	GPI	Glucose-6-phosphate_A <-> Fructose-6-phosphate_A
R3	Glycolysis	PFKL; PFKM; PFKP	Fructose-6-phosphate_A + ATP_A -> Fructose-1-6-biphosphate_A + ADP_A
R4	Glycolysis	ALDOA; ALDOB	Fructose-1-6-biphosphate_A <-> Glyceraldehyde-3-phosphate_A + Dihydroxyacetone-phosphate_A
R5	Glycolysis	HS16708; HS17626; TPI1	Dihydroxyacetone-phosphate_A <-> Glyceraldehyde-3-phosphate_A
R6	Glycolysis	GAPDH; GAPDHS; HS15058; HS16973; HS17086; HS17248; HS17313; HS17391; HS17569; HS17733; HS17738	Glyceraldehyde-3-phosphate_A + NAD_A <-> 1-3-biphosphoglycerate_A + NADH_A
R7	Glycolysis	HS16267; PGK1; PGK2	1-3-biphosphoglycerate_A + ADP_A <-> 3-phosphoglycerate_A + ATP_A
R8	Glycolysis	BPGM; HS09900; HS16251; HS16751; HS17109; HS17587; PGAM1; PGAM2; VCAN	3-phosphoglycerate_A <-> 2-phosphoglycerate_A
R9	Glycolysis	ENO1; ENO2; ENO3	2-phosphoglycerate_A <-> Phosphoenol-pyruvate_A
R10	Glycolysis	PKLR; PKM2	Phosphoenol-pyruvate_A + ADP_A -> Pyruvate_A + ATP_A
R11	Glycolysis	HS16547; HS16965; HS17383; HS17676; LDHA; LDHAL6A; LDHAL6B; LDHB; LDHC	Pyruvate_A + NADH_A <-> Lactate_A + NAD_A
R12	Glycolysis	PC	Pyruvate_A + ATP_A + Bicarbonate_A -> Oxoloacetate_A + ADP_A
R13	Glycolysis	DLAT; DLD; PDHA1; PDHB; PDHX	Pyruvate_A + NAD_AM -> Acetyl-CoA_A + CO2_A + NADH_AM
R14	Glycolysis	PCK1; PCK2	Oxoloacetate_A + GTP_A -> Phosphoenol-pyruvate_A + CO2_A + GDP_A
R15	Glycolysis	BPGM; HS16251; HS16751; HS17109; HS17587; PGAM1; PGAM2	2-3-Disphospho-D-glycerate_A -> 3-phosphoglycerate_A
R16	Glycolysis	BPGM; HS16251; HS16751; HS17109; HS17587; PGAM1; PGAM2	1-3-biphosphoglycerate_A <-> 2-3-Disphospho-D-glycerate_A
R17	PPP	G6PD	Glucose-6-phosphate_A + NADP_A <-> 6-phosphoglucone_A + NADPH_A
R18	PPP	H6PD; PGLS	6-phosphoglucone_A -> 6-phosphogluconate_A
R19	PPP		6-phosphogluconate_A + NADP_A -> Ribulose-5-phosphate_A + NADPH_A + CO2_A
R20	PPP	RPE	Ribulose-5-phosphate_A <-> Xylulose-5-phosphate_A
R21	PPP	RPIA	Ribulose-5-phosphate_A <-> Ribose-5-phosphate_A
R22	PPP	TKT; TKTL1; TKTL2	Ribose-5-phosphate_A + Xylulose-5-phosphate_A <-> Sedoheptulose-7-phosphate_A + Glyceraldehyde-3-phosphate_A

Table E.1. Metabolic reactions and genes in the developed brain model (cont.).

Reaction No	Metabolism	Gene Symbol	Reaction
R23	PPP	TALDO1	Sedoheptulose-7-phosphate_A + Glyceraldehyde-3-phosphate_A <-> Fructose-6-phosphate_A + Erythrose-4-phosphate_A
R24	PPP	TKT; TKTL1; TKTL2	Xylulose-5-phosphate_A + Erythrose-4-phosphate_A <-> Fructose-6-phosphate_A + Glyceraldehyde-3-phosphate_A
R25	TCA Cycle	CS; FLJ40154	Oxoloacetate_A + Acetyl-CoA_A -> Citrate_A
R26	TCA Cycle	ACO1; ACO2	Citrate_A <-> Cis_aconitate_A
R27	TCA Cycle	ACO1; ACO2	Cis_aconitate_A <-> Isocitrate_A
R28	TCA Cycle	ACLY	ATP_A + Citrate_A -> Oxoloacetate_A + Acetyl-CoA_A + ADP_A
R29	TCA Cycle	CLYBL	Citrate_A <-> Oxoloacetate_A + Acetate_A
R30	TCA Cycle	IDH3A; IDH3B; IDH3G	Isocitrate_A + NAD_AM -> alpha-ketoglutarate_A + NADH_AM + CO2_A
R31	TCA Cycle	HS09852; IDH1; IDH2	Isocitrate_A + NADP_A -> alpha-ketoglutarate_A + NADPH_A + CO2_A
R32	TCA Cycle	HS09852; IDH1; IDH2	Isocitrate_A + NADP_AM -> alpha-ketoglutarate_A + NADPH_AM + CO2_A
R33	TCA Cycle	OGDHL; DHTKD1; OGDH; DLST; DLD	alpha-ketoglutarate_A + NAD_AM -> Succinyl-CoA_A + NADH_AM + CO2_A
R34	TCA Cycle	SUCLA2; SUCLG1	Succinyl-CoA_A + ADP_A <-> Succinate_A + ATP_A
R35	TCA Cycle	SDHC; HSSUCCDH; HS12683; SDHB; SDHA; PGL2	Succinate_A + FAD_AM <-> Fumarate_A + FADH2_AM
R36	TCA Cycle	FH	Fumarate_A <-> Malate_A
R37	TCA Cycle	MDH1; MDH2	Malate_A + NAD_AM -> Oxoloacetate_A + NADH_AM
R38	TCA Cycle	MDH1; MDH2	Malate_A + NAD_A -> Oxoloacetate_A + NADH_A
R39	TCA Cycle	ME1; ME2; ME3	Malate_A + NADP_A -> Pyruvate_A + NADPH_A + CO2_A
R40	TCA Cycle	NNT	NADP_AM + NADH_AM -> NADPH_AM + NAD_AM

Table E.1. Metabolic reactions and genes in the developed brain model (cont.).

Reaction No	Metabolism	Gene Symbol	Reaction
R41	Oxidative Phosphorylation and ATPase	HS13127; HS13575; HS13941; HS14053; HS15241; HS15997; HS16080; HS16135; HS16463; HS16554; HS16828; HS16990; HS17072; HS17222; HS17235; HS17481; MT-ND1; MT-ND2; MT-ND3; MT-ND4; MT-ND4L; MT-ND5; MT-ND6; ND1; ND3; ND4; ND6; NDUFA1; NDUFA10; NDUFA11; NDUFA12; NDUFA13; NDUFA2; NDUFA3; NDUFA4; NDUFA5; NDUFA6; NDUFA7; NDUFA8; NDUFA9; NDUFAF1; NDUFAF2; NDUFAF3; NDUFAF4; NDUFB1; NDUFB10; NDUFB11; NDUFB2; NDUFB3; NDUFB4; NDUFB5; NDUFB6; NDUFB7; NDUFB8; NDUFB9; NDUFC1; NDUFC2; NDUFS1; NDUFS2; NDUFS3; NDUFS7; NDUFS8; NDUFV1; NDUFV2; NDUFV3	NADH_AM + Ubiquinone_A -> NAD_AM + Ubiquinol_A + 4 Hc_A
R42	Oxidative Phosphorylation and ATPase	CYC1; HS14919; HS16142; MT-CYB; UQCR; UQCR10; UQCRB; UQCRC1; UQCRC2; UQCRFS1; UQCRFSL1; UQCRH; UQCRQ	Ubiquinol_A + CytCox_A -> Ubiquinone_A + CytCred_A + 4 Hc_A
R43	Oxidative Phosphorylation and ATPase	COX1; COX2; COX3; COX4I1; COX4I2; COX5A; COX5B; COX6A1; COX6A2; COX6B1; COX6B2; COX6C; COX7A1; COX7A2; COX7A2L; COX7AP2; COX7B; COX7B2; COX7C; COX8A; HS09101; HS16039; HS16147; HS17660; HS17765; MT-CO1; MT-CO2; MT-CO3	CytCred_A + 0.5 O2_A -> CytCox_A + 2 Hc_A
R44	Oxidative Phosphorylation and ATPase	ETFDH	FADH2_AM + Ubiquinone_A -> FAD_AM + Ubiquinol_A

Table E.1. Metabolic reactions and genes in the developed brain model (cont.).

Reaction No	Metabolism	Gene Symbol	Reaction
R45	Oxidative Phosphorylation and ATPase	ATP5A1; ATP5B; ATP5C1; ATP5D; ATP5E; ATP5EP2; ATP5F1; ATP5H; ATP5I; ATP5J2; ATP5L; ATP5L2; ATP5S; ATP6; ATP8; HS15678; HS16048; HS16291; HS16707; HS16872; HS16911; HS16919; HS17378; HS17406; MTATP6; MTATP8	ADP_A + 4 Hc_A -> ATP_A
R46	Glycolysis	GCK; HK1; HK2; HK3; HKDC1; HS15971	Glucose_N + ATP_N -> Glucose-6-phosphate_N + ADP_N
R47	Glycolysis	GPI	Glucose-6-phosphate_N <-> Fructose-6-phosphate_N
R48	Glycolysis	PFKL; PFKM; PFKP	Fructose-6-phosphate_N + ATP_N -> Fructose-1-6-biphosphate_N + ADP_N
R49	Glycolysis	ALDOA; ALDOB	Fructose-1-6-biphosphate_N <-> Glyceraldehyde-3-phosphate_N + Dihydroxyacetone-phosphate_N
R50	Glycolysis	HS16708; HS17626; TPI1	Dihydroxyacetone-phosphate_N <-> Glyceraldehyde-3-phosphate_N
R51	Glycolysis	GAPDH; GAPDHS; HS15058; HS16973; HS17086; HS17248; HS17313; HS17391; HS17569; HS17733; HS17738	Glyceraldehyde-3-phosphate_N + NAD_N <-> 1-3-biphosphoglycerate_N + NADH_N
R52	Glycolysis	HS16267; PGK1; PGK2	1-3-biphosphoglycerate_N + ADP_N <-> 3-phosphoglycerate_N + ATP_N
R53	Glycolysis	BPGM; HS09900; HS16251; HS16751; HS17109; HS17587; PGAM1; PGAM2; VCAN	3-phosphoglycerate_N <-> 2-phosphoglycerate_N
R54	Glycolysis	ENO1; ENO2; ENO3	2-phosphoglycerate_N <-> Phosphoenol-pyruvate_N
R55	Glycolysis	PKLR; PKM2	Phosphoenol-pyruvate_N + ADP_N -> Pyruvate_N + ATP_N
R56	Glycolysis	HS16547; HS16965; HS17383; HS17676; LDHA; LDHAL6A; LDHAL6B; LDHB; LDHC	Pyruvate_N + NADH_N <-> Lactate_N + NAD_N
R57	Glycolysis	DLAT; DLD; PDHA1; PDHB; PDHX	Pyruvate_N + NAD_NM -> Acetyl-CoA_N + CO2_N + NADH_NM
R58	Glycolysis	PCK1; PCK2	Oxoloacetate_N + GTP_N -> Phosphoenol-pyruvate_N + CO2_N + GDP_N
R59	Glycolysis	BPGM; HS16251; HS16751; HS17109; HS17587; PGAM1; PGAM2	2-3-Disphospho-D-glycerate_N -> 3-phosphoglycerate_N
R60	Glycolysis	BPGM; HS16251; HS16751; HS17109; HS17587; PGAM1; PGAM2	1-3-biphosphoglycerate_N <-> 2-3-Disphospho-D-glycerate_N
R61	PPP	G6PD	Glucose-6-phosphate_N + NADP_N <-> 6-phosphoglucone_N + NADPH_N
R62	PPP	H6PD; PGLS	6-phosphoglucone_N -> 6-phosphogluconate_N
R63	PPP		6-phosphogluconate_N + NADP_N -> Ribulose-5-phosphate_N + NADPH_N + CO2_N
R64	PPP	RPE	Ribulose-5-phosphate_N <-> Xylulose-5-phosphate_N

Table E.1. Metabolic reactions and genes in the developed brain model (cont.).

Reaction No	Metabolism	Gene Symbol	Reaction
R65	PPP	RPIA	Ribulose-5-phosphate_N <-> Ribose-5-phosphate_N
R66	PPP	TKT; TKTL1; TKTL2	Ribose-5-phosphate_N + Xylulose-5-phosphate_N <-> Sedoheptulose-7-phosphate_N + Glyceraldehyde-3-phosphate_N
R67	PPP	TALDO1	Sedoheptulose-7-phosphate_N + Glyceraldehyde-3-phosphate_N <-> Fructose-6-phosphate_N + Erythrose-4-phosphate_N
R68	PPP	TKT; TKTL1; TKTL2	Xylulose-5-phosphate_N + Erythrose-4-phosphate_N <-> Fructose-6-phosphate_N + Glyceraldehyde-3-phosphate_N
R69	TCA Cycle	CS; FLJ40154	Oxoloacetate_N + Acetyl-CoA_N -> Citrate_N
R70	TCA Cycle	ACO1; ACO2	Citrate_N <-> Cis_aconitate_N
R71	TCA Cycle	ACO1; ACO2	Cis_aconitate_N <-> Isocitrate_N
R72	TCA Cycle	ACLY	ATP_N + Citrate_N -> Oxoloacetate_N + Acetyl-CoA_N + ADP_N
R73	TCA Cycle	IDH3A; IDH3B; IDH3G	Isocitrate_N + NAD_NM -> alpha-ketoglutarate_N + NADH_NM + CO2_N
R74	TCA Cycle	HS09852; IDH1; IDH2	Isocitrate_N + NADP_NM -> alpha-ketoglutarate_N + NADPH_NM + CO2_N
R75	TCA Cycle	HS09852; IDH1; IDH2	Isocitrate_N + NADP_N -> alpha-ketoglutarate_N + NADPH_N + CO2_N
R76	TCA Cycle	OGDHL; DHTKD1; OGDH; DLST; DLD	alpha-ketoglutarate_N + NAD_NM -> Succinyl-CoA_N + NADH_NM + CO2_N
R77	TCA Cycle	SUCLA2; SUCLG1	Succinyl-CoA_N + ADP_N <-> Succinate_N + ATP_N
R78	TCA Cycle	SDHC; HSSUCCDH; HS12683; SDHB; SDHA; PGL2	Succinate_N + FAD_NM <-> Fumarate_N + FADH2_NM
R79	TCA Cycle	FH	Fumarate_N <-> Malate_N
R80	TCA Cycle	MDH1; MDH2	Malate_N + NAD_NM -> Oxoloacetate_N + NADH_NM
R81	TCA Cycle	MDH1; MDH2	Oxoloacetate_N + NADH_N -> Malate_N + NAD_N
R82	TCA Cycle	ME1; ME2; ME3	Malate_N + NADP_NM -> Pyruvate_N + NADPH_NM + CO2_N
R83	TCA Cycle	NNT	NADP_NM + NADH_NM -> NADPH_NM + NAD_NM

Table E.1. Metabolic reactions and genes in the developed brain model (cont.).

Reaction No	Metabolism	Gene Symbol	Reaction
R84	Oxidative Phosphorylation and ATPase	HS13127; HS13575; HS13941; HS14053; HS15241; HS15997; HS16080; HS16135; HS16463; HS16554; HS16828; HS16990; HS17072; HS17222; HS17235; HS17481; MT-ND1; MT-ND2; MT-ND3; MT-ND4; MT-ND4L; MT-ND5; MT-ND6; ND1; ND3; ND4; ND6; NDUFA1; NDUFA10; NDUFA11; NDUFA12; NDUFA13; NDUFA2; NDUFA3; NDUFA4; NDUFA5; NDUFA6; NDUFA7; NDUFA8; NDUFA9; NDUFAF1; NDUFAF2; NDUFAF3; NDUFAF4; NDUFB1; NDUFB10; NDUFB11; NDUFB2; NDUFB3; NDUFB4; NDUFB5; NDUFB6; NDUFB7; NDUFB8; NDUFB9; NDUFC1; NDUFC2; NDUFS1; NDUFS2; NDUFS3; NDUFS7; NDUFS8; NDUFV1; NDUFV2; NDUFV3	NADH_NM + Ubiquinone_N -> NAD_NM + Ubiquinol_N + 4 Hc_N
R85	Oxidative Phosphorylation and ATPase	CYC1; HS14919; HS16142; MT-CYB; UQCR; UQCR10; UQCRB; UQCRC1; UQCRC2; UQCRFS1; UQCRFSL1; UQCRH; UQCRQ	Ubiquinol_N + CytCox_N -> Ubiquinone_N + CytCred_N + 4 Hc_N
R86	Oxidative Phosphorylation and ATPase	COX1; COX2; COX3; COX4I1; COX4I2; COX5A; COX5B; COX6A1; COX6A2; COX6B1; COX6B2; COX6C; COX7A1; COX7A2; COX7A2L; COX7AP2; COX7B; COX7B2; COX7C; COX8A; HS09101; HS16039; HS16147; HS17660; HS17765; MT-CO1; MT-CO2; MT-CO3	CytCred_N + 0.5 O2_N -> CytCox_N + 2 Hc_N
R87	Oxidative Phosphorylation and ATPase	ETFDH	FADH2_NM + Ubiquinone_N -> FAD_NM + Ubiquinol_N

Table E.1. Metabolic reactions and genes in the developed brain model (cont.).

Reaction No	Metabolism	Gene Symbol	Reaction
R88	Oxidative Phosphorylation and ATPase	ATP5A1; ATP5B; ATP5C1; ATP5D; ATP5E; ATP5EP2; ATP5F1; ATP5H; ATP5I; ATP5J2; ATP5L; ATP5L2; ATP5S; ATP6; ATP8; HS15678; HS16048; HS16291; HS16707; HS16872; HS16911; HS16919; HS17378; HS17406; MTATP6; MTATP8	ADP_N + 4 Hc_N -> ATP_N
R89	Glutamate - Glutamine Cycle	GLUD1; GLUD2	alpha-ketoglutarate_N + NH3_N + NADPH_NM <-> Glutamate_N + NADP_NM
R90	Glutamate - Glutamine Cycle	GLUD1; GLUD2	alpha-ketoglutarate_A + NH3_A + NADH_AM <-> Glutamate_A + NAD_AM
R91	Glutamate - Glutamine Cycle		Glutamate_N + ATP_A -> Glutamate_A + ADP_A
R92	Glutamate - Glutamine Cycle	GLUD1; GLUD2	alpha-ketoglutarate_A + NH3_A + NADPH_AM <-> Glutamate_A + NADP_AM
R93	Glutamate - Glutamine Cycle	GLUD1; GLUD2	alpha-ketoglutarate_N + NH3_N + NADH_NM <-> Glutamate_N + NAD_NM
R94	Glutamate - Glutamine Cycle	GLUL; HS17115	Glutamate_A + NH3_A + ATP_A -> Glutamine_A + ADP_A
R95	Glutamate - Glutamine Cycle		Glutamine_A -> Glutamine_N
R96	Glutamate - Glutamine Cycle	ASNS; GLS; GLS2	Glutamine_N -> Glutamate_N + NH3_N
R97	GABA Cycle	GAD1; GAD2; HS13905	Glutamate_N -> GABA_N + CO2_N
R98	GABA Cycle		GABA_N <-> GABA_A
R99	GABA Cycle	ABAT	GABA_A + alpha-ketoglutarate_A -> Glutamate_A + SuccinateSAL_A
R100	GABA Cycle	ALDH5A1	SuccinateSAL_A + NAD_AM -> NADH_AM + Succinate_A
R101	GABA Cycle	ABAT	GABA_N + alpha-ketoglutarate_N -> Glutamate_N + SuccinateSAL_N
R102	GABA Cycle	ALDH5A1	SuccinateSAL_N + NAD_NM -> NADH_NM + Succinate_N
R103	Aspartate Metabolism	GOT1; GOT1L1; GOT2; HS14628; HS16074	Oxoloacetate_N + Glutamate_N <-> Aspartate_N + alpha-ketoglutarate_N
R104	Aspartate Metabolism		Aspartate_N <-> Aspartate_A
R105	Aspartate Metabolism	GOT1; GOT1L1; GOT2; HS14628; HS16074	Aspartate_A + alpha-ketoglutarate_A <-> Oxoloacetate_A + Glutamate_A
R106	Asparagine Metabolism	ASNS	Glutamine_N + Aspartate_N + ATP_N <-> Glutamate_N + Asparagine_N + AMP_N
R107	Histamine Metabolism	HDC	Histidine_N <-> Histamine_N + CO2_N
R108	Histamine Metabolism	HNMT	Histamine_N + S-adenosyl-L-methionine_N -> S-adenosyl-L-homocysteine_N + methylhistamine_N
R109	Alanine Metabolism	GPT; GPT2	Pyruvate_N + Glutamate_N <-> alpha-ketoglutarate_N + Alanine_N

Table E.1. Metabolic reactions and genes in the developed brain model (cont.).

Reaction No	Metabolism	Gene Symbol	Reaction
R110	Alanine Metabolism		Alanine_N <-> Alanine_A
R111	Alanine Metabolism	GPT; GPT2	Alanine_A + alpha-ketoglutarate_A <-> Pyruvate_A + Glutamate_A
R112	Glycine-Serine Metabolism	PHGDH; PHGDHL1	3-phosphoglycerate_A + NAD_A <-> 3-phosphohydroxypyruvate_A + NADH_A
R113	Glycine-Serine Metabolism	PSAT1	3_phospho_serine_A + alpha-ketoglutarate_A <-> 3-phosphohydroxypyruvate_A + Glutamate_A
R114	Glycine-Serine Metabolism	PSPH; PSPHL	3_phospho_serine_A -> Serine_A
R115	Glycine-Serine Metabolism	SDS; SDSL	Serine_A -> Pyruvate_A + NH3_A
R116	Glycine-Serine Metabolism		Serine_A -> Serine_N
R117	Glycine-Serine Metabolism	SHMT1; SHMT2	Serine_N + tetrahydrofolate_N -> Glycine_N
R118	Glycine-Serine Metabolism		Glycine_N -> Glycine_A
R119	Glycine-Serine Metabolism		Glycine_A + NAD_AM + tetrahydrofolate_A -> CO2_A + NH3_A + NADH_AM
R120	Glycine-Serine Metabolism	SHMT1; SHMT2	Glycine_A -> tetrahydrofolate_A + Serine_A
R121	Leucine Metabolism	BCAT1; BCAT2	Leucine_A + alpha-ketoglutarate_A <-> KIC_A + Glutamate_A
R122	Leucine Metabolism		KIC_A + NAD_AM -> Isovaleryl-CoA_A + CO2_A + NADH_AM
R123	Leucine Metabolism	IVD	Isovaleryl-CoA_A + FAD_AM <-> 3_methylcrotonyl-Coa_A + FADH2_AM
R124	Leucine Metabolism	MCCC1; MCCC2	Bicarbonate_A + 3_methylcrotonyl-Coa_A + ATP_A <-> ADP_A + 3_methylglutaconyl-Coa_A
R125	Leucine Metabolism	AUH	3_methylglutaconyl-Coa_A <-> 3_hydroxy_3_methylglutaryl-Coa_A
R126	Leucine Metabolism	HMGCL; HMGCLL1	3_hydroxy_3_methylglutaryl-Coa_A <-> Acetoacetate_A + Acetyl-CoA_A
R127	Leucine Metabolism; Ketone Body Metabolism	OXCT1	Acetoacetate_A + Succinyl-CoA_A -> Acetoacetyl-CoA_A + Succinate_A
R128	Leucine Metabolism; Ketone Body Metabolism	ACAA1; ACAT1; ACAT2; HADHB	Acetoacetyl-CoA_A <-> 2 Acetyl-CoA_A
R129	Leucine Metabolism		KIC_A -> KIC_N
R130	Leucine Metabolism	BCAT1; BCAT2	KIC_N + Glutamate_N <-> Leucine_N + alpha-ketoglutarate_N
R131	Leucine Metabolism		Leucine_N -> Leucine_A
R132	Valine Metabolism	BCAT1; BCAT2	Valine_A + alpha-ketoglutarate_A <-> KIV_A + Glutamate_A
R133	Valine Metabolism	BCKDHA; BCKDHB; DBT; DLD	KIV_A + NAD_AM -> Isobutyryl-CoA_A + CO2_A + NADH_AM
R134	Valine Metabolism	ACAD8; ACADSB	Isobutyryl-CoA_A + FAD_AM -> FADH2_AM + methylacrylyl-CoA_A
R135	Valine Metabolism	ECHS1; EHHADH; HADHA; HS15845; HS17054	methylacrylyl-CoA_A -> S-3-hydroxy-isobutyryl-CoA_A
R136	Valine Metabolism	HIBCH	S-3-hydroxy-isobutyryl-CoA_A -> S-3-hydroxy-isobutyrate_A

Table E.1. Metabolic reactions and genes in the developed brain model (cont.).

Reaction No	Metabolism	Gene Symbol	Reaction
R137	Valine Metabolism	HIBADH	S-3-hydroxy-isobutyrate_A + NAD_AM -> S-methylmalonate-semialdehyde + NADH_AM
R138	Valine Metabolism	ALDH6A1	S-methylmalonate-semialdehyde + NAD_AM -> NADH_AM + Propionyl-CoA_A + Bicarbonate_A
R139	Valine Metabolism; Isoleucine Metabolism	PCCA; PCCB	Propionyl-CoA_A + Bicarbonate_A + ATP_A -> S-methylmalonyl-CoA_A + ADP_A
R140	Valine Metabolism; Isoleucine Metabolism	MCEE	S-methylmalonyl-CoA_A -> R-methylmalonyl-CoA_A
R141	Valine Metabolism; Isoleucine Metabolism	MUT	R-methylmalonyl-CoA_A -> Succinyl-CoA_A
R142	Valine Metabolism		KIV_A -> KIV_N
R143	Valine Metabolism	BCAT1; BCAT2	KIV_N + Glutamate_N <-> Valine_N + alpha-ketoglutarate_N
R144	Valine Metabolism		Valine_N -> Valine_A
R145	Isoleucine Metabolism	BCAT1; BCAT2	Isoleucine_A + alpha-ketoglutarate_A <-> KMV_A + Glutamate_A
R146	Isoleucine Metabolism	DLD; DBT; BCKDHA; BCKDHB	KMV_A + NAD_AM -> Methylbutyryl-CoA_A + CO2_A + NADH_AM
R147	Isoleucine Metabolism	ACADSB	Methylbutyryl-CoA_A + FAD_AM -> FADH2_AM + E-2-methylcrotonoyl-CoA_A
R148	Isoleucine Metabolism	ECHS1; EHHADH; HADHA; HS15845; HS17054	E-2-methylcrotonoyl-CoA_A -> 2-methyl-3-hydroxybutyryl-CoA_A
R149	Isoleucine Metabolism	HSD17B10	2-methyl-3-hydroxybutyryl-CoA_A + NAD_AM -> NADH_AM + 2-methylacetoacetyl-CoA_A
R150	Isoleucine Metabolism	ACAT1; ACAT2; HADHB	2-methylacetoacetyl-CoA_A <-> Propionyl-CoA_A + Acetyl-CoA_A
R151	Isoleucine Metabolism		KMV_A -> KMV_N
R152	Isoleucine Metabolism	BCAT1; BCAT2	KMV_N + Glutamate_N <-> Isoleucine_N + alpha-ketoglutarate_N
R153	Isoleucine Metabolism		Isoleucine_N -> Isoleucine_A
R154	Lysine Metabolism	AASS	Lysine_N + alpha-ketoglutarate_N + NADPH_N -> Saccharopine_N + NADP_N
R155	Lysine Metabolism	AASS; SCCPDH	Saccharopine_N + NAD_N -> Glutamate_N + NADH_N + 2-aminoadipate_semialdehyde_N
R156	Lysine Metabolism	ALDH7A1	2-aminoadipate_semialdehyde_N <-> S-2,3,4,5-tetrahydropiperidine-2-carboxylate_N
R157	Lysine Metabolism	ALDH7A1	S-2,3,4,5-tetrahydropiperidine-2-carboxylate_N + NAD_N -> 2-aminoadipate_N + NADH_N
R158	Lysine Metabolism		2-aminoadipate_N + alpha-ketoglutarate_N -> alpha-ketoadipate_N + Glutamate_N
R159	Lysine Metabolism		alpha-ketoadipate_N + NAD_NM -> CO2_N + NADH_NM + glutaryl-CoA_N
R160	Lysine Metabolism	GCDH	FAD_NM + glutaryl-CoA_N -> glutaconyl-CoA_N + FADH2_NM
R161	Lysine Metabolism	GCDH	glutaconyl-CoA_N -> CO2_N + crotonyl-CoA_N
R162	Lysine Metabolism		crotonyl-CoA_N -> S-3-hydroxybutanoyl-CoA_N

Table E.1. Metabolic reactions and genes in the developed brain model (cont.).

Reaction No	Metabolism	Gene Symbol	Reaction
R163	Lysine Metabolism		S-3-hydroxybutanoyl-CoA_N + NAD_NM -> Acetoacetyl-CoA_N + NADH_NM
R164	Lysine Metabolism; Ketone Body Metabolism	ACAA1; ACAT1; ACAT2; HADHB	Acetoacetyl-CoA_N <-> 2 Acetyl-CoA_N
R165	Phenylalanine - Tyrosine Metabolism	PAH	Phenylalanine_N + Tetrahydrobiopterin_N + O2_N -> Tyrosine_N + 4-alpha-hydroxy-tetrahydrobiopterin_N
R166	Phenylalanine - Tyrosine Metabolism	PCBD1; PCBD2	4-alpha-hydroxy-tetrahydrobiopterin_N -> Dihydrobiopterin_N
R167	Phenylalanine - Tyrosine Metabolism	QDPR	Dihydrobiopterin_N + NADH_N -> Tetrahydrobiopterin_N + NAD_N
R168	Phenylalanine - Tyrosine Metabolism	TH	Tyrosine_N + Tetrahydrobiopterin_N + O2_N -> L-DOPA_N + 4-alpha-hydroxy-tetrahydrobiopterin_N
R169	Phenylalanine - Tyrosine Metabolism	DDC	L-DOPA_N -> Dopamine_N + CO2_N
R170	Phenylalanine - Tyrosine Metabolism	DBH	Dopamine_N + O2_N -> Norepinephrine_N
R171	Phenylalanine - Tyrosine Metabolism	PNMT	Norepinephrine_N + S-adenosyl-L-methionine_N -> S-adenosyl-L-homocysteine_N + Epinephrine_N
R172	Phenylalanine - Tyrosine Metabolism		Dopamine_N -> Dopamine_A
R173	Phenylalanine - Tyrosine Metabolism	DBH	Dopamine_A + O2_A -> Norepinephrine_A
R174	Tryptophan Metabolism	TPH1; TPH2	Tryptophan_N + Tetrahydrobiopterin_N + O2_N -> 5-hydroxytryptophan_N + 4-alpha-hydroxy-tetrahydrobiopterin_N
R175	Tryptophan Metabolism	DDC	5-hydroxytryptophan_N -> Seratonin_N + CO2_N
R176	Tryptophan Metabolism	AANAT	Seratonin_N + Acetyl-CoA_N -> N-acetyl-serotonin_N
R177	Tryptophan Metabolism	ASMT	N-acetyl-serotonin_N + S-adenosyl-L-methionine_N -> S-adenosyl-L-homocysteine_N + Melatonin_N
R178	Acetylcholine Metabolism	CHAT	Choline_N + Acetyl-CoA_N <-> Acetylcholine_N
R179	Proline metabolism	P5CR2; PYCR1; PYCRL	S-1-pyrroline-5-carboxylate_A + NADPH_A -> proline_A + NADP_A
R180	Proline metabolism	KIAA1653; PRODH	proline_A + FAD_AM -> S-1-pyrroline-5-carboxylate_A + FADH2_AM
R181	Methionine Metabolism		methionine -> methionine_A
R182	Methionine Metabolism	MAT1A; MAT2A; MAT2B	ATP_A + methionine_A -> S-adenosyl-L-methionine_A
R183	Methionine Metabolism		S-adenosyl-L-methionine_A -> S-adenosyl-L-homocysteine_A
R184	Methionine Metabolism	AHCY; AHCYL1; AHCYL2; HS15808; HS15871; HS17583	S-adenosyl-L-homocysteine_A -> L-homocysteine_A + adenosine_A
R185	Methionine Metabolism	CBS	L-homocysteine_A + Serine_A -> L-cystathionine_A
R186	Methionine Metabolism	CTH	L-cystathionine_A -> NH3_A + 2-oxobutanoate_A + Cysteine_A

Table E.1. Metabolic reactions and genes in the developed brain model (cont.).

Reaction No	Metabolism	Gene Symbol	Reaction
R187	Methionine Metabolism	MTR	L-homocysteine_A -> methionine_A + tetrahydrofolate_A
R188	Methionine Metabolism	BCKDHA; BCKDHB; DBT; DLD	2-oxobutanoate_A + NAD_A -> Propionyl-CoA_A + CO2_A + NADH_A
R189	Methionine Metabolism		methionine -> methionine_N
R190	Methionine Metabolism	MAT1A; MAT2A; MAT2B	ATP_N + methionine_N -> S-adenosyl-L-methionine_N
R191	Methionine Metabolism		S-adenosyl-L-methionine_N -> S-adenosyl-L-homocysteine_N
R192	Methionine Metabolism	AHCY; AHCYL1; AHCYL2; HS15808; HS15871; HS17583	S-adenosyl-L-homocysteine_N -> L-homocysteine_N + adenosine_N
R193	Methionine Metabolism	CBS	L-homocysteine_N + Serine_N -> L-cystathionine_N
R194	Methionine Metabolism	CTH	L-cystathionine_N -> NH3_N + 2-oxobutanoate_N + Cysteine_N
R195	Methionine Metabolism	MTR	L-homocysteine_N -> methionine_N + tetrahydrofolate_N
R196	Threonine Metabolism		threonine -> threonine_A
R197	Threonine Metabolism		threonine_A + NAD_A -> 2-amino-3-oxobutanoate_A + NADH_A
R198	Threonine Metabolism	GCAT	2-amino-3-oxobutanoate_A -> Glycine_A + Acetyl-CoA_A
R199	Threonine Metabolism		threonine -> threonine_N
R200	Threonine Metabolism		threonine_N + NAD_N -> 2-amino-3-oxobutanoate_N + NADH_N
R201	Threonine Metabolism	GCAT	2-amino-3-oxobutanoate_N -> Glycine_N + Acetyl-CoA_N
R202	Cholesterol Synthesis	HMGCS1; HMGCS2	Acetyl-CoA_A + Acetoacetyl-CoA_A -> s3_hydroxy_3_methylglutaryl-Coa_A
R203	Cholesterol Synthesis	HMGCR	s3_hydroxy_3_methylglutaryl-Coa_A + 2 NADPH_A -> R-mevalonate_A + 2 NADP_A
R204	Cholesterol Synthesis	MVK	R-mevalonate_A + ATP_A -> mevalonate-5-phosphate_A + ADP_A
R205	Cholesterol Synthesis	PMVK	mevalonate-5-phosphate_A + ATP_A <-> mevalonate-diphosphate_A + ADP_A
R206	Cholesterol Synthesis	MVD	mevalonate-diphosphate_A + ATP_A -> isopentenyl_diphosphate_A + CO2_A + ADP_A
R207	Cholesterol Synthesis	IDI1; IDI2	isopentenyl_diphosphate_A -> dimethylallyl_diphosphate_A
R208	Cholesterol Synthesis	FDPS; GGPS1; HS17470	dimethylallyl_diphosphate_A + isopentenyl_diphosphate_A -> geranyl_diphosphate_A
R209	Cholesterol Synthesis	FDPS; GGPS1; HS17470	isopentenyl_diphosphate_A + geranyl_diphosphate_A -> 2E_6E_farnesyl_diphosphate_A
R210	Cholesterol Synthesis	FDFT1	2 2E_6E_farnesyl_diphosphate_A -> presqualene_diphosphate_A
R211	Cholesterol Synthesis	FDFT1	presqualene_diphosphate_A + NADPH_A -> squalene_A + NADP_A
R212	Cholesterol Synthesis	SQLE	squalene_A + NADPH_A + O2_A -> S_2_3_epoxysqualene_A + NADP_A
R213	Cholesterol Synthesis	LSS	S_2_3_epoxysqualene_A -> lanosterol_A
R214	Cholesterol Synthesis	CYP51A1	lanosterol_A + NADPH_A + O2_A -> 4-4-dimethyl-14alpha-hydroxymethyl-5alpha-cholesta-8-24-dien-3beta-ol_A + NADP_A

Table E.1. Metabolic reactions and genes in the developed brain model (cont.).

Reaction No	Metabolism	Gene Symbol	Reaction
R215	Cholesterol Synthesis	CYP51A1	4-4-dimethyl-14alpha-hydroxymethyl-5alpha-cholesta-8-24-dien-3beta-ol_A + NADPH_A + O2_A -> 4-4-dimethyl-14alpha-formyl-5alpha-cholesta-8-24-dien-3beta-ol_A + NADP_A
R216	Cholesterol Synthesis	CYP51A1	4-4-dimethyl-14alpha-formyl-5alpha-cholesta-8-24-dien-3beta-ol_A + NADPH_A + O2_A -> 4-4-dimethyl-5-alpha-cholesta-8-14-24-trien-3-beta-ol_A + NADP_A + formate_A
R217	Cholesterol Synthesis	LBR; TM7SF2	4-4-dimethyl-5-alpha-cholesta-8-14-24-trien-3-beta-ol_A + NADPH_A -> 4_4-dimethylzymosterol_A + NADP_A
R218	Cholesterol Synthesis	SC4MOL	4_4-dimethylzymosterol_A + NADPH_A + O2_A -> 4alpha-hydroxymethyl-4beta-methyl-5alpha-cholesta-8-24-dien-3beta-ol_A + NADP_A
R219	Cholesterol Synthesis	SC4MOL	4alpha-hydroxymethyl-4beta-methyl-5alpha-cholesta-8-24-dien-3beta-ol_A + NADPH_A + O2_A -> 4alpha-formyl-4beta-methyl-5alpha-cholesta-8-24-dien-3beta-ol_A + NADP_A
R220	Cholesterol Synthesis	SC4MOL	4alpha-formyl-4beta-methyl-5alpha-cholesta-8-24-dien-3beta-ol_A + NADPH_A + O2_A -> 4alpha-carboxy-4beta-methyl-5alpha-cholesta-8-24-dien-3beta-ol_A + NADP_A
R221	Cholesterol Synthesis	NSDHL	4alpha-carboxy-4beta-methyl-5alpha-cholesta-8-24-dien-3beta-ol_A + NADP_A -> 3-keto-4-methylzymosterol_A + NADPH_A + CO2_A
R222	Cholesterol Synthesis	HSD17B7	3-keto-4-methylzymosterol_A + NADPH_A -> 4alpha-methyl-zymosterol_A + NADP_A
R223	Cholesterol Synthesis	SC4MOL	4alpha-methyl-zymosterol_A + NADPH_A + O2_A -> 4alpha-hydroxymethyl-5alpha-cholesta-8-24-dien-3beta-ol_A + NADP_A
R224	Cholesterol Synthesis	SC4MOL	4alpha-hydroxymethyl-5alpha-cholesta-8-24-dien-3beta-ol_A + NADPH_A + O2_A -> 4alpha-formyl-5alpha-cholesta-8-24-dien-3beta-ol_A + NADP_A
R225	Cholesterol Synthesis	SC4MOL	4alpha-formyl-5alpha-cholesta-8-24-dien-3beta-ol_A + NADPH_A + O2_A -> 4alpha-carboxy-5alpha-cholesta-8-24-dien-3beta-ol_A + NADP_A
R226	Cholesterol Synthesis	NSDHL	4alpha-carboxy-5alpha-cholesta-8-24-dien-3beta-ol_A + NADP_A -> 5alpha-cholesta-8-24-dien-3-one_A + NADPH_A + CO2_A
R227	Cholesterol Synthesis	HSD17B7	5alpha-cholesta-8-24-dien-3-one_A + NADPH_A -> zymosterol_A + NADP_A
R228	Cholesterol Synthesis	EBP	zymosterol_A -> 5alpha-cholesta-7-24-dien-3beta-ol_A
R229	Cholesterol Synthesis	SC5DL	5alpha-cholesta-7-24-dien-3beta-ol_A + NADPH_A + O2_A -> 7-dehydrodesmosterol_A + NADP_A
R230	Cholesterol Synthesis	DHCR7	7-dehydrodesmosterol_A + NADPH_A -> desmosterol_A + NADP_A
R231	Cholesterol Synthesis	DHCR24	desmosterol_A + NADPH_A -> Cholesterol_A + NADP_A
R232	Cholesterol Synthesis	DHCR24	5alpha-cholesta-7-24-dien-3beta-ol_A + NADPH_A -> lathosterol_A + NADP_A
R233	Cholesterol Synthesis	SC5DL	lathosterol_A + NADPH_A + O2_A -> 7-dehydro-cholesterol_A + NADP_A
R234	Cholesterol Synthesis	DHCR7	7-dehydro-cholesterol_A + NADPH_A -> Cholesterol_A + NADP_A
R235	Cholesterol Synthesis	DHCR24	lanosterol_A + NADPH_A -> 24-25-dihydrolanosterol_A + NADP_A
R236	Cholesterol Synthesis	CYP51A1	24-25-dihydrolanosterol_A + NADPH_A + O2_A -> 4-4-dimethyl-14alpha-hydroxymethyl-5alpha-cholesta-8-en-3beta-ol_A + NADP_A

Table E.1. Metabolic reactions and genes in the developed brain model (cont.).

Reaction No	Metabolism	Gene Symbol	Reaction
R237	Cholesterol Synthesis	CYP51A1	4-4-dimethyl-14alpha-hydroxymethyl-5alpha-cholesta-8-en-3beta-ol_A + NADPH_A + O2_A -> 4-4-dimethyl-14alpha-formyl-5alpha-cholesta-8-en-3beta-ol_A + NADP_A
R238	Cholesterol Synthesis	CYP51A1	4-4-dimethyl-14alpha-formyl-5alpha-cholesta-8-en-3beta-ol_A + NADPH_A + O2_A -> 4-4-dimethyl-5-alpha-cholesta-8-14-dien-3-beta-ol_A + NADP_A + formate_A
R239	Cholesterol Synthesis	LBR; TM7SF2	4-4-dimethyl-5-alpha-cholesta-8-14-dien-3-beta-ol_A + NADPH_A -> 4-4-dimethyl-5alpha-cholesta-8-en-3-beta-ol_A + NADP_A
R240	Cholesterol Synthesis	SC4MOL	4-4-dimethyl-5alpha-cholesta-8-en-3-beta-ol_A + NADPH_A + O2_A -> 4alpha-hydroxymethyl-4beta-methyl-5alpha-cholesta-8-en-3beta-ol_A + NADP_A
R241	Cholesterol Synthesis	SC4MOL	4alpha-hydroxymethyl-4beta-methyl-5alpha-cholesta-8-en-3beta-ol_A + NADPH_A + O2_A -> 4alpha-formyl-4beta-methyl-5alpha-cholesta-8-en-3beta-ol_A + NADP_A
R242	Cholesterol Synthesis	SC4MOL	4alpha-formyl-4beta-methyl-5alpha-cholesta-8-en-3beta-ol_A + NADPH_A + O2_A -> 4alpha-carboxy-4beta-methyl-5alpha-cholesta-8-en-3beta-ol_A + NADP_A
R243	Cholesterol Synthesis	NSDHL	4alpha-carboxy-4beta-methyl-5alpha-cholesta-8-en-3beta-ol_A + NADP_A -> 4alpha-methyl-5alpha-cholesta-8-en-3-one_A + NADPH_A + CO2_A
R244	Cholesterol Synthesis	HSD17B7	4alpha-methyl-5alpha-cholesta-8-en-3-one_A + NADPH_A -> 4alpha-methyl-cholesta-8-enol_A + NADP_A
R245	Cholesterol Synthesis	SC4MOL	4alpha-methyl-cholesta-8-enol_A + NADPH_A + O2_A -> 4alpha-hydroxymethyl-5alpha-cholesta-8-en-3beta-ol_A + NADP_A
R246	Cholesterol Synthesis	SC4MOL	4alpha-hydroxymethyl-5alpha-cholesta-8-en-3beta-ol_A + NADPH_A + O2_A -> 4alpha-formyl-5alpha-cholesta-8-en-3beta-ol_A + NADP_A
R247	Cholesterol Synthesis	SC4MOL	4alpha-formyl-5alpha-cholesta-8-en-3beta-ol_A + NADPH_A + O2_A -> 4alpha-carboxy-5alpha-cholesta-8-en-3beta-ol_A + NADP_A
R248	Cholesterol Synthesis	NSDHL	4alpha-carboxy-5alpha-cholesta-8-en-3beta-ol_A + NADP_A -> 5alpha-cholesta-8-en-3-one_A + CO2_A + NADPH_A
R249	Cholesterol Synthesis	HSD17B7	5alpha-cholesta-8-en-3-one_A + NADPH_A -> zymostenol_A + NADP_A
R250	Cholesterol Synthesis	EBP	zymostenol_A -> lathosterol_A
R251	Cholesterol Synthesis		formate_A <-> CO2_A
R252	Cholesterol Synthesis		Cholesterol_A -> Cholesterol_N
R253	Fatty Acid Synthesis	FASN	Acetoacetyl-acp_A + NADPH_A -> R-3-hydroxybutanoyl-acp_A + NADP_A
R254	Fatty Acid Synthesis	FASN; RPP14	R-3-hydroxybutanoyl-acp_A -> Crotonyl-acp_A
R255	Fatty Acid Synthesis	FASN	Crotonyl-acp_A + NADPH_A -> Butyryl-acp_A + NADP_A
R256	Fatty Acid Synthesis	FASN; FLJ40154; OXSM	Butyryl-acp_A + Malonyl-CoA_A -> 3-oxo-hexanoyl-acp_A + CO2_A
R257	Fatty Acid Synthesis		3-oxo-hexanoyl-acp_A + NADPH_A -> R-3-hydroxyhexanoyl-acp_A + NADP_A
R258	Fatty Acid Synthesis	FASN; RPP14	R-3-hydroxyhexanoyl-acp_A -> trans_hex-2-enoyl-acp_A
R259	Fatty Acid Synthesis	FASN	trans_hex-2-enoyl-acp_A + NADPH_A -> Hexanoyl-acp_A + NADP_A
R260	Fatty Acid Synthesis	FASN; FLJ40154; OXSM	Hexanoyl-acp_A + Malonyl-CoA_A -> 3-oxo-octanoyl-acp_A + CO2_A

Table E.1. Metabolic reactions and genes in the developed brain model (cont.).

Reaction No	Metabolism	Gene Symbol	Reaction
R261	Fatty Acid Synthesis		3-oxo-octanoyl-acp_A + NADPH_A -> R-3-hydroxyoctanoyl-acp_A + NADP_A
R262	Fatty Acid Synthesis	FASN; RPP14	R-3-hydroxyoctanoyl-acp_A -> trans_oct-2-enoyl-acp_A
R263	Fatty Acid Synthesis	FASN	trans_oct-2-enoyl-acp_A + NADPH_A -> Octanoyl-acp_A + NADP_A
R264	Fatty Acid Synthesis	FASN; FLJ40154; OXSM	Octanoyl-acp_A + Malonyl-CoA_A -> 3-oxo-decanoyl-acp_A + CO2_A
R265	Fatty Acid Synthesis		3-oxo-decanoyl-acp_A + NADPH_A -> R-3-hydroxydecanoyl-acp_A + NADP_A
R266	Fatty Acid Synthesis	FASN; RPP14	R-3-hydroxydecanoyl-acp_A -> trans-delta2-decenoyl-acp_A
R267	Fatty Acid Synthesis	FASN	trans-delta2-decenoyl-acp_A + NADPH_A -> Decanoyl-acp_A + NADP_A
R268	Fatty Acid Synthesis	FASN; FLJ40154; OXSM	Decanoyl-acp_A + Malonyl-CoA_A -> 3-oxo-dodecanoyl-acp_A + CO2_A
R269	Fatty Acid Synthesis		3-oxo-dodecanoyl-acp_A + NADPH_A -> R-3-hydroxydodecanoyl-acp_A + NADP_A
R270	Fatty Acid Synthesis	FASN; RPP14	R-3-hydroxydodecanoyl-acp_A -> trans_dodec-2-enoyl-acp_A
R271	Fatty Acid Synthesis	FASN	trans_dodec-2-enoyl-acp_A + NADPH_A -> Dodecanoyl-acp_A + NADP_A
R272	Fatty Acid Synthesis		Dodecanoyl-acp_A -> Laurate_A
R273	Fatty Acid Synthesis	FASN; FLJ40154; OXSM	Dodecanoyl-acp_A + Malonyl-CoA_A -> 3-oxo-myristoyl-acp_A + CO2_A
R274	Fatty Acid Synthesis		3-oxo-myristoyl-acp_A + NADPH_A -> 3R-3-hydroxymyristoyl-acp_A + NADP_A
R275	Fatty Acid Synthesis	FASN; RPP14	3R-3-hydroxymyristoyl-acp_A -> trans_tetradec-2-enoyl-acp_A
R276	Fatty Acid Synthesis	FASN	trans_tetradec-2-enoyl-acp_A + NADPH_A -> Myristoyl-acp_A + NADP_A
R277	Fatty Acid Synthesis	FASN; FLJ40154; OXSM	Myristoyl-acp_A + Malonyl-CoA_A -> 3-oxo-palmitoyl-acp_A + CO2_A
R278	Fatty Acid Synthesis		3-oxo-palmitoyl-acp_A + NADPH_A -> R-3-hydroxypalmitoyl-acp_A + NADP_A
R279	Fatty Acid Synthesis	FASN; RPP14	R-3-hydroxypalmitoyl-acp_A -> trans_hexadecenoyl-acp_A
R280	Fatty Acid Synthesis	FASN	trans_hexadecenoyl-acp_A + NADPH_A -> Palmitoyl-acp_A + NADP_A
R281	Fatty Acid Synthesis	FASN	Palmitoyl-acp_A <-> Palmitate_A
R282	Fatty Acid Synthesis	MLYCD	Acetyl-CoA_A + CO2_A <-> Malonyl-CoA_A
R283	Fatty Acid Synthesis	FASN	Acetyl-CoA_A <-> Acetyl-acp_A
R284	Fatty Acid Synthesis	FASN; MCAT	Malonyl-CoA_A <-> Malonyl-acp_A
R285	Fatty Acid Synthesis	FASN; FLJ40154; OXSM	Malonyl-acp_A + Acetyl-acp_A <-> Acetoacetyl-acp_A + CO2_A
R286	Fatty Acid Synthesis	ACACA; ACACB; PCCA; PCCB	Acetyl-CoA_A + ATP_A + Bicarbonate_A <-> Malonyl-CoA_A + ADP_A
R287	Fatty Acid Synthesis	CA1; CA10; CA11; CA13; CA3; CA4; CA5A; CA5B; CA6; CA7; CA8; CA9; HS15759	Bicarbonate_A <-> CO2_A
R288	Fatty Acid Synthesis	ACSBG1; ACSBG2; ACSL1; ACSL3; ACSL4; ACSL5; SLC27A2	Palmitate_A + ATP_A -> Palmitoyl-CoA_A + AMP_A

Table E.1. Metabolic reactions and genes in the developed brain model (cont.).

Reaction No	Metabolism	Gene Symbol	Reaction
R289	Fatty Acid Synthesis	ELOVL1; ELOVL6	Palmitoyl-CoA_A + Malonyl-CoA_A -> 3-oxo-stearoyl-CoA_A + CO2_A
R290	Fatty Acid Synthesis		3-oxo-stearoyl-CoA_A + NADPH_A -> 3-hydroxy-stearoyl-CoA_A + NADP_A
R291	Fatty Acid Synthesis		3-hydroxy-stearoyl-CoA_A -> trans-2-3-stearoyl-CoA_A
R292	Fatty Acid Synthesis		trans-2-3-stearoyl-CoA_A + NADPH_A -> Stearoyl-CoA_A + NADP_A
R293	Fatty Acid Synthesis	ACOT2; ACOT4; ACOT7	Stearoyl-CoA_A -> Stearate_A
R294	Fatty Acid Synthesis	FADS1; FADS2; FADS6; SCD; SCD5	Stearoyl-CoA_A + O2_A -> Oleoyl-CoA_A
R295	Fatty Acid Synthesis	ACOT2; ACOT4	Oleoyl-CoA_A -> Oleate_A
R296	Fatty Acid Synthesis		Linoleate_A + 2 O2_A + 2 NADH_A + ATP_A + CO2_A + Acetyl-CoA_A -> Arachidonate_A + ADP_A + 2 NAD_A
R297	Fatty Acid Synthesis		Linolenate_A + 3 O2_A + 3 NADH_A + 2 ATP_A + 2 CO2_A + 2 Acetyl-CoA_A -> Decosahexenoate_A + 2 ADP_A + 3 NAD_A
R298	Fatty Acid Synthesis	FASN	Acetoacetyl-acp_N + NADPH_N -> R-3-hydroxybutanoyl-acp_N + NADP_N
R299	Fatty Acid Synthesis	FASN; RPP14	R-3-hydroxybutanoyl-acp_N -> Crotonyl-acp_N
R300	Fatty Acid Synthesis	FASN	Crotonyl-acp_N + NADPH_N -> Butyryl-acp_N + NADP_N
R301	Fatty Acid Synthesis	FASN; FLJ40154; OXSM	Butyryl-acp_N + Malonyl-CoA_N -> 3-oxo-hexanoyl-acp_N + CO2_N
R302	Fatty Acid Synthesis		3-oxo-hexanoyl-acp_N + NADPH_N -> R-3-hydroxyhexanoyl-acp_N + NADP_N
R303	Fatty Acid Synthesis	FASN; RPP14	R-3-hydroxyhexanoyl-acp_N -> trans_hex-2-enoyl-acp_N
R304	Fatty Acid Synthesis	FASN	trans_hex-2-enoyl-acp_N + NADPH_N -> Hexanoyl-acp_N + NADP_N
R305	Fatty Acid Synthesis	FASN; FLJ40154; OXSM	Hexanoyl-acp_N + Malonyl-CoA_N -> 3-oxo-octanoyl-acp_N + CO2_N
R306	Fatty Acid Synthesis		3-oxo-octanoyl-acp_N + NADPH_N -> R-3-hydroxyoctanoyl-acp_N + NADP_N
R307	Fatty Acid Synthesis	FASN; RPP14	R-3-hydroxyoctanoyl-acp_N -> trans_oct-2-enoyl-acp_N
R308	Fatty Acid Synthesis	FASN	trans_oct-2-enoyl-acp_N + NADPH_N -> Octanoyl-acp_N + NADP_N
R309	Fatty Acid Synthesis	FASN; FLJ40154; OXSM	Octanoyl-acp_N + Malonyl-CoA_N -> 3-oxo-decanoyl-acp_N + CO2_N
R310	Fatty Acid Synthesis		3-oxo-decanoyl-acp_N + NADPH_N -> R-3-hydroxydecanoyl-acp_N + NADP_N
R311	Fatty Acid Synthesis	FASN; RPP14	R-3-hydroxydecanoyl-acp_N -> trans-delta2-decenoyl-acp_N
R312	Fatty Acid Synthesis	FASN	trans-delta2-decenoyl-acp_N + NADPH_N -> Decanoyl-acp_N + NADP_N
R313	Fatty Acid Synthesis	FASN; FLJ40154; OXSM	Decanoyl-acp_N + Malonyl-CoA_N -> 3-oxo-dodecanoyl-acp_N + CO2_N
R314	Fatty Acid Synthesis		3-oxo-dodecanoyl-acp_N + NADPH_N -> R-3-hydroxydodecanoyl-acp_N + NADP_N
R315	Fatty Acid Synthesis	FASN; RPP14	R-3-hydroxydodecanoyl-acp_N -> trans_dodec-2-enoyl-acp_N
R316	Fatty Acid Synthesis	FASN	trans_dodec-2-enoyl-acp_N + NADPH_N -> Dodecanoyl-acp_N + NADP_N
R317	Fatty Acid Synthesis		Dodecanoyl-acp_N -> Laurate_N

Table E.1. Metabolic reactions and genes in the developed brain model (cont.).

Reaction No	Metabolism	Gene Symbol	Reaction
R318	Fatty Acid Synthesis	FASN; FLJ40154; OXSM	Dodecanoyl-acp_N + Malonyl-CoA_N -> 3-oxo-myristoyl-acp_N + CO2_N
R319	Fatty Acid Synthesis		3-oxo-myristoyl-acp_N + NADPH_N -> 3R-3-hydroxymyristoyl-acp_N + NADP_N
R320	Fatty Acid Synthesis	FASN; RPP14	3R-3-hydroxymyristoyl-acp_N -> trans_tetradec-2-enoyl-acp_N
R321	Fatty Acid Synthesis	FASN	trans_tetradec-2-enoyl-acp_N + NADPH_N -> Myristoyl-acp_N + NADP_N
R322	Fatty Acid Synthesis	FASN; FLJ40154; OXSM	Myristoyl-acp_N + Malonyl-CoA_N -> 3-oxo-palmitoyl-acp_N + CO2_N
R323	Fatty Acid Synthesis		3-oxo-palmitoyl-acp_N + NADPH_N -> R-3-hydroxypalmitoyl-acp_N + NADP_N
R324	Fatty Acid Synthesis	FASN; RPP14	R-3-hydroxypalmitoyl-acp_N -> trans_hexadecenoyl-acp_N
R325	Fatty Acid Synthesis	FASN	trans_hexadecenoyl-acp_N + NADPH_N -> Palmitoyl-acp_N + NADP_N
R326	Fatty Acid Synthesis	FASN	Palmitoyl-acp_N <-> Palmitate_N
R327	Fatty Acid Synthesis	MLYCD	Acetyl-CoA_N + CO2_N <-> Malonyl-CoA_N
R328	Fatty Acid Synthesis	FASN	Acetyl-CoA_N <-> Acetyl-acp_N
R329	Fatty Acid Synthesis	FASN; MCAT	Malonyl-CoA_N <-> Malonyl-acp_N
R330	Fatty Acid Synthesis	FASN; FLJ40154; OXSM	Malonyl-acp_N + Acetyl-acp_N <-> Acetoacetyl-acp_N + CO2_N
R331	Fatty Acid Synthesis	ACACA; ACACB; PCCA; PCCB	Acetyl-CoA_N + ATP_N + Bicarbonate_N <-> Malonyl-CoA_N + ADP_N
R332	Fatty Acid Synthesis	CA1; CA10; CA11; CA13; CA3; CA4; CA5A; CA5B; CA6; CA7; CA8; CA9; HS15759	Bicarbonate_N <-> CO2_N
R333	Fatty Acid Synthesis	ACSBG1; ACSBG2; ACSL1; ACSL3; ACSL4; ACSL5; SLC27A2	Palmitate_N + ATP_N -> Palmitoyl-CoA_N + AMP_N
R334	Fatty Acid Synthesis	ELOVL1; ELOVL6	Palmitoyl-CoA_N + Malonyl-CoA_N -> 3-oxo-stearoyl-CoA_N + CO2_N
R335	Fatty Acid Synthesis		3-oxo-stearoyl-CoA_N + NADPH_N -> 3-hydroxy-stearoyl-CoA_N + NADP_N
R336	Fatty Acid Synthesis		3-hydroxy-stearoyl-CoA_N -> trans-2-3-stearoyl-CoA_N
R337	Fatty Acid Synthesis		trans-2-3-stearoyl-CoA_N + NADPH_N -> Stearoyl-CoA_N + NADP_N
R338	Fatty Acid Synthesis	ACOT2; ACOT4; ACOT7	Stearoyl-CoA_N -> Stearate_N
R339	Fatty Acid Synthesis	FADS1; FADS2; FADS6; SCD; SCD5	Stearoyl-CoA_N + O2_N -> Oleoyl-CoA_N
R340	Fatty Acid Synthesis	ACOT2; ACOT4	Oleoyl-CoA_N -> Oleate_N
R341	Fatty Acid Synthesis		Arachidonate_A -> Arachidonate_N
R342	Fatty Acid Synthesis		Decosahexenoate_A -> Decosahexenoate_N
R343	Fatty Acid Synthesis		0.243 Palmitate_A + 0.249 Stearate_A + 0.224 Oleate_A + 0.098 Arachidonate_A + 0.186 Decosahexenoate_A -> 1 FattyAcid_A
R344	Fatty Acid Synthesis		0.243 Palmitate_N + 0.249 Stearate_N + 0.224 Oleate_N + 0.098 Arachidonate_N + 0.186 Decosahexenoate_N -> 1 FattyAcid_N

Table E.1. Metabolic reactions and genes in the developed brain model (cont.).

Reaction No	Metabolism	Gene Symbol	Reaction
R345	Glycerol-3-phosphate Shuttle	GPD1	Dihydroxyacetone-phosphate_A + NADH_A -> Glycerol-3-phosphate_A + NAD_A
R346	Glycerol-3-phosphate Shuttle	GPD2; HS17122	Glycerol-3-phosphate_A + FAD_AM -> Dihydroxyacetone-phosphate_A + FADH2_AM
R347	Glycerol-3-phosphate Shuttle	GPD2; HS17122	Dihydroxyacetone-phosphate_N + FADH2_NM -> Glycerol-3-phosphate_N + FAD_NM
R348	Phosphatidyl ethanolamine Metabolism	CHKB; ETNK1; ETNK2	ATP_A + Ethanolamine_A -> Phosphoryl-ethanolamine_A + ADP_A
R349	Phosphatidyl ethanolamine Metabolism	PCYT2	Phosphoryl-ethanolamine_A + CTP_A -> CDP-ethanolamine_A
R350	Phosphatidyl ethanolamine Metabolism	CEPT1; SELI	1_2-diacylglycerol_A + CDP-ethanolamine_A -> Phosphatidyl-ethanolamine_A + CMP_A
R351	Phosphatidyl ethanolamine Metabolism Phosphatidyl choline Metabolism	PEMT	Phosphatidyl-ethanolamine_A -> Phosphatidyl-choline_A
R352	Phosphatidyl ethanolamine Metabolism	PTDSS2	Phosphatidyl-ethanolamine_A + Serine_A -> Ethanolamine_A + Phosphatidyl-serine_A
R353	Phosphatidyl ethanolamine Metabolism	PISD	Phosphatidyl-serine_A -> Phosphatidyl-ethanolamine_A + CO2_A
R354	Phosphatidyl ethanolamine Metabolism	CHKB; ETNK1; ETNK2	ATP_N + Ethanolamine_N -> Phosphoryl-ethanolamine_N + ADP_N
R355	Phosphatidyl ethanolamine Metabolism	PCYT2	Phosphoryl-ethanolamine_N + CTP_N -> CDP-ethanolamine_N
R356	Phosphatidyl ethanolamine Metabolism	CEPT1; SELI	1_2-diacylglycerol_N + CDP-ethanolamine_N -> Phosphatidyl-ethanolamine_N + CMP_N
R357	Phosphatidyl ethanolamine Metabolism; Phosphatidyl choline Metabolism	PEMT	Phosphatidyl-ethanolamine_N -> Phosphatidyl-choline_N
R358	Phosphatidyl ethanolamine Metabolism	PTDSS2	Phosphatidyl-ethanolamine_N + Serine_N -> Ethanolamine_N + Phosphatidyl-serine_N
R359	Phosphatidyl ethanolamine Metabolism	PISD	Phosphatidyl-serine_N -> Phosphatidyl-ethanolamine_N + CO2_N
R360	Phosphatidyl choline Metabolism	CHKA; CHKB	Choline_A + ATP_A -> Phosphoryl-choline_A + ADP_A
R361	Phosphatidyl choline Metabolism	PCYT1A; PCYT1B	Phosphoryl-choline_A + CTP_A -> CDP-choline_A
R362	Phosphatidyl choline Metabolism	CEPT1; CHPT1	1_2-diacylglycerol_A + CDP-choline_A -> Phosphatidyl-choline_A + CMP_A

Table E.1. Metabolic reactions and genes in the developed brain model (cont.).

Reaction No	Metabolism	Gene Symbol	Reaction
R363	Phosphatidyl choline Metabolism	CHKA; CHKB	Choline_N + ATP_N -> Phosphoryl-choline_N + ADP_N
R364	Phosphatidyl choline Metabolism	PCYT1A; PCYT1B	Phosphoryl-choline_N + CTP_N -> CDP-choline_N
R365	Phosphatidyl choline Metabolism	CEPT1; CHPT1	1_2-diacylglycerol_N + CDP-choline_N -> Phosphatidyl-choline_N + CMP_N
R366	Cardiolipin Metabolism	PGS1	CDP-diacylglycerol_A + Glycerol-3-phosphate_A -> CMP_A + phosphatidylglycerol-phosphate_A
R367	Cardiolipin Metabolism		phosphatidylglycerol-phosphate_A -> phosphatidyl-glycerol_A
R368	Cardiolipin Metabolism	CRLS1	phosphatidyl-glycerol_A + CDP-diacylglycerol_A -> cardiolipin_A + CMP_A
R369	Cardiolipin Metabolism	PGS1	CDP-diacylglycerol_N + Glycerol-3-phosphate_N -> CMP_N + phosphatidylglycerol-phosphate_N
R370	Cardiolipin Metabolism		phosphatidylglycerol-phosphate_N -> phosphatidyl-glycerol_N
R371	Cardiolipin Metabolism	CRLS1	phosphatidyl-glycerol_N + CDP-diacylglycerol_N -> cardiolipin_N + CMP_N
R372	Sphingomyelin Metabolism	SPTLC1; SPTLC2; SPTLC3	Serine_A + Palmitoyl-CoA_A -> CO2_A + 3-dehydrosphinganine_A
R373	Sphingomyelin Metabolism	KDSR	3-dehydrosphinganine_A + NADPH_A <-> sphinganine_A + NADP_A
R374	Sphingomyelin Metabolism		sphinganine_A + FattyAcid_A <-> dihydroceramide_A
R375	Sphingomyelin Metabolism	DEGS2	dihydroceramide_A <-> ceramide_A
R376	Sphingomyelin Metabolism	SAMD8; SGMS1; SGMS2	ceramide_A + Phosphatidyl-choline_A <-> 1_2-diacylglycerol_A + sphingomyelin_A
R377	Sphingomyelin Metabolism	ENPP7; LOC51190; SMPD1; SMPD2; SMPD3; SMPD4	sphingomyelin_A -> ceramide_A + Phosphoryl-choline_A
R378	Sphingomyelin Metabolism	SPTLC1; SPTLC2; SPTLC3	Serine_N + Palmitoyl-CoA_N -> CO2_N + 3-dehydrosphinganine_N
R379	Sphingomyelin Metabolism	KDSR	3-dehydrosphinganine_N + NADPH_N <-> sphinganine_N + NADP_N
R380	Sphingomyelin Metabolism		sphinganine_N + FattyAcid_N <-> dihydroceramide_N
R381	Sphingomyelin Metabolism	DEGS2	dihydroceramide_N <-> ceramide_N
R382	Sphingomyelin Metabolism	SAMD8; SGMS1; SGMS2	ceramide_N + Phosphatidyl-choline_N <-> 1_2-diacylglycerol_N + sphingomyelin_N
R383	Sphingomyelin Metabolism	ENPP7; LOC51190; SMPD1; SMPD2; SMPD3; SMPD4	sphingomyelin_N -> ceramide_N + Phosphoryl-choline_N
R384	CDP-Diacylglycerol Biosynthesis	AGPAT6; AGPAT9; GPAM; GPAT2; HS14692; HS15014	Glycerol-3-phosphate_A + FattyAcid_A -> 1-acyl-sn-glycerol-3-phosphate_A
R385	CDP-Diacylglycerol Biosynthesis	ABHD5; AGPAT1; AGPAT2; AGPAT3; AGPAT4; AGPAT5; LCLAT1; LPCAT3; LPCAT4; MBOAT1; MBOAT2; MBOAT7	1-acyl-sn-glycerol-3-phosphate_A + FattyAcid_A -> Phosphatidate_A
R386	CDP-Diacylglycerol Biosynthesis	AGPAT6; AGPAT9; GPAM; GPAT2; HS14692; HS15014	Glycerol-3-phosphate_N + FattyAcid_N -> 1-acyl-sn-glycerol-3-phosphate_N

Table E.1. Metabolic reactions and genes in the developed brain model (cont.).

Reaction No	Metabolism	Gene Symbol	Reaction
R387	CDP-Diacylglycerol Biosynthesis	ABHD5; AGPAT1; AGPAT2; AGPAT3; AGPAT4; AGPAT5; LCLAT1; LPCAT3; LPCAT4; MBOAT1; MBOAT2; MBOAT7	1-acyl-sn-glycerol-3-phosphate_N + FattyAcid_N -> Phosphatidate_N
R388	Inositol Metabolism		myo-inositol -> myo-inositol_A
R389	Inositol Metabolism	CDIPT	myo-inositol_A + CDP-diacylglycerol_A -> phosphatidyl-inositol_A + CMP_A
R390	Inositol Metabolism; CDP-Diacylglycerol Biosynthesis	CDS1; CDS2	CTP_A + Phosphatidate_A -> CDP-diacylglycerol_A
R391	Inositol Metabolism	PI4K2B; PI4KA; PI4KB; PI4KII; PIK4CA	phosphatidyl-inositol_A + ATP_A -> phosphatidyl-1D-myo-inositol-4-phosphate_A + ADP_A
R392	Inositol Metabolism	MGC26597; PIK4CA; PIP4K2B; PIP5K1A; PIP5K1B; PIP5K1C; PIP5KL1	phosphatidyl-1D-myo-inositol-4-phosphate_A + ATP_A <-> phosphatidyl-1D-myo-inositol-4-5-bisphosphate_A + ADP_A
R393	Inositol Metabolism	HS17073; PLCB1; PLCB2; PLCB3; PLCB4; PLCD1; PLCD3; PLCD4; PLCE1; PLCG1; PLCG2; PLCH1; PLCH2; PLCZ1	phosphatidyl-1D-myo-inositol-4-5-bisphosphate_A -> 1_2-diacylglycerol_A + myo-inositol-(1-4-5)-trisphosphate_A
R394	Inositol Metabolism	INPP5A; INPP5B; INPP5F; INPP5J; INPP5K; INPPL1; OCRL; SYNJ1; SYNJ2	myo-inositol-(1-4-5)-trisphosphate_A -> myo-inositol-(1-4)-bisphosphate_A
R395	Inositol Metabolism	INPP1	myo-inositol-(1-4)-bisphosphate_A <-> myo-inositol-(4)-monophosphate_A
R396	Inositol Metabolism	IMPA1; IMPA2; IMPAD1	myo-inositol-(4)-monophosphate_A <-> myo-inositol_A
R397	Inositol Metabolism	AGK; DGKA; DGKB; DGKD; DGKE; DGKG; DGKH; DGKI; DGKK; DGKQ; DGKZ; HS14711; HS17318; HS17545	ATP_A + 1_2-diacylglycerol_A -> Phosphatidate_A + ADP_A
R398	Inositol Metabolism	IPMK; ITPKA; ITPKB; ITPKC	myo-inositol-(1-4-5)-trisphosphate_A + ATP_A -> myo-inositol-(1-3-4-5)-tetrakisphosphate_A + ADP_A
R399	Inositol Metabolism	INPP5A; INPP5B; INPP5D; INPP5J; INPP5K; INPPL1; OCRL; SYNJ1; SYNJ2	myo-inositol-(1-3-4-5)-tetrakisphosphate_A <-> myo-inositol-(1-3-4)-trisphosphate_A
R400	Inositol Metabolism	INPP1	myo-inositol-(1-3-4)-trisphosphate_A -> myo-inositol-(3-4)-bisphosphate_A
R401	Inositol Metabolism	INPP4A; INPP4B	myo-inositol-(3-4)-bisphosphate_A -> myo-inositol-3-monophosphate_A
R402	Inositol Metabolism		myo-inositol -> myo-inositol_N
R403	Inositol Metabolism	CDIPT	myo-inositol_N + CDP-diacylglycerol_N -> phosphatidyl-inositol_N + CMP_N
R404	Inositol Metabolism; CDP-Diacylglycerol Biosynthesis	CDS1; CDS2	CTP_N + Phosphatidate_N -> CDP-diacylglycerol_N
R405	Inositol Metabolism	PI4K2B; PI4KA; PI4KB; PI4KII; PIK4CA	phosphatidyl-inositol_N + ATP_N -> phosphatidyl-1D-myo-inositol-4-phosphate_N + ADP_N

Table E.1. Metabolic reactions and genes in the developed brain model (cont.).

Reaction No	Metabolism	Gene Symbol	Reaction
R406	Inositol Metabolism	MGC26597; PIK4CA; PIP4K2B; PIP5K1A; PIP5K1B; PIP5K1C; PIP5KL1	phosphatidyl-1D-myo-inositol-4-phosphate_N + ATP_N <-> phosphatidyl-1D-myo-inositol-4-5-bisphosphate_N + ADP_N
R407	Inositol Metabolism	HS17073; PLCB1; PLCB2; PLCB3; PLCB4; PLCD1; PLCD3; PLCD4; PLCE1; PLCG1; PLCG2; PLCH1; PLCH2; PLCZ1	phosphatidyl-1D-myo-inositol-4-5-bisphosphate_N -> 1_2-diacylglycerol_N + myo-inositol-(1-4-5)-trisphosphate_N
R408	Inositol Metabolism	INPP5A; INPP5B; INPP5F; INPP5J; INPP5K; INPPL1; OCRL; SYNJ1; SYNJ2	myo-inositol-(1-4-5)-trisphosphate_N -> myo-inositol-(1-4)-bisphosphate_N
R409	Inositol Metabolism	INPP1	myo-inositol-(1-4)-bisphosphate_N <-> myo-inositol-(4)-monophosphate_N
R410	Inositol Metabolism	IMPA1; IMPA2; IMPAD1	myo-inositol-(4)-monophosphate_N <-> myo-inositol_N
R411	Inositol Metabolism	AGK; DGKA; DGKB; DGKD; DGKE; DGKG; DGKH; DGKI; DGKK; DGKQ; DGKZ; HS14711; HS17318; HS17545	ATP_N + 1_2-diacylglycerol_N -> Phosphatidate_N + ADP_N
R412	Inositol Metabolism	IPMK; ITPKA; ITPKB; ITPKC	myo-inositol-(1-4-5)-trisphosphate_N + ATP_N -> myo-inositol-(1-3-4-5)-tetrakisphosphate_N + ADP_N
R413	Inositol Metabolism	INPP5A; INPP5B; INPP5D; INPP5J; INPP5K; INPPL1; OCRL; SYNJ1; SYNJ2	myo-inositol-(1-3-4-5)-tetrakisphosphate_N <-> myo-inositol-(1-3-4)-trisphosphate_N
R414	Inositol Metabolism	INPP1	myo-inositol-(1-3-4)-trisphosphate_N -> myo-inositol-(3-4)-bisphosphate_N
R415	Inositol Metabolism	INPP4A; INPP4B	myo-inositol-(3-4)-bisphosphate_N -> myo-inositol-3-monophosphate_N
R416	Lipid Synthesis		0.448 Cholesterol_A + 0.210 Phosphatidyl-ethanolamine_A + 0.202 Phosphatidyl-choline_A + 0.081 Phosphatidyl-serine_A + 0.037 sphingomyelin_A + 0.021 phosphatidyl-inositol_A + 0.010 cardiolipin_A -> Lipid_A
R417	Lipid Synthesis		0.448 Cholesterol_N + 0.210 Phosphatidyl-ethanolamine_N + 0.202 Phosphatidyl-choline_N + 0.081 Phosphatidyl-serine_N + 0.037 sphingomyelin_N + 0.021 phosphatidyl-inositol_N + 0.010 cardiolipin_N -> Lipid_N
R418	ROS Pathway		Cystine_A + NADH_A -> 2 Cysteine_A + NAD_A
R419	ROS Pathway	GCLC; GCLM	Cysteine_A + Glutamate_A + ATP_A -> L-gamma-glutamylcysteine_A + ADP_A
R420	ROS Pathway	GSS	L-gamma-glutamylcysteine_A + Glycine_A + ATP_A -> ReducedGlutathione_A + ADP_A
R421	ROS Pathway		O2_A -> H2O2_A
R422	ROS Pathway	GPX1; GPX2; GPX3; GPX5; GPX6; GPX7; GPX8; HS17068	2 ReducedGlutathione_A + H2O2_A -> OxidizedGlutathione_A
R423	ROS Pathway	GSR	OxidizedGlutathione_A + NADPH_A -> 2 ReducedGlutathione_A + NADP_A
R424	ROS Pathway	GSR	OxidizedGlutathione_A + NADPH_AM -> 2 ReducedGlutathione_A + NADP_AM
R425	ROS Pathway	CAT; TYRP1	H2O2_A -> O2_A
R426	ROS Pathway		ReducedGlutathione_A + Glutamine_A -> Glutamate_A + NH3_A + CysteinylGlycine_A
R427	ROS Pathway		CysteinylGlycine_A -> CysteinylGlycine_N
R428	ROS Pathway	ANPEP; CNDP2; DPP8	CysteinylGlycine_N -> Cysteine_N + Glycine_N
R429	ROS Pathway	GCLC; GCLM	Cysteine_N + Glutamate_N + ATP_N -> L-gamma-glutamylcysteine_N + ADP_N

Table E.1. Metabolic reactions and genes in the developed brain model (cont.).

Reaction No	Metabolism	Gene Symbol	Reaction
R430	ROS Pathway	GSS	L-gamma-glutamylcysteine_N + Glycine_N + ATP_N -> ReducedGlutathione_N + ADP_N
R431	ROS Pathway		O2_N -> H2O2_N
R432	ROS Pathway	GPX1; GPX2; GPX3; GPX5; GPX6; GPX7; GPX8; HS17068	2 ReducedGlutathione_N + H2O2_N -> OxidizedGlutathione_N
R433	ROS Pathway	GSR	OxidizedGlutathione_N + NADPH_N -> 2 ReducedGlutathione_N + NADP_N
R434	ROS Pathway	GSR	OxidizedGlutathione_N + NADPH_NM -> 2 ReducedGlutathione_N + NADP_NM
R435	ROS Pathway	CAT; TYRP1	H2O2_N -> O2_N
R436	Glycogen Degradation Metabolism	PYGB; PYGL; PYGM	Glycogen -> Glucose-1-phosphate_A
R437	Glycogen Degradation Metabolism	HS10556; HS14226; HS15853; PGM1; PGM2; PGM5	Glucose-1-phosphate_A <-> Glucose-6-phosphate_A
R438	Ketone Body Metabolism		BHB -> BHB_A
R439	Ketone Body Metabolism		BHB -> BHB_N
R440	Ketone Body Metabolism		Acetoacetate -> Acetoacetate_A
R441	Ketone Body Metabolism		Acetoacetate -> Acetoacetate_N
R442	Ketone Body Metabolism	BDH1; BDH2	BHB_A + NAD_AM <-> Acetoacetate_A + NADH_AM
R443	Ketone Body Metabolism	BDH1; BDH2	BHB_N + NAD_NM <-> Acetoacetate_N + NADH_NM
R444	Ketone Body Metabolism	OXCT1	Acetoacetate_N + Succinyl-CoA_N -> Acetoacetyl-CoA_N + Succinate_N
R445	Arginine Metabolism		Ornithine -> Ornithine_A
R446	Arginine Metabolism	ADC	Arginine_A <-> Agmatine_A + CO2_A
R447	Arginine Metabolism	ARG1; ARG2	Arginine_A -> Ornithine_A + Urea_A
R448	Arginine Metabolism	OAT	Ornithine_A + alpha-ketoglutarate_A <-> Glutamate_A + Glutamate_semialdehyde_A
R449	Arginine Metabolism		Glutamate_semialdehyde_A <-> S-1-pyrroline-5-carboxylate_A
R450	Arginine Metabolism	ALDH4A1	S-1-pyrroline-5-carboxylate_A + NAD_A -> Glutamate_A + NADH_A
R451	Arginine Metabolism		Ornithine -> Ornithine_N
R452	Arginine Metabolism		Arginine_A -> Arginine_N
R453	Arginine Metabolism	ADC	Arginine_N <-> Agmatine_N + CO2_N
R454	Arginine Metabolism	AGMAT	Agmatine_N <-> Putrescine_N + Urea_N
R455	Arginine Metabolism	NOS1; NOS2; NOS2B; NOS3	2 Arginine_N + 3 NADPH_N + 4 O2_N <-> 2 Citrulline_N + 3 NADP_N
R456	Arginine Metabolism	ASS1; HS05204; HS13756; HS15303; HS16608; HS17316; HS17447	Aspartate_N + Citrulline_N + ATP_N -> L_Arginino_Succinate_N + AMP_N
R457	Arginine Metabolism	ASL; HS12378	L_Arginino_Succinate_N -> Arginine_N + Fumarate_N

Table E.1. Metabolic reactions and genes in the developed brain model (cont.).

Reaction No	Metabolism	Gene Symbol	Reaction
R458	Arginine Metabolism	ARG1; ARG2	Arginine_N -> Ornithine_N + Urea_N
R459	Arginine Metabolism	ADC; HS16994; ODC1	Ornithine_N <-> CO2_N + Putrescine_N
R460	Arginine Metabolism		Putrescine_N -> Putrescine_A
R461	Polyamine Metabolism	SAT1; SAT2	Putrescine_A + Acetyl-CoA_A -> N-acetylputrescine_A
R462	Polyamine Metabolism	MAOA; MAOB	N-acetylputrescine_A + O2_A -> Acetamidobutanal_A + NH3_A + H2O2_A
R463	Polyamine Metabolism	ALDH1B1; ALDH2; ALDH3A1; ALDH3A2; ALDH3B1; ALDH3B2; HS17339	Acetamidobutanal_A + NAD_A -> Acetamidobutanoate_A + NADH_A
R464	Polyamine Metabolism		Acetamidobutanoate_A -> GABA_A
R465	Polyamine Metabolism	AMD1	S-adenosyl-L-methionine_A -> S-adenosyl-L-methioninamine_A + CO2_A
R466	Polyamine Metabolism	AMD1	S-adenosyl-L-methionine_N -> S-adenosyl-L-methioninamine_N + CO2_N
R467	Polyamine Metabolism	SRM	Putrescine_N + S-adenosyl-L-methioninamine_N -> Spermidine_N + S-methyl-5-thioadenosine_N
R468	Polyamine Metabolism	HS17321; SMS	Spermidine_N + S-adenosyl-L-methioninamine_N -> Spermine_N + S-methyl-5-thioadenosine_N
R469	Polyamine Metabolism	SAT1; SAT2	Spermine_N + Acetyl-CoA_N -> N_1_Acetylspermine_N
R470	Polyamine Metabolism	AOC3; PAOX	N_1_Acetylspermine_N + O2_N -> H2O2_N + Spermidine_N
R471	Polyamine Metabolism	SMOX	Spermine_N + O2_N -> H2O2_N + Spermidine_N
R472	Polyamine Metabolism	SAT1; SAT2	Spermidine_N + Acetyl-CoA_N -> N_1_Acetylspermidine_N
R473	Polyamine Metabolism	AOC3; PAOX	N_1_Acetylspermidine_N + O2_N -> H2O2_N + Putrescine_N
R474	Creatine Metabolism	GATM	Glycine_A + Arginine_A -> Ornithine_A + Guanidinoacetate_A
R475	Creatine Metabolism	GAMT	Guanidinoacetate_A + S-adenosyl-L-methionine_A -> S-adenosyl-L-homocysteine_A + Creatine_A
R476	Creatine Metabolism	CKB; CKM; CKMT1A; CKMT1B; CKMT2	Creatine_A + ATP_A <-> CreatinePhosphate_A + ADP_A
R477	Creatine Metabolism	GATM	Glycine_N + Arginine_N -> Ornithine_N + Guanidinoacetate_N
R478	Creatine Metabolism	GAMT	Guanidinoacetate_N + S-adenosyl-L-methionine_N -> S-adenosyl-L-homocysteine_N + Creatine_N
R479	Creatine Metabolism	CKB; CKM; CKMT1A; CKMT1B; CKMT2	Creatine_N + ATP_N <-> CreatinePhosphate_N + ADP_N
R480	Heme Metabolism	ALAS1; ALAS2; HS17216	Glycine_A + Succinyl-CoA_A -> CO2_A + 5-amino-levulinate_A
R481	Heme Metabolism	ALAD	2 5-amino-levulinate_A -> porphobilinogen_A
R482	Heme Metabolism	HMBS	4 porphobilinogen_A -> 4 NH3_A + hydroxymethylbilane_A
R483	Heme Metabolism	UROS	hydroxymethylbilane_A -> uroporphyrinogen_A
R484	Heme Metabolism	UROD	uroporphyrinogen_A -> 4 CO2_A + coproporphyrinogen_A
R485	Heme Metabolism	CPOX	coproporphyrinogen_A + O2_A -> protoporphyrinogen_A + 2 CO2_A

Table E.1. Metabolic reactions and genes in the developed brain model (cont.).

Reaction No	Metabolism	Gene Symbol	Reaction
R486	Heme Metabolism	PPOX	protoporphyrinogen_A + 3 O2_A -> protoporphyrin_A + 3 H2O2_A
R487	Heme Metabolism	FECH	protoporphyrin_A -> protoheme_A
R488	Heme Metabolism	HMOX1; HMOX2	protoheme_A + 3 O2_A + FADH2_AM -> biliverdin_A + FAD_AM
R489	Heme Metabolism	BLVRA; BLVRB	biliverdin_A + NADPH_A -> bilirubin_A + NADP_A
R490	Heme Metabolism	ALAS1; ALAS2; HS17216	Glycine_N + Succinyl-CoA_N -> CO2_N + 5-amino-levulinate_N
R491	Heme Metabolism	ALAD	2 5-amino-levulinate_N -> porphobilinogen_N
R492	Heme Metabolism	HMBS	4 porphobilinogen_N -> 4 NH3_N + hydroxymethylbilane_N
R493	Heme Metabolism	UROS	hydroxymethylbilane_N -> uroporphyrinogen_N
R494	Heme Metabolism	UROD	uroporphyrinogen_N -> 4 CO2_N + coproporphyrinogen_N
R495	Heme Metabolism	CPOX	coproporphyrinogen_N + O2_N -> protoporphyrinogen_N + 2 CO2_N
R496	Heme Metabolism	PPOX	protoporphyrinogen_N + 3 O2_N -> protoporphyrin_N + 3 H2O2_N
R497	Heme Metabolism	FECH	protoporphyrin_N -> protoheme_N
R498	Heme Metabolism	HMOX1; HMOX2	protoheme_N + 3 O2_N + FADH2_NM -> biliverdin_N + FAD_NM
R499	Heme Metabolism	BLVRA; BLVRB	biliverdin_N + NADPH_N -> bilirubin_N + NADP_N
R500	Purine Nucleoside Metabolism		adenosine -> adenosine_A
R501	Purine Nucleoside Metabolism	ADK	adenosine_A + ATP_A -> AMP_A + ADP_A
R502	Purine Nucleoside Metabolism	AK1; AK2; AK3; AK5; AK7; C9orf98	AMP_A + ATP_A -> 2 ADP_A
R503	Purine Nucleoside Metabolism	CANT1; ENTPD1; ENTPD3; ENTPD8	ATP_A -> AMP_A
R504	Purine Nucleoside Metabolism	ENTPD1; ENTPD3; ENTPD8	ADP_A -> AMP_A
R505	Purine Nucleoside Metabolism	NT5C1A; NT5C1B; NT5C2; NT5C3; NT5E	AMP_A -> adenosine_A

Table E.1. Metabolic reactions and genes in the developed brain model (cont.).

Reaction No	Metabolism	Gene Symbol	Reaction
R506	Purine Nucleoside Metabolism	ATP12A; ATP1A1; ATP1A2; ATP1A3; ATP1A4; ATP1B1; ATP1B2; ATP1B3; ATP1B4; ATP2B1; ATP2B2; ATP2B3; ATP2B4; ATP4A; ATP4B; ATP6AP1; ATP6V0D1; ATP6V0D2; ATP6V0E1; ATP6V0E2; ATP6V1A; ATP6V1B1; ATP6V1B2; ATP6V1C1; ATP6V1C2; ATP6V1D; ATP6V1E1; ATP6V1E2; ATP6V1F; ATP6V1G2; ATP6V1G3; ATP6V1H; FXYD2; NKAIN1; NKAIN2; NKAIN3; NKAIN4	ATP_A -> ADP_A
R507	Purine Nucleoside Metabolism		guanosine -> guanosine_A
R508	Purine Nucleoside Metabolism	PNP	guanosine_A <-> ribose-1-phosphate_A + guanine_A
R509	Purine Nucleoside Metabolism	HPRT1	5-phospho-D-ribose-1-diphosphate_A + guanine_A -> GMP_A
R510	Purine Nucleoside Metabolism	HS07900; PRPS1; PRPS1L1; PRPS2	Ribose-5-phosphate_A + ATP_A -> AMP_A + 5-phospho-D-ribose-1-diphosphate_A
R511	Purine Nucleoside Metabolism		ribose-1-phosphate_A -> Ribose-5-phosphate_A
R512	Purine Nucleoside Metabolism	GUK1	GMP_A + ATP_A -> GDP_A + ADP_A
R513	Purine Nucleoside Metabolism	LOC283458; NME1; NME2; NME2P1; NME3; NME4; NME5; NME6; NME7	GDP_A + ATP_A -> GTP_A + ADP_A
R514	Purine Nucleoside Metabolism	LSG1; MTG1	GTP_A -> GDP_A
R515	Purine Nucleoside Metabolism	NT5C2	GMP_A -> guanosine_A
R516	Purine Nucleoside Metabolism		GTP_A -> GMP_A
R517	Purine Nucleoside Metabolism		GDP_A -> GMP_A
R518	Pirimidine Nucleoside Metabolism		uridine -> uridine_A
R519	Pirimidine Nucleoside Metabolism		UTP_A -> UDP_A
R520	Pirimidine Nucleoside Metabolism	NME1; NME2; NME2P1; NME3; NME4; NME5; NME6; NME7	UDP_A + ATP_A -> UTP_A + ADP_A

Table E.1. Metabolic reactions and genes in the developed brain model (cont.).

Reaction No	Metabolism	Gene Symbol	Reaction
R521	Pirimidine Nucleoside Metabolism		UDP_A -> UMP_A
R522	Pirimidine Nucleoside Metabolism		UMP_A + ATP_A -> UDP_A + ADP_A
R523	Pirimidine Nucleoside Metabolism	CANT1	UTP_A -> UMP_A
R524	Pirimidine Nucleoside Metabolism	UCK1; UCK2; UCKL1	uridine_A + ATP_A -> UMP_A + ADP_A
R525	Pirimidine Nucleoside Metabolism	UPP1; UPP2	uridine_A -> ribose-1-phosphate_A + uracil_A
R526	Pirimidine Nucleoside Metabolism		UMP_A -> uridine_A
R527	Pirimidine Nucleoside Metabolism		cytidine -> cytidine_A
R528	Pirimidine Nucleoside Metabolism	AICDA; CDA	cytidine_A -> NH3_A + uridine_A
R529	Pirimidine Nucleoside Metabolism	CMPK1; CMPK2	CMP_A + ATP_A -> CDP_A + ADP_A
R530	Pirimidine Nucleoside Metabolism		CDP_A -> CMP_A
R531	Pirimidine Nucleoside Metabolism	NME1; NME2; NME2P1; NME3; NME4; NME5; NME6; NME7	CDP_A + ATP_A -> CTP_A + ADP_A
R532	Pirimidine Nucleoside Metabolism	CANT1	CTP_A -> CMP_A
R533	Pirimidine Nucleoside Metabolism		CTP_A -> CDP_A
R534	Pirimidine Nucleoside Metabolism		CMP_A -> cytidine_A
R535	Pirimidine Nucleoside Metabolism		cytidine_A + ATP_A -> ADP_A + CMP_A
R536	Purine Nucleoside Metabolism		adenosine -> adenosine_N
R537	Purine Nucleoside Metabolism	ADK	adenosine_N + ATP_N -> AMP_N + ADP_N
R538	Purine Nucleoside Metabolism	AK1; AK2; AK3; AK5; AK7; C9orf98	AMP_N + ATP_N -> 2 ADP_N
R539	Purine Nucleoside Metabolism	CANT1; ENTPD1; ENTPD3; ENTPD8	ATP_N -> AMP_N
R540	Purine Nucleoside Metabolism	ENTPD1; ENTPD3; ENTPD8	ADP_N -> AMP_N

Table E.1. Metabolic reactions and genes in the developed brain model (cont.).

Reaction No	Metabolism	Gene Symbol	Reaction
R541	Purine Nucleoside Metabolism	NT5C1A; NT5C1B; NT5C2; NT5C3; NT5E	AMP_N -> adenosine_N
R542	Purine Nucleoside Metabolism	ATP12A; ATP1A1; ATP1A2; ATP1A3; ATP1A4; ATP1B1; ATP1B2; ATP1B3; ATP1B4; ATP2B1; ATP2B2; ATP2B3; ATP2B4; ATP4A; ATP4B; ATP6AP1; ATP6V0D1; ATP6V0D2; ATP6V0E1; ATP6V0E2; ATP6V1A; ATP6V1B1; ATP6V1B2; ATP6V1C1; ATP6V1C2; ATP6V1D; ATP6V1E1; ATP6V1E2; ATP6V1F; ATP6V1G2; ATP6V1G3; ATP6V1H; FXYD2; NKAIN1; NKAIN2; NKAIN3; NKAIN4	ATP_N -> ADP_N
R543	Purine Nucleoside Metabolism		guanosine -> guanosine_N
R544	Purine Nucleoside Metabolism	PNP	guanosine_N <-> ribose-1-phosphate_N + guanine_N
R545	Purine Nucleoside Metabolism	HPRT1	5-phospho-D-ribose-1-diphosphate_N + guanine_N -> GMP_N
R546	Purine Nucleoside Metabolism	HS07900; PRPS1; PRPS1L1; PRPS2	Ribose-5-phosphate_N + ATP_N -> AMP_N + 5-phospho-D-ribose-1-diphosphate_N
R547	Purine Nucleoside Metabolism		ribose-1-phosphate_N -> Ribose-5-phosphate_N
R548	Purine Nucleoside Metabolism	GUK1	GMP_N + ATP_N -> GDP_N + ADP_N
R549	Purine Nucleoside Metabolism	LOC283458; NME1; NME2; NME2P1; NME3; NME4; NME5; NME6; NME7	GDP_N + ATP_N -> GTP_N + ADP_N
R550	Purine Nucleoside Metabolism	LSG1; MTG1	GTP_N -> GDP_N
R551	Purine Nucleoside Metabolism	NT5C2	GMP_N -> guanosine_N
R552	Purine Nucleoside Metabolism		GTP_N -> GMP_N
R553	Purine Nucleoside Metabolism		GDP_N -> GMP_N
R554	Pirimidine Nucleoside Metabolism		uridine -> uridine_N
R555	Pirimidine Nucleoside Metabolism		UTP_N -> UDP_N

Table E.1. Metabolic reactions and genes in the developed brain model (cont.).

Reaction No	Metabolism	Gene Symbol	Reaction
R556	Pirimidine Nucleoside Metabolism	NME1; NME2; NME2P1; NME3; NME4; NME5; NME6; NME7	UDP_N + ATP_N -> UTP_N + ADP_N
R557	Pirimidine Nucleoside Metabolism		UDP_N -> UMP_N
R558	Pirimidine Nucleoside Metabolism		UMP_N + ATP_N -> UDP_N + ADP_N
R559	Pirimidine Nucleoside Metabolism	CANT1	UTP_N -> UMP_N
R560	Pirimidine Nucleoside Metabolism	UCK1; UCK2; UCKL1	uridine_N + ATP_N -> UMP_N + ADP_N
R561	Pirimidine Nucleoside Metabolism	UPP1; UPP2	uridine_N -> ribose-1-phosphate_N + uracil_N
R562	Pirimidine Nucleoside Metabolism		UMP_N -> uridine_N
R563	Pirimidine Nucleoside Metabolism		cytidine -> cytidine_N
R564	Pirimidine Nucleoside Metabolism	AICDA; CDA	cytidine_N -> NH3_N + uridine_N
R565	Pirimidine Nucleoside Metabolism	CMPK1; CMPK2	CMP_N + ATP_N -> CDP_N + ADP_N
R566	Pirimidine Nucleoside Metabolism		CDP_N -> CMP_N
R567	Pirimidine Nucleoside Metabolism	NME1; NME2; NME2P1; NME3; NME4; NME5; NME6; NME7	CDP_N + ATP_N -> CTP_N + ADP_N
R568	Pirimidine Nucleoside Metabolism	CANT1	CTP_N -> CMP_N
R569	Pirimidine Nucleoside Metabolism		CTP_N -> CDP_N
R570	Pirimidine Nucleoside Metabolism		CMP_N -> cytidine_N
R571	Pirimidine Nucleoside Metabolism		cytidine_N + ATP_N -> ADP_N + CMP_N
R572			EXT -> Glycogen
R573			Lactate_A -> EXT
R574			Lactate_N -> EXT
R575			CO2_A -> EXT
R576			CO2_N -> EXT
R577			Glutamine_A -> EXT
R578			Dopamine_N -> EXT
R579			Norepinephrine_N -> EXT

Table E.1. Metabolic reactions and genes in the developed brain model (cont.).

Reaction No	Metabolism	Gene Symbol	Reaction
R580			Epinephrine_N -> EXT
R581			Norepinephrine_A -> EXT
R582			Seratonin_N -> EXT
R583			Melatonin_N -> EXT
R584			Acetylcholine_N -> EXT
R585			Lipid_N -> EXT
R586			Lipid_A -> EXT
R587			EXT -> Linoleate_A
R588			EXT -> Linolenate_A
R589			EXT -> Choline_N
R590			EXT -> Choline_A
R591			EXT -> Cystine_A
R592			ReducedGlutathione_N -> EXT
R593			EXT -> Glucose_A
R594			EXT -> Glucose_N
R595			EXT -> O2_A
R596			EXT -> O2_N
R597			EXT -> Leucine_A
R598			EXT -> Isoleucine_A
R599			EXT -> Valine_A
R600			EXT -> Tyrosine_N
R601			EXT -> Tryptophan_N
R602			EXT -> Lysine_N
R603			EXT -> Phenylalanine_N
R604			EXT -> NH3_A
R605			EXT -> BHB
R606			EXT -> Acetoacetate
R607			EXT -> Arginine_A
R608			EXT -> Ornithine
R609			CreatinePhosphate_N -> EXT
R610			CreatinePhosphate_A -> EXT
R611			EXT -> Histidine_N
R612			EXT -> methionine
R613			adenosine_A -> EXT
R614			adenosine_N -> EXT
R615			2-oxobutanoate_N -> EXT
R616			EXT -> tetrahydrofolate_N
R617			EXT -> tetrahydrofolate_A
R618			EXT -> myo-inositol
R619			bilirubin_A -> EXT
R620			bilirubin_N -> EXT

Table E.1. Metabolic reactions and genes in the developed brain model (cont.).

Reaction No	Metabolism	Gene Symbol	Reaction
R621			EXT -> threonine
R622			EXT -> adenosine
R623			EXT -> guanosine
R624			EXT -> uridine
R625			EXT -> cytidine
R626			Urea_N -> EXT
R627			Urea_A -> EXT
R628			S-methyl-5-thioadenosine_N -> EXT
R629			Asparagine_N -> EXT
R630			methylhistamine_N -> EXT

REFERENCES

1. Kitano, H., “Systems biology: a brief overview,” *Science*, vol. 295, pp. 1662–1664, 2002.

2. Westerhoff , H. V., and B. O. Palsson, “The evolution of molecular biology into systems biology,” Nat. Biotechnol., vol. 22, pp. 1249–1252, 2004.

3. Palsson, B., “In silico biology through ‘omics’,” *Nat. Biotechnol.*, vol. 20, pp. 649–650, 2002.

4. Gehlenborg, N., S. I. O’Donoghue, N. S. Baliga, A. Goesmann, M. A. Hibbs, H. Kitano, O. Kohlbacher, H. Neuweger, R. Schneider, and D. Tenenbaum, “Visualization of omics data for systems biology,” *Nat. methods*, vol. 7, 2010.

5. Patil, K. R., and J. Nielsen, “Uncovering transcriptional regulation of metabolism by using metabolic network topology,” *Proc. Natl. Acad. Sci. United States Am.*, vol. 102, pp. 2685–2689, 2005.

6. Çakır, T., S. Alsan, H. Saybaşılı, A. Akın, and K. Ö. Ülgen, “Reconstruction and flux analysis of coupling between metabolic pathways of astrocytes and neurons: application to cerebral hypoxia.”

7. Johnson, M. B., Y. I. Kawasawa, C. E. Mason, Ž. Krsnik, G. Coppola, D. Bogdanović, D. H. Geschwind, S. M. Mane, M. W. State, and N. Šestan, “Functional and Evolutionary Insights into Human Brain Development through Global Transcriptome Analysis,” *Neuron*, vol. 62, no. 4, pp. 494–509, May 2009.

8. Hartl, D., M. Irmler, I. Römer, M. T. Mader, L. Mao, C. Zabel, M. H. de Angelis, J. Beckers, and J. Klose, “Transcriptome and proteome analysis of early embryonic mouse brain development,” *Proteomics*, vol. 8, no. 6, pp. 1257–1265, 2008.

9. Cahoy, J. D., B. Emery, A. Kaushal, L. C. Foo, J. L. Zamanian, K. S. Christopherson, Y. Xing, J. L. Lubischer, P. A. Krieg, and S. A. Krupenko, “A transcriptome database for astrocytes, neurons, and oligodendrocytes: a new resource for understanding brain development and function,” *J. Neurosci.*, vol. 28, pp. 264–278, 2008.

10. Palsson, B. O., “Properties of Reconstructed Networks,” *Cambridge: Syst. Biol.*, 2006.

11. Ge, H., A. J. M. Walhout, and M. Vidal, “Integrating ‘omic’ information: a bridge between genomics and systems biology,” *Trends Genet.*, vol. 19, no. 10, pp. 551–560, Oct. 2003.

12. Chen, L., R.-S. Wang, and X.-S. Zhang, *Biomolecular networks: methods and applications in systems biology*, vol. 10. Wiley. com, 2009.

13. Bronk, J. R., *Human metabolism: functional diversity and integration*. Addison-Wesley Longman, 1999.

14. Jankovic, J., “Parkinson’s disease: clinical features and diagnosis,” *J. Neurol. Neurosurg. & Psychiatry*, vol. 79, pp. 368–376, 2008.

15. Warner, T. T., and A. H. V. Schapira, “Genetic and environmental factors in the cause of Parkinson’s disease,” *Ann. Neurol.*, vol. 53, no. S3, pp. S16–S25, 2003.

16. Veldman, B. A. J., A. M. Wijn, N. Knoers, P. Praamstra, and M. W. I. M. Horstink, “Genetic and environmental risk factors in Parkinson’s disease,” *Clin. Neurol. Neurosurg.*, vol. 100, no. 1, pp. 15–26, Mar. 1998.

17. Hardy, J., “Genetic Analysis of Pathways to Parkinson Disease,” *Neuron*, vol. 68, no. 2, pp. 201–206, Oct. 2010.

18. Nuytemans, K., J. Theuns, M. Cruts, and C. Van Broeckhoven, “Genetic etiology

of Parkinson disease associated with mutations in the SNCA, PARK2, PINK1, PARK7, and LRRK2 genes: a mutation update," *Hum. Mutat.*, vol. 31, no. 7, pp. 763–780, 2010.

19. Shulman, J. M., P. L. De Jager, and M. B. Feany, "Parkinson's disease: genetics and pathogenesis," *Annu. Rev. Pathol. Mech. Dis.*, vol. 6, pp. 193–222, 2011.

20. Brady, S., G. Siegel, R. W. Albers, and D. Price, *Basic neurochemistry: molecular, cellular and medical aspects*. Academic Press, 2005.

21. Büeler, H., "Impaired mitochondrial dynamics and function in the pathogenesis of Parkinson's disease," *Exp. Neurol.*, vol. 218, no. 2, pp. 235–246, Aug. 2009.

22. Morris, M. E., "Movement disorders in people with Parkinson disease: a model for physical therapy," *Phys. Ther.*, vol. 80, pp. 578–597, 2000.

23. Elsworth, J. D., and R. H. Roth, "Dopamine Synthesis, Uptake, Metabolism, and Receptors: Relevance to Gene Therapy of Parkinson's Disease," *Exp. Neurol.*, vol. 144, no. 1, pp. 4–9, Mar. 1997.

24. Schapira, A. H. V., "Neurobiology and treatment of Parkinson's disease," *Trends Pharmacol. Sci.*, vol. 30, no. 1, pp. 41–47, Jan. 2009.

25. Scarpini, E., P. Schelterns, and H. Feldman, "Treatment of Alzheimer's disease; current status and new perspectives," *Lancet Neurol.*, vol. 2, no. 9, pp. 539–547, Sep. 2003.

26. Zheng, Z., and M. I. Diamond, "Huntington Disease and the huntingtin protein," *Prog. Mol. Biol. Transl. Sci.*, vol. 107, 2012.

27. Bensimon, G., L. Lacomblez, and V. Meininger, "A controlled trial of riluzole in amyotrophic lateral sclerosis," *New Engl. J. Med.*, vol. 330, pp. 585–591, 1994.

28. Goldenberg, M. M., “Multiple sclerosis review,” *Pharm. Ther.*, vol. 37, 2012.

29. Bear, M. F., B. W. Connors, and M. A. Paradiso, *Neuroscience*. Wolters Kluwer Health, 2007.

30. Kauffman, K. J., P. Prakash, and J. S. Edwards, “Advances in flux balance analysis,” *Curr. Opin. Biotechnol.*, vol. 14, no. 5, pp. 491–496, Oct. 2003.

31. Orth, J. D., I. Thiele, and B. Ø. Palsson, “What is flux balance analysis?,” *Nat. Biotechnol.*, vol. 28, pp. 245–248, 2010.

32. Varma, A., and B. O. Palsson, “Stoichiometric flux balance models quantitatively predict growth and metabolic by-product secretion in wild-type Escherichia coli W3110.,” *Appl. Environ. Microbiol.*, vol. 60, pp. 3724–3731, 1994.

33. Segre, D., D. Vitkup, and G. M. Church, “Analysis of optimality in natural and perturbed metabolic networks,” *Proc. Natl. Acad. Sci.*, vol. 99, pp. 15112–15117, 2002.

34. Shlomi, T., O. Berkman, and E. Ruppin, “Regulatory on/off minimization of metabolic flux changes after genetic perturbations,” *Proc. Natl. Acad. Sci. United States Am.*, vol. 102, pp. 7695–7700, 2005.

35. Zelezniak, A., T. H. Pers, S. Soares, M. E. Patti, and K. R. Patil, “Metabolic network topology reveals transcriptional regulatory signatures of type 2 diabetes,” *PLoS Comput. Biol.*, vol. 6, 2010.

36. Cvijovic, M., R. Olivares-Hernández, R. Agren, N. Dahr, W. Vongsangnak, I. Nookaew, K. R. Patil, and J. Nielsen, “BioMet Toolbox: genome-wide analysis of metabolism,” *Nucleic acids Res.*, vol. 38, 2010.

37. Sandelin, A., W. Alkema, P. Engström, W. W. Wasserman, and B. Lenhard, “JASPAR: an open-access database for eukaryotic transcription factor binding

profiles," *Nucleic Acids Res.*, vol. 32, no. suppl 1, pp. D91–D94, Jan. 2004.

38. Matys, V., E. Fricke, R. Geffers, E. Gößling, M. Haubrock, R. Hehl, K. Hornischer, D. Karas, A. E. Kel, and O. V. Kel-Margoulis, "TRANSFAC¯: transcriptional regulation, from patterns to profiles," *Nucleic acids Res.*, vol. 31, pp. 374–378, 2003.

39. Wasserman, W. W., and A. Sandelin, "Applied bioinformatics for the identification of regulatory elements," *Nat. Rev. Genet.*, vol. 5, pp. 276–287, 2004.

40. Schneider, T. D., and R. M. Stephens, "Sequence logos: a new way to display consensus sequences," *Nucleic acids Res.*, vol. 18, pp. 6097–6100, 1990.

41. Zambelli, F., G. Pesole, and G. Pavesi, "Pscan: finding over-represented transcription factor binding site motifs in sequences from co-regulated or co-expressed genes," *Nucleic acids Res.*, vol. 37, 2009.

42. Chatziioannou, A., G. Palaiologos, and F. N. Kolisis, "Metabolic flux analysis as a tool for the elucidation of the metabolism of neurotransmitter glutamate," *Metab. Eng.*, vol. 5, no. 3, pp. 201–210, Jul. 2003.

43. Occhipinti, R., M. A. Puchowicz, J. C. LaManna, E. Somersalo, and D. Calvetti, "Statistical analysis of metabolic pathways of brain metabolism at steady state," *Ann. Biomed. Eng.*, vol. 35, pp. 886–902, 2007.

44. Lewis, N. E., G. Schramm, A. Bordbar, J. Schellenberger, M. P. Andersen, J. K. Cheng, N. Patel, A. Yee, R. A. Lewis, and R. Eils, "Large-scale in silico modeling of metabolic interactions between cell types in the human brain," *Nat. Biotechnol.*, vol. 28, pp. 1279–1285, 2010.

45. Romero, P., J. Wagg, M. L. Green, D. Kaiser, M. Krummenacker, and P. D. Karp, "Computational prediction of human metabolic pathways from the complete human genome," *Genome Biol.*, vol. 6, 2004.

46. Rosenthal, M. D., and R. H. Glew, *Medical biochemistry: human metabolism in health and disease*. Wiley. com, 2011.

47. Durany, N., J. Joseph, and F. F. Cruz-SÃ, "Phosphoglycerate mutase, 2, 3-bisphosphoglycerate phosphatase and creatine kinase activity and isoenzymes in human brain tumours.," *Br. J. Cancer*, vol. 76, 1997.

48. Burbaeva, G. S., M. S. Turishcheva, E. A. Vorobyeva, O. K. Savushkina, E. B. Tereshkina, and I. S. Boksha, "Diversity of glutamate dehydrogenase in human brain," *Prog. Neuro-Psychopharmacology Biol. Psychiatry*, vol. 26, no. 3, pp. 427–435, Apr. 2002.

49. Schmoll, D., E. Führmann, R. Gebhardt, and B. Hamprecht, "Significant Amounts of Glycogen are Synthesized from 3-Carbon Compounds in Astroglial Primary Cultures from Mice with Participation of the Mitochondrial Phosphoenolpyruvate Carboxykinase Isoenzyme," *Eur. J. Biochem.*, vol. 227, no. 1–2, pp. 308–315, 1995.

50. Cruz, F., S. R. Scott, I. Barroso, P. Santisteban, and S. Cerdán, "Ontogeny and Cellular Localization of the Pyruvate Recycling System in Rat Brain," *J. Neurochem.*, vol. 70, no. 6, pp. 2613–2619, 1998.

51. Beigneux, A. P., C. Kosinski, B. Gavino, J. D. Horton, W. C. Skarnes, and S. G. Young, "ATP-citrate lyase deficiency in the mouse," *J. Biol. Chem.*, vol. 279, pp. 9557–9564, 2004.

52. Melø, T. M., A. Nehlig, and U. Sonnewald, "Neuronal–glial interactions in rats fed a ketogenic diet," *Neurochem. International*, vol. 48, no. 6–7, pp. 498–507, May 2006.

53. Hasselbalch, S. G., G. M. Knudsen, J. Jakobsen, L. P. Hageman, S. Holm, and O. B. Paulson, "Brain metabolism during short-term starvation in humans," *J. Cereb.*

Blood Flow & Metab., vol. 14, pp. 125–131, 1994.

54. Chechik, T., L. M. Roeder, J. T. Tildon, and S. E. Poduslo, "Ketone body enzyme activities in purified neurons, astrocytes and oligodendroglia," *Neurochem. International*, vol. 10, no. 1, pp. 95–99, 1987.

55. Wiesinger, H., "Glia-specific enzyme systems." Oxford University Press, New York, pp. 488–499, 1995.

56. Regunathan, S., D. L. Feinstein, W. Raasch, and D. J. Reis, "Agmatine (decarboxylated arginine) is synthesized and stored in astrocytes," *Neuroreport*, vol. 6, pp. 1897–1900, 1995.

57. Braissant, O., T. Gotoh, M. Loup, M. Mori, and C. Bachmann, "l-arginine uptake, the citrulline–NO cycle and arginase II in the rat brain: an in situ hybridization study," *Mol. Brain Res.*, vol. 70, no. 2, pp. 231–241, Jul. 1999.

58. Iyo, A. H., M.-Y. Zhu, G. A. Ordway, and S. Regunathan, "Expression of arginine decarboxylase in brain regions and neuronal cells," *J. Neurochem.*, vol. 96, no. 4, pp. 1042–1050, 2006.

59. Wiesinger, H., "Arginine metabolism and the synthesis of nitric oxide in the nervous system," *Prog. Neurobiol.*, vol. 64, no. 4, pp. 365–391, Jul. 2001.

60. Molderings, G. J., and B. Haenisch, "Agmatine (decarboxylated l-arginine): Physiological role and therapeutic potential," *Pharmacol. & Ther.*, vol. 133, no. 3, pp. 351–365, Mar. 2012.

61. Bernstein, H. G., C. Stich, K. Jäger, H. Dobrowolny, M. Wick, J. Steiner, R. Veh, B. Bogerts, and G. Laube, "Agmatinase, an inactivator of the putative endogenous antidepressant agmatine, is strongly upregulated in hippocampal interneurons of subjects with mood disorders," *Neuropharmacology*, vol. 62, no. 1, pp. 237–246, Jan. 2012.

62. Krauss, M., T. Weiss, K. Langnaese, K. Richter, A. Kowski, R. W. Veh, and G. Laube, “Cellular and subcellular rat brain spermidine synthase expression patterns suggest region-specific roles for polyamines, including cerebellar pre-synaptic function,” *J. Neurochem.*, vol. 103, no. 2, pp. 679–693, 2007.

63. Angulo, M. C., K. Le Meur, A. S. Kozlov, S. Charpak, and E. Audinat, “GABA, a forgotten gliotransmitter,” *Prog. Neurobiol.*, vol. 86, no. 3, pp. 297–303, Nov. 2008.

64. Laschet, J., T. Grisar, M. Bureau, and D. Guillaume, “Characteristics of putrescine uptake and subsequent GABA formation in primary cultured astrocytes from normal C57BL/6J and epileptic DBA/2J mouse brain cortices,” *Neuroscience*, vol. 48, no. 1, pp. 151–157, May 1992.

65. Arnt-Ramos, L. R., W. E. O’Brien, and S. R. Vincent, “Immunohistochemical localization of argininosuccinate synthetase in the rat brain in relation to nitric oxide synthase-containing neurons,” *Neuroscience*, vol. 51, no. 4, pp. 773–789, Dec. 1992.

66. Nakamura, H., K. Itoh, and M. Kawabuchi, “NADPH-diaphorase and cytosolic urea cycle enzymes in the rat accessory olfactory bulb,” *J. Chem. Neuroanat.*, vol. 17, no. 2, pp. 109–117, Oct. 1999.

67. Shank, R. P., and G. LeM. Campbell, “Ornithine as a precursor of glutamate and GABA: Uptake and metabolism by neuronal and glial enriched cellular material,” *J. Neurosci. Res.*, vol. 9, no. 1, pp. 47–57, Jan. 1983.

68. Bernstein, H.G., and M. Müller, “The cellular localization of the l-ornithine decarboxylase/polyamine system in normal and diseased central nervous systems,” *Prog. Neurobiol.*, vol. 57, no. 5, pp. 485–505, Apr. 1999.

69. Thompson, S. G., P. T.-H. Wong, S. F. Leong, and E. G. McGeer, “Regional

Distribution in Rat Brain of 1-Pyrroline-5-Carboxylate Dehydrogenase and Its Localization to Specific Glial Cells," *J. Neurochem.*, vol. 45, no. 6, pp. 1791–1796, 1985.

70. Braissant, O., H. Henry, M. Loup, B. Eilers, and C. Bachmann, "Endogenous synthesis and transport of creatine in the rat brain: an in situ hybridization study," *Mol. Brain Res.*, vol. 86, no. 1–2, pp. 193–201, Jan. 2001.

71. Smith, Q. R., "Transport of glutamate and other amino acids at the blood-brain barrier," *J. Nutr.*, vol. 130, pp. 1016–1022, 2000.

72. Krusong, K., A. G. Ercan-Sencicek, M. Xu, H. Ohtsu, G. M. Anderson, M. W. State, and C. Pittenger, "High levels of histidine decarboxylase in the striatum of mice and rats," *Neurosci. Lett.*, vol. 495, no. 2, pp. 110–114, May 2011.

73. Brown, R. E., D. R. Stevens, and H. L. Haas, "The physiology of brain histamine," *Prog. Neurobiol.*, vol. 63, no. 6, pp. 637–672, Apr. 2001.

74. Nishibori, M., A. Tahara, K. Sawada, J. Sakiyama, N. Nakaya, and K. Saeki, "Neuronal and vascular localization of histamine N-methyltransferase in the bovine central nervous system," *Eur. J. Neurosci.*, vol. 12, no. 2, pp. 415–424, 2000.

75. McBean, G. J., "The transsulfuration pathway: a source of cysteine for glutathione in astrocytes," *Amino acids*, vol. 42, pp. 199–205, 2012.

76. Vitvitsky, V., M. Thomas, A. Ghorpade, H. E. Gendelman, and R. Banerjee, "A functional transsulfuration pathway in the brain links to glutathione homeostasis," *J. Biol. Chem.*, vol. 281, pp. 35785–35793, 2006.

77. Spector, R., G. Coakley, and R. Blakely, "Methionine Recycling in Brain: A Role for Folates and Vitamin B-12," *J. Neurochem.*, vol. 34, no. 1, pp. 132–137, 1980.

78. Lajtha, A., P. Saransaari, and A. Schousboe, *Handbook of Neurochemistry and Molecular Neurobiology: Amino Acids and Peptides in the Nervous System*, vol. 4. Springer, 2007.

79. Ellis, C. E., E. J. Murphy, D. C. Mitchell, M. Y. Golovko, F. Scaglia, G. C. Barceló-Coblijn, and R. L. Nussbaum, "Mitochondrial lipid abnormality and electron transport chain impairment in mice lacking α-synuclein," *Mol. Cell. Biol.*, vol. 25, pp. 10190–10201, 2005.

80. Pope, S., J. M. Land, and S. J. R. Heales, "Oxidative stress and mitochondrial dysfunction in neurodegeneration; cardiolipin a critical target?," *Biochim. et Biophys. Acta*, vol. 1777, no. 7–8, pp. 794–799, Jul. 2008.

81. Ma, K., R. Langenbach, S. I. Rapoport, and M. Basselin, "Altered brain lipid composition in cyclooxygenase-2 knockout mouse," *J. Lipid Res.*, vol. 48, pp. 848–854, 2007.

82. Pahan, K., F. G. Sheikh, M. Khan, A. M. Namboodiri, and I. Singh, "Sphingomyelinase and ceramide stimulate the expression of inducible nitric-oxide synthase in rat primary astrocytes," *J. Biol. Chem.*, vol. 273, pp. 2591–2600, 1998.

83. Mitoma, J., T. Kasama, S. Furuya, and Y. Hirabayashi, "Occurrence of an Unusual Phospholipid, Phosphatidyl-l-threonine, in Cultured Hippocampal Neurons EXOGENOUS l-SERINE IS REQUIRED FOR THE SYNTHESIS OF NEURONAL PHOSPHATIDYL-l-SERINE AND SPHINGOLIPIDS," *J. Biol. Chem.*, vol. 273, pp. 19363–19366, 1998.

84. Hirabayashi, Y., and S. Furuya, "Roles of l-serine and sphingolipid synthesis in brain development and neuronal survival," *Prog. Lipid Res.*, vol. 47, no. 3, pp. 188–203, May 2008.

85. Yamanaka, T., E. Hanada, and K. Suzuki, "Acid sphingomyelinase of human brain. Improved purification procedures and characterization.," *J. Biol. Chem.*, vol.

256, pp. 3884–3889, 1981.

86. Ma, K., J. Deutsch, N. E. Villacreses, T. A. Rosenberger, S. I. Rapoport, and H. U. Shetty, “Measuring Brain Uptake and Incorporation into Brain Phosphatidylinositol of Plasma myo-[2H6] Inositol in Unanesthetized Rats: An Approach to Estimate In vivo Brain Phosphatidylinositol Turnover,” *Neurochem. Res.*, vol. 31, pp. 759–765, 2006.

87. Hauser, G., and V. N. Finelli, “The biosynthesis of free and phosphatide myo-inositol from glucose by mammalian tissue slices,” *J. Biol. Chem.*, vol. 238, pp. 3224–3228, 1963.

88. Inhorn, R. C., V. S. Bansal, and P. W. Majerus, “Pathway for inositol 1, 3, 4-trisphosphate and 1, 4-bisphosphate metabolism,” *Proc. Natl. Acad. Sci.*, vol. 84, pp. 2170–2174, 1987.

89. Fisher, S. K., J. E. Novak, and B. W. Agranoff, “Inositol and higher inositol phosphates in neural tissues: homeostasis, metabolism and functional significance,” *J. Neurochem.*, vol. 82, no. 4, pp. 736–754, 2002.

90. Vincent, S. R., S. Das, and M. D. Maines, “Brain heme oxygenase isoenzymes and nitric oxide synthase are co-localized in select neurons,” *Neuroscience*, vol. 63, no. 1, pp. 223–231, Nov. 1994.

91. Schipper, H. M., “Heme oxygenase-1: role in brain aging and neurodegeneration,” *Exp. Gerontol.*, vol. 35, no. 6–7, pp. 821–830, Sep. 2000.

92. Ryter, S. W., and R. M. Tyrrell, “The heme synthesis and degradation pathways: role in oxidant sensitivity Heme oxygenase has both pro- and antioxidant properties,” *Free. Radic. Biol. Med.*, vol. 28, no. 2, pp. 289–309, Jan. 2000.

93. Ipata, P. L., “Origin, utilization, and recycling of nucleosides in the central nervous system,” *Adv. Physiol. Educ.*, vol. 35, pp. 342–346, 2011.

94. Lubow, J. M., I. G. Piñón, A. Avogaro, C. Cobelli, D. M. Treeson, K. A. Mandeville, G. Toffolo, and P. J. Boyle, "Brain oxygen utilization is unchanged by hypoglycemia in normal humans: lactate, alanine, and leucine uptake are not sufficient to offset energy deficit," *Am. J. Physiol. Metab.*, vol. 290, 2006.

95. Madsen, P. L., N. F. Cruz, L. Sokoloff, and G. A. Dienel, "Cerebral Oxygen/Glucose Ratio is Low During Sensory Stimulation and Rises Above Normal During Recovery: Excess Glucose Consumption During Stimulation Is Not Accounted for by Lactate Efflux From or Accumulation in Brain Tissue," *J. Cereb. Blood Flow & Metab.*, vol. 19, pp. 393–400, 1999.

96. Nybo, L., B. Nielsen, E. Blomstrand, K. Møller, and N. Secher, "Neurohumoral responses during prolonged exercise in humans," *J. Appl. Physiol.*, vol. 95, pp. 1125–1131, 2003.

97. Wahren, J., K. Ekberg, E. Fernqvist-Forbes, and S. Nair, "Brain substrate utilisation during acute hypoglycaemia," *Diabetologia*, vol. 42, pp. 812–818, 1999.

98. Gruetter, R., E. R. Seaquist, and K. Ugurbil, "A mathematical model of compartmentalized neurotransmitter metabolism in the human brain," *Am. J. Physiol. Metab.*, vol. 281, 2001.

99. Gruetter, V., K. F. Petersen, G. W. Cline, J. Shen, G. F. Mason, S. Dufour, K. L. Behar, G. I. Shulman, and D. L. Rothman, "Astroglial contribution to brain energy metabolism in humans revealed by 13C nuclear magnetic resonance spectroscopy: elucidation of the dominant pathway for neurotransmitter glutamate repletion and measurement of astrocytic oxidative metabolism," *J. Neurosci.*, vol. 22, pp. 1523–1531, 2002.

100. Shen, J., K. F. Petersen, K. L. Behar, P. Brown, T. W. Nixon, G. F. Mason, O. A. Petroff, G. I. Shulman, R. G. Shulman, and D. L. Rothman, "Determination of the rate of the glutamate/glutamine cycle in the human brain by in vivo 13C NMR,"

Proc. Natl. Acad. Sci., vol. 96, pp. 8235–8240, 1999.

101. Öz, G., D. A. Berkich, P.-G. Henry, Y. Xu, K. LaNoue, S. M. Hutson, and R. Gruetter, "Neuroglial metabolism in the awake rat brain: CO2 fixation increases with brain activity," *J. Neurosci.*, vol. 24, pp. 11273–11279, 2004.

102. Hertz, L., L. Peng, and G. A. Dienel, "Energy metabolism in astrocytes: high rate of oxidative metabolism and spatiotemporal dependence on glycolysis/glycogenolysis," *J. Cereb. Blood Flow & Metab.*, vol. 27, pp. 219–249, 2006.

103. Siegel, G. J., B. W. Agranoff, R. W. Albers, and P. B. Molinoff, *Basic neurochemistry: molecular, cellular, and medical aspects*. Raven Press, 1994.

104. Wiesinger, H., B. Hamprecht, and R. Dringen, "Metabolic pathways for glucose in astrocytes," *Glia*, vol. 21, pp. 22–34, 1997.

105. Ben-Yoseph, O., D. M. Camp, T. E. Robinson, and B. D. Ross, "Dynamic measurements of cerebral pentose phosphate pathway activity in vivo using [1, 6-13C2, 6, 6-2H2] glucose and microdialysis," *J. Neurochem.*, vol. 64, pp. 1336–1342, 1995.

106. Aureli, T., M. E. Di Cocco, M. Calvani, and F. Conti, "The entry of [1-13C] glucose into biochemical pathways reveals a complex compartmentation and metabolite trafficking between glia and neurons: a study by 13C-NMR spectroscopy," *Brain Res.*, vol. 765, pp. 218–227, 1997.

107. Schapira, A. H. V., J. M. Cooper, D. Dexter, J. B. Clark, P. Jenner, and C. D. Marsden, "Mitochondrial Complex I Deficiency in Parkinson's Disease," *J. Neurochem.*, vol. 54, no. 3, pp. 823–827, 1990.

108. Mizuno, Y., S. Matuda, H. Yoshino, H. Mori, N. Hattori, and S.-I. Ikebe, "An immunohistochemical study on α-ketoglutarate dehydrogenase complex in

Parkinson's disease," *Ann. Neurol.*, vol. 35, no. 2, pp. 204–210, 1994.

109. Gibson, G. E., A. E. Kingsbury, H. Xu, J. G. Lindsay, S. Daniel, O. J. F. Foster, A. J. Lees, and J. P. Blass, "Deficits in a tricarboxylic acid cycle enzyme in brains from patients with Parkinson's disease," *Neurochem. International*, vol. 43, no. 2, pp. 129–135, Jul. 2003.

110. Müller, T., D. Woitalla, B. Hauptmann, B. Fowler, and W. Kuhn, "Decrease of methionine and S-adenosylmethionine and increase of homocysteine in treated patients with Parkinson's disease," *Neurosci. Lett.*, vol. 308, no. 1, pp. 54–56, Jul. 2001.

111. Piccinini, M., F. Scandroglio, S. Prioni, B. Buccinnà, N. Loberto, M. Aureli, V. Chigorno, E. Lupino, G. DeMarco, and A. Lomartire, "Deregulated sphingolipid metabolism and membrane organization in neurodegenerative disorders," *Mol. Neurobiol.*, vol. 41, pp. 314–340, 2010.

112. Stokes, C. E., and J. N. Hawthorne, "Reduced Phosphoinositide Concentrations in Anterior Temporal Cortex of Alzheimer-Diseased Brains," *J. Neurochem.*, vol. 48, no. 4, pp. 1018–1021, 1987.

113. Miller, B. L., R. A. Moats, T. Shonk, T. Ernst, S. Woolley, and B. D. Ross, "Alzheimer disease: depiction of increased cerebral myo-inositol with proton MR spectroscopy.," *Radiology*, vol. 187, pp. 433–437, 1993.

114. Kalra, S., C. C. Hanstock, W. R. Martin, P. S. Allen, and W. S. Johnston, "Detection of cerebral degeneration in amyotrophic lateral sclerosis using high-field magnetic resonance spectroscopy," *Arch. Neurol.*, vol. 63, 2006.

115. Teunissen, C. E., C. D. Dijkstra, C. H. Polman, E. L. J. Hoogervorst, K. von Bergmann, and D. Lütjohann, "Decreased levels of the brain specific 24S-hydroxycholesterol and cholesterol precursors in serum of multiple sclerosis patients," *Neurosci. Lett.*, vol. 347, no. 3, pp. 159–162, Aug. 2003.

116. Antonio Molina, J., F. Javier Jiménez-Jiménez, P. Gómez, C. Vargas, J. Antonio Navarro, M. Ortí-Pareja, T. Gasalla, J. Benito-León, F. Bermejo, and J. Arenas, "Decreased cerebrospinal fluid levels of neutral and basic amino acids in patients with Parkinson's disease," *J. Neurol. Sci.*, vol. 150, no. 2, pp. 123–127, Sep. 1997.

117. Reilmann, R., L. H. Rolf, and H. W. Lange, "Decreased plasma alanine and isoleucine in Huntington's disease," *Acta Neurol. Scand.*, vol. 91, no. 3, pp. 222–224, 1995.

118. Kim, J. S., H. H. Kornhuber, B. Holzmüller, W. Schmid-Burgk, T. Mergner, and G. Krzepinski, "Reduction of cerebrospinal fluid glutamic acid in Huntington's chorea and in schizophrenic patients," *Arch. für Psychiatr. und Nervenkrankh.*, vol. 228, pp. 7–10, 1980.

119. Monaco, F., S. Fumero, A. Mondino, and R. Mutani, "Plasma and cerebrospinal fluid tryptophan in multiple sclerosis and degenerative diseases.," *J. Neurol. Neurosurg. & Psychiatry*, vol. 42, pp. 640–641, 1979.

120. Bjerkenstedt, L., G. Edman, L. Hagenfeldt, G. Sedvall, and F. A. Wiesel, "Plasma amino acids in relation to cerebrospinal fluid monoamine metabolites in schizophrenic patients and healthy controls.," *Br. J. Psychiatry*, vol. 147, pp. 276–282, 1985.

121. Adhihetty, P. J., and M. F. Beal, "Creatine and its potential therapeutic value for targeting cellular energy impairment in neurodegenerative diseases," *Neuromolecular Med.*, vol. 10, pp. 275–290, 2008.

122. Tarnopolsky, M. A., and M. F. Beal, "Potential for creatine and other therapies targeting cellular energy dysfunction in neurological disorders," *Ann. Neurol.*, vol. 49, no. 5, pp. 561–574, 2001.

123. Klein, A. M., and R. J. Ferrante, "The neuroprotective role of creatine," in

Creatine and Creatine Kinase in Health and Disease, Springer, 2008, pp. 205–243.

124. Kashiwaya, Y., T. Takeshima, N. Mori, K. Nakashima, K. Clarke, and R. L. Veech, "d-β-Hydroxybutyrate protects neurons in models of Alzheimer's and Parkinson's disease," *Proc. Natl. Acad. Sci.*, vol. 97, pp. 5440–5444, 2000.

125. Zhang, Y., M. James, F. A. Middleton, and R. L. Davis, "Transcriptional analysis of multiple brain regions in Parkinson's disease supports the involvement of specific protein processing, energy metabolism, and signaling pathways, and suggests novel disease mechanisms," *Am. J. Med. Genet. Part B: Neuropsychiatr. Genet.*, vol. 137B, no. 1, pp. 5–16, 2005.

126. Lesnick, T. G., S. Papapetropoulos, D. C. Mash, J. Ffrench-Mullen, L. Shehadeh, M. de Andrade, J. R. Henley, W. A. Rocca, J. E. Ahlskog, and D. M. Maraganore, "A genomic pathway approach to a complex disease: axon guidance and Parkinson disease," *PLoS Genet.*, vol. 3, 2007.

127. Sammon, J. W., "A nonlinear mapping for data structure analysis," *Comput. IEEE Trans.*, vol. 100, pp. 401–409, 1969.

128. McClure, J., and E. Wit, *Statistics for Microarrays: Design, Analysis and Inference*. Wiley, 2004.